DISS ETH NO. 23086

Transformations of Silver Nanoparticles in Urban Wastewater and Water Systems

A dissertation submitted to

ETH Zürich

to obtain the degree of

Doctor of Sciences

presented by

Basilius Adam Daniel Thalmann

Msc. ETH in Interdisciplinary Sciences

born on 14.03.1986

citizen of Küsnacht (ZH), Switzerland

accepted on the recommendation of

Prof. Dr. Eberhard Morgenroth, examiner

Dr. Ralf Kägi, co-examiner

Dr. Andreas Voegelin, co-examiner

Prof. Dr. Greg Lowry, co-examiner

Zürich, 2015

Abstract

Metallic silver nanoparticles (AgNP) are increasingly applied in consumer products from which they are probably released to the urban wastewater and water system. Due to the antimicrobial activity of AgNP, they are of high ecotoxicological concern and an engineered nanomaterial of priority for environmental risk assessment. Transformations of AgNP can have large effects on their toxicity toward aquatic organism. Most importantly, the sulfidation of AgNP is known to reduce the toxicity of Ag by several orders of magnitude. Thus, a proper understanding of the sulfidation of AgNP in the urban wastewater and water system is crucial for in-depth environmental risk assessments. Furthermore, the ozonation of the effluent of wastewater treatment plant (WWTP) to mitigate micropollutants is likely to further change the Ag speciation. The first objective of this thesis was to understand the sulfidation kinetics of AgNP with bisulfide (HS^-) and metal sulfides. The second objective was to study the impact of ozone treatment on sulfidized AgNP.

The sulfidation with HS^- was best described by a diffusion limited solid-state kinetic model. The rate increased with increasing humic acid concentrations and half-life times were between one to twelve minutes. Analytical transmission electron microscopy revealed a change from asymmetrical to concentric sulfidation of AgNP with increasing humic acid concentrations. In addition, the formation of hollow sphere nanoparticles through the Kirkendall effect was observed. The sulfidation with copper and zinc sulfides followed pseudo-first order kinetics with increasing rates for decreasing AgNP diameters and increasing metal sulfide concentrations. Furthermore, the rate was dependent on the metal sulfide type. The half-life times were a few hours to days. Furthermore, complex sulfidation patterns were observed possibly due to the polycrystallinity of the AgNP. While the sulfidation of AgNP with HS^- is likely to occur in urban wastewater systems due to the presence of elevated HS^- concentrations, the reaction with metal sulfides is more likely in oxic surface waters, as HS^- is oxidized by oxygen within a couple of hours, whereas metal sulfides are persistent for weeks to months.

To address the second objective, the reaction of nano-Ag_2S with ozone was assessed. Oxidation of the sulfide in Ag_2S requires 2.91 mol Ozone per Ag_2S and the second-order rate constant was comparable to the rate constant of fast reacting organic micropollutants. Furthermore, the Ag speciation in the WWTP effluent changed from Ag_2S to AgCl. The short-term toxicity of Ag toward the green algae *Chlamydomonas reinhardtii* increased from not detectable to ionic Ag^+ in effluent.

In conclusion, the sulfidation of AgNP in urban wastewater and water systems is estimated to be completed within minutes up to a few days. The ozone treatment of WWTP effluent containing nano-Ag_2S leads to the formation of new Ag species which show an increased short-term toxicity towards algae.

Zusammenfassung

Silber Nanopartikel (AgNP) werden vermehrt in Konsumgütern angewandt, von welchen die Partikel durch den Gebrauch in das urbane Abwasser und Wasser ausgewaschen werden können. Aufgrund ihrer antimikrobieller Wirkung stellen sie ein potentielles Risiko für die Umwelt dar, welches abgeschätzt werden sollte. Durch Umwandlung in der Umwelt ändert sich die Speziierung der AgNP was die Toxizität gegenüber aquatischen Organismen und Pflanzen beeinflusst. Die Reaktion von AgNP mit Sulfiden, genannt Sulfidierung, zum Beispiel reduziert die Ag Toxizität um mehrere Grössenordnungen. Deshalb ist es für eine Risikoeinschätzung der AgNP in der Umwelt wichtig die Sulfidierung im urbanen Abwasser und Wasser zu verstehen. Im Abwasser ist die dominante Sulfid Quelle Bisulfid (HS^-), welches in erhöhten Konzentrationen zu finden ist. Für das Oberflächengewässer hingegen ist die Sulfidierung mit Metallsulfiden wahrscheinlicher, da sie persistenter gegen die Oxidation mit Sauerstoff sind. Das erste Ziel dieser Dissertation war deshalb die Sulfidierung von AgNP mit HS^- und Metallsulfiden zu verstehen.

Mit HS^- war die Reaktion diffusionslimitiert und hatte Halbwertszeiten zwischen einer und zwölf Minuten. Wobei die Rate mit abnehmender AgNP Grösse und zunehmender Konzentration an Huminsäuren schneller wurde. Mittels analytischer Elektronenmikroskopie konnte gezeigt werden, dass die Huminsäure zu einer Änderung des Reaktionsverlauf von asymmetrischer zu konzentrischer Sulfidierung führte. Die Sulfidierung mit Metallsulfiden war mit Halbwertszeiten von einigen Stunden bis Tagen signifikant langsamer als mit HS^-. Die Reaktion war schneller mit kleineren AgNP und zunehmender Metallsulfid Konzentration. Zusätzlich war die Geschwindigkeitsrate von der Metallsulfid Art abhängig.

Zur Reduktion von Mikroverunreinigungen im Abwasser werden in der nächsten Jahren bis zu 100 Schweizer Kläranlagen mit einer zusätzlichen Ozonung des Ablaufs ausgerüstet. Dies könnte zu einer weiteren Änderung der Speziierung von AgNP führen. Deshalb wurde als zweites Forschungsziel der Einfluss der Ozonung auf sulfidierte AgNP untersucht. Das Sulfid wurde dabei durch das Ozon zu Sulfat oxidiert und es bildete sich vorwiegend Silberchlorid. Die Reaktionsgeschwindigkeit war vergleichbar mit schnell oxidierenden Mikroverunreinigungen. Die Änderung der Speziierung führte zu einer Erhöhung der kurzzeitigen, toxischen Wirkung auf Grünalgen von unter der Nachweisgrenze auf Werte vergleichbar mit ionischem Ag^+.

Zusammenfassend, AgNP sind im urbanen Abwasser und Wasser innerhalb von Minuten bis Tagen vollständig sulfidiert. Überdies führt die Ozonung von sulfidierten AgNP zur Bildung von neuen Silberspezien und Erhöhung der Toxizität.

Graphical Abstract

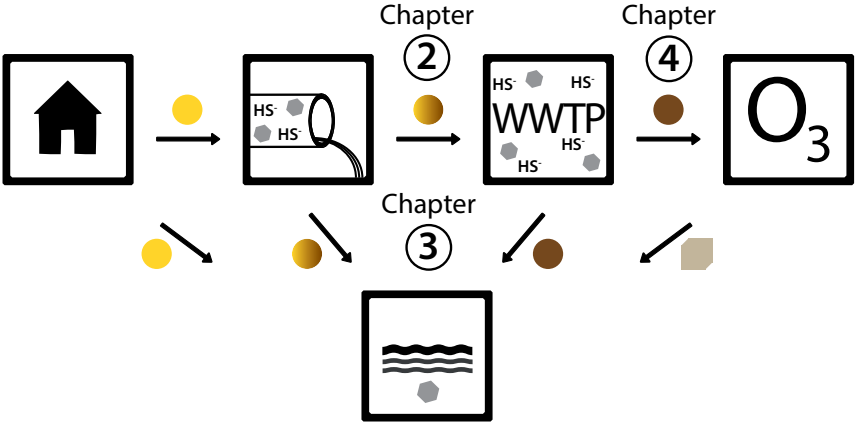

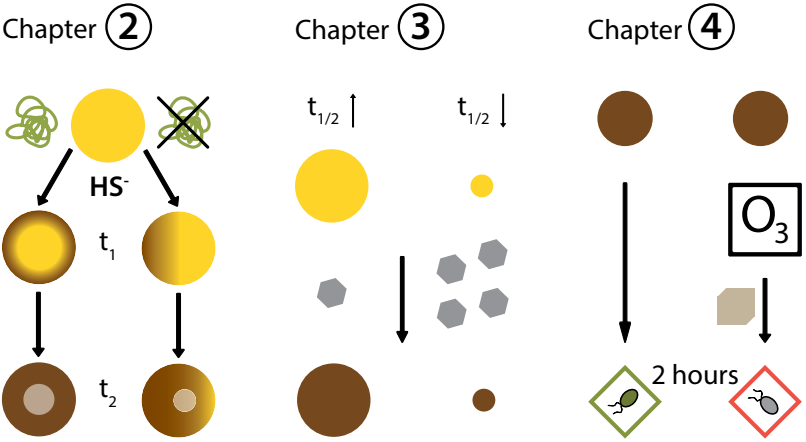

AgNP
Metal Sulfide
nano-Ag_2S
HS- Bisulfide
AgCl
Humic Acid (HA)

Table of Contents

Glossary

AgNP	Silver nanoparticles
Sulfidation	The reaction of a metal, alloy or mineral (*e.g.* Ag, CuO) with sulfur (most importantly sulfide) and its incorporation to form a sulfidic compound, such as metal sulfides (Ag_2S, CuS)
Chalcophile	Elements (*e.g.* Ag, Cu, Ga) that combine readily with sulfur or another element from the chalcogen period except oxygen
Oxic	The presence of molecular oxygen (O_2), mostly dissolved in water
Anoxic	The absence of O_2, does not exclude the presence of other oxygen containing substances (*e.g.* NO_3^-)
NOM	Natural organic matter
HA	Humic acid, a fraction of NOM is defined as a complex mixture of organic substances containing acidic groups
DOM	Dissolved organic matter
DOC	Dissolved organic carbon
TSS	Total suspended solids
WWTP	Wastewater treatment plant
HS^-	Bisulfide, the dominant dissolved sulfide species at circumneutral pH
K_{sp}	Solubility product
EC_{50}	Half maximum effective concentration of a chemical substance on an organism
XAS	X-ray absorption spectroscopy
EXAFS	Extended X-ray absorption fine structure
XANES	X-ray absorption near edge structure
ICP-MS	Inductively coupled plasma mass spectroscopy
ICP-OES	Inductively coupled plasma optical emission spectroscopy
IC	Ion chromatography
(S)TEM	(Scanning) transmission electron microscopy
SEM	Scanning electron microscopy
HAADF	High-angle annular dark field used for electron microscopy

1. Introduction

1.1 Nanotechnology

In 1959 Richard Feynman gave his visionary talk entitled "There's Plenty of Room at the Bottom", where he introduced the idea and the potential of making materials smaller, down to the nanoscale. He proposed that nanotechnology has the potential to create new possibilities in miniaturization (*e.g.* tiny machines or computer chips) and to improve material properties. Although nanotechnology was already used by humans for centuries unnamed (Freestone et al. 2007), it took almost another 30 years after his talk until research efforts started to increase. During the 1990s about 100'000 studies were published and only recently nanotechnology started to be a fast growing research field with over 700'000 publications and 30'000 patents between 2001 and 2012 (Chen et al. 2013).

Nanomaterials, defined as materials with the shortest dimension being one to one hundred nanometers, can be classified into two groups: carbon-based (*e.g.* fullerenes, carbon nanotubes (CNTs), graphene) and inorganic materials, including quantum dots (*e.g.* cadmium sulfide (CdS), lead selenide (PbSe), indium arsenide (InAs)), metal oxides (*e.g.* titanium dioxide (TiO_2), zinc oxide (ZnO), copper oxide (CuO)) and pure metals (*e.g.* silver (Ag), zerovalent iron (Fe), gold (Au)). Besides the miniaturizing effect, which is mostly applied for electronic devices, nanomaterials show new physical properties due to their small dimension. Moreover, the shrinking of the particles to the nanosize increases the surface to volume ratio, which results in an increased reactivity.

Today, one of the most produced nanomaterials in the EU is nano-TiO_2 (~10'000 t $year^{-1}$ in 2012) followed by nano-ZnO (~1'600 t $year^{-1}$) (Sun et al. 2014). Nano-TiO_2 has its main application either as catalysts or as an Ultra-Violet (UV) light attenuator (especially for UV radiation protection like sunscreen) and nano-ZnO is mainly used in paints and cosmetics. It is very likely, that the use and application of nanomaterials in commercial products will continue to increase in the future. Despite the opportunities provided by nanomaterials, environmental and health concerns increased. Thus, governmental regulations of nano-products are required.

The US environmental protection agency (EPA) defined nanotechnology as "research and technology development at the atomic, molecular, or macromolecular levels using a length scale of approximately one to one hundred nanometers in any dimension" (Usepa 2007). The European Union, on the other hand, defined nanomaterials more generally as natural, incidental or manufactured materials which consist of 50% particles with a diameter between one to one hundred nanometers (2011/696/EU). By the completion of this thesis there is no other nano specific

regulation enacted, however, discussions on national and international basis are ongoing.

Within this context the Swiss National Science Foundation (SNSF) introduced in 2010 the National Research Program 64 (NRP 64) to investigate the "Opportunities and Risks of Nanomaterials". The aim of the program is to bridge existing knowledge gaps on nanomaterials with respect to opportunities and risks for human health and the environment. This thesis is financed through the NRP 64 and focuses on the transformations of silver nanoparticles in urban wastewater and water systems.

1.2 Silver Nanoparticles

Although nano-TiO_2 and -ZnO had the highest production loads, nano-Ag, with an annual production of 30 t in 2012 in the EU was the most applied nanomaterial by number of products. Nano-Ag is widely incorporated into textiles, cleaning agents, plastics, cosmetics or other household products (Mueller and Nowack 2008), mainly due to the antimicrobial activity of Ag^+ (Ratte 1999). It can be produced in different shapes like cubes, plates or rods, however, most importantly as spherical Ag nanoparticles (AgNP). Due to their wide application further on the specific case for AgNP is discussed, however, most of it is generally also applicable for other shapes of nano-Ag.

AgNP are dominantly synthesized via wet chemistry methods. Although there exists a wide variety of procedures, typically a silver salt such as silver nitrate ($AgNO_3$) is reduced with a reducing agent, for example sodium borohydride ($NaBH_4$), to form metallic AgNP. An additional stabilizer / surfactant is added during the synthesis, which forms a coating layer around the particle and prevents AgNP from agglomerating with other particles (Figure 1.1) (Kim et al. 2006). Current surfactants available on the market can be grouped into either steric (*e.g.* polyethylene glycol (PEG), polyvinylpyrrolidone (PVP)) or charged molecules (*e.g.* citrate, tannic acid, branched polyethyleneimine (BPEI)) (Figure 1.2 top) (http://www.nanocomposix.com).

AgNP might get released to the environment throughout their entire life cycle, from production and application in products to the use and end of the life cycle. During production and application of AgNP in products they can be release to the environment due to carless disposal or failures during the manufacturing. During the use of AgNP containing products such as socks, wash detergents or cosmetics wash out to the sewers is the most likely release pathway. At the end of the products life cycle it is estimated that approximately a third of the incorporated Ag is recycled. Therefore, mass-flow modeling studies estimated that the primary release pathway to the environment from production and consumption of AgNP is to the wastewater system. A smaller fraction of AgNP is either directly disposed to land-

Figure 1.1: Citrate coated AgNP dispersed in water (20 mg_{Ag} L^{-1}). The nominal diameter of the particles is increasing from left to right (10, 20, 40, 100 nm AgNP).

fills or indirectly through waste incineration plants (Blaser et al. 2008, Gottschalk et al. 2009, Hendren et al. 2013, Keller et al. 2013, Mueller and Nowack 2008, Sun et al. 2014).

1.3 Toxicity of Silver Nanoparticles

Once released, AgNP are of high environmental concern due to their antimicrobial activity and toxicity toward higher organisms. The toxicity of metallic Ag is mostly attributed to the slow oxidative dissolution and release of Ag^+. Ag is prone to bind to thiol groups and, hence, vital proteins, enzymes or cell walls can be damaged or disturbed (Ratte 1999). There is evidence that the same processes are responsible for the toxicity of AgNP (Kittler et al. 2010, Navarro et al. 2008b). However, for some AgNP a nano-specific toxicity has been observed, especially for smaller particles (< 10 nm), which may penetrate the cell wall and dissolve within the cell, which has been described as Trojan horse effect (Fabrega et al. 2009, Sotiriou and Pratsinis 2010). Another possible toxicological mechanism of AgNP is oxidative stress caused by reactive oxygen species (ROS) potentially formed on the surface of AgNP (Choi and Hu 2008). In recent years the potential risk of AgNP to humans and other biological organisms has been intensely studied and adverse effects were not only observed for bacteria, but also the interaction of Ag with other cells can lead to serious damage (up to tissue failure) for example for algae, plants, fungi, vertebrates and human cells (Asharani et al. 2008, Lu et al. 2010, Meyer et al. 2010, Navarro et al. 2008a, Navarro et al. 2008b, Sondi and Salopek-Sondi 2004, Yin et al. 2011).

The knowledge of the AgNP exposure dose and the toxic response of the aquatic organism is important for environmental risk assessments. However, environmental transformations of AgNP can significantly influence their toxicity. Therefore, to evaluate the possible ecotoxicological risk of AgNP reaching the aquatic environ-

ment it is very important to understand what specific Ag species will be present at any given point in the environmental system (Levard et al. 2012).

1.4 Environmental Transformations

AgNP in the environment are likely to undergo a wide variety of transformations. The following environmental transformations are discussed and their influence on the toxicity is mentioned: replacement of the surfactant, oxidative dissolution, interaction with chloride (Cl^-) and reaction with sulfide.

The surfactant of AgNP is likely to get replaced by natural organic matter (NOM) or proteins present in water (Figure 1.2 left) (Lowry et al. 2012, Ostermeyer et al. 2013). Humic acid (HA) as a surrogate of NOM has been shown to stabilize nanoparticles efficiently, with the highest stability for a mixture of HA with different molecular weights (Louie et al. 2013). The HA interaction depends on the type of AgNP surfactant (Yin et al. 2015). In the presence of sunlight HA can reduce Ag^+ to nanosized metallic Ag (Akaighe et al. 2011). Furthermore, the toxicity of AgNP to Daphnia (water fleas) decreases with increasing NOM (Gao et al. 2012).

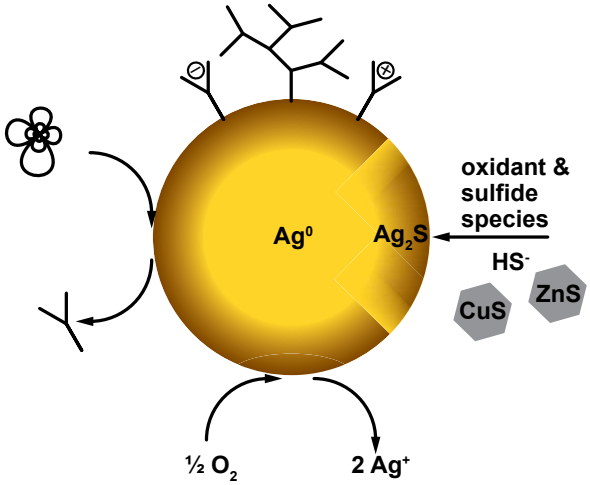

Figure 1.2: Schematic drawing of a single AgNP. AgNP are stabilized against agglomeration using either steric or electrostatic surfactants (top). Surfactants are likely to be replaced by other substances, and environmentally most relevant are NOM especially thiol containing organics and proteins (left). In the presence of O_2 metallic Ag undergoes oxidative dissolution, where ionic Ag^+ is released (bottom). In the presence of sulfide species such as bisulfide (HS^-) and an oxidant, AgNP transform to Ag_2S (right).

The oxidative dissolution of AgNP in oxic waters is another important environmental transformation pathway. In the presence of O_2 metallic Ag is thermodynamically unstable (change in Gibbs free energy from Ag^0 to Ag_2O: $\Delta G^0_{298°K}$ = -11.25 kJ/mol) and gets oxidized by oxygen followed by the formation a silver oxide (Ag_2O) layer, which then is dissolved in water at low Ag concentrations (solubility product: K_{sp} = 1.8×10^{-8} M^3, 25 mg_{Ag2O} L^{-1}, Figure 1.2 bottom, Table 1.1) (Haynes 2014). In general, the oxidative dissolution kinetic is faster at low pH and high O_2 concentrations due to the reaction's consumption of both H^+ and O_2 (Table 1.1). For AgNP the rate is furthermore dependent on the particle size, surfactant and presence of natural organic matter (NOM). Smaller particles are known to be oxidized faster due to their higher surface-to-volume ratio (Dobias and Bernier-Latmani 2013, Ma et al. 2012, Peretyazhko et al. 2014). Additionally it was shown that the standard electrode potential (E_0) is decreasing for particles with a diameter below 30 nm (Ivanova and Zamborini 2010). AgNP surfactants and NOM reduce the oxidative dissolution possibly by shielding the particle surface from oxygen and dissolution of the Ag_2O layer (Gunsolus et al. 2015, Liu and Hurt 2010). One of the primary toxicological pathways of AgNP is through the interaction of released Ag^+ with a cell, hence, the extent and rate of AgNP dissolution is known to strongly affect the toxicity (Kittler et al. 2010, Navarro et al. 2008b).

Table 1.1: Overview of Selected, Relevant Environmental Reactions and Solubility Products with their Respective Constants.

Reaction Name	Chemical Equation / Solubility Product	Constant *k*	Reference
oxidative dissolution	$2Ag + \frac{1}{2}O_2 + 2H^+ \underset{}{\overset{k_{ox}}{\rightleftharpoons}} 2Ag^+ + H_2O$	0.15 - 1.24 d^{-1}	(Peretyazhko et al. 2014)
sulfidation	$2Ag + \frac{1}{2}O_2 + HS^- \xrightarrow{k_{sulf}} Ag_2S + OH^-$	0.018 mM min^{-1}	(Liu et al. 2011)
sulfide oxidation	$HS^- + \frac{1}{2}O_2 \xrightarrow{k_{HS^-\_Ox}} S + OH^-$	0.6 - 34.6 µM min^{-1}	(Luther et al. 2011)
silver oxide	$\left[Ag^+\right]^2\left[OH^-\right] = K_{sp,Ag_2O}$	3.6×10^{-11} M^3	(Haynes 2014)
silver chloride	$\left[Ag^+\right]\left[Cl^-\right] = K_{sp,\mathrm{AgCl}}$	1.77×10^{-10} M^2	(Haynes 2014)
silver sulfide	$\left[Ag^+\right]^2\left[O^{2-}\right] = K_{sp,Ag_2O}$	6×10^{-30} M^3	(Haynes 2014)

Ag is known to form complexes and precipitates with halides. In most natural waters chloride (Cl^-) is present at elevated concentrations (surface waters ~1-10 mM Cl^-, sea water ~500 mM Cl^-) where Ag^+ can form complexes ($AgCl^{2-}$, $AgCl_3^{2-}$, $AgCl_4^{3-}$) or precipitates as AgCl (K_{sp} =1.77×10^{-10}, Table 1.1) (Haynes 2014). A recent study showed, that the presence of low Cl^- levels decreased the dissolution kinetics of AgNP through scavenging of Ag^+ and formation of a AgCl passivation layer, whereas high Cl^- concentrations increased the dissolution and led to the formation of Cl^- complexes. Furthermore, the toxicity of Ag decreased when AgCl precipitated and increased at levels were Cl^- complexes formed (Levard et al. 2013b).

Sulfide, a soft base, forms complexes and solid minerals with type-B metal cations such as Ag^+ (Stumm and Morgan 1981). The reaction of a metal, alloy or mineral (*e.g.* Ag, CuO) with sulfur (most importantly sulfide) and its incorporation to form a sulfidic compound (such as metal sulfides (Ag_2S, CuS)) is called sulfidation. Silver sulfide (Ag_2S) has a K_{spa} of 6×10^{-30} M^{-3} (Table 1.1), thus, in the presence of sulfide Ag^+ concentrations are particularly low (Figure 1.2 right) (Haynes 2014). In anoxic waters, especially in wastewater, the existence of sulfate reducing bacteria lead to elevated concentrations of bisulfide (up to 0.44 mM, HS^-) and other sulfide species (*e.g.* metal sulfides and polysulfides (HS_n^-)) (Gramp et al. 2007, Gramp et al. 2006, Hao et al. 1996, Kamyshny et al. 2008, Nielsen et al. 1998).

For the sulfidation of AgNP with HS^- the presence of an oxidant (*e.g.* O_2 or H_2O_2) to oxidize the metallic Ag is required (Levard et al. 2011, Liu et al. 2011). However, HS^- is also oxidized with oxygen ($k_{pH=7.2,\ abiotic}$ = ~0.6 µM min^{-1}, biotic oxidation up to 34.6 µM min^{-1}, Table 1.1), hence, the sulfidation with HS^- in the presence of O_2 is only possible for a limited time (Chen and Morris 1972, Luther et al. 2011). The sulfidation kinetics of AgNP have been assessed assuming an adapted pseudo-first-order kinetic model, based on the observed decline of HS^- concentrations. Half-life times of AgNP in wastewater were estimated to be between 10 min and 1.5 days. Furthermore, the sulfidation was considered to progress via some kind of solid-fluid reaction pathways. However, the sulfidation mechanism and the influence of AgNP size and NOM remained unclear (Liu et al. 2011).

Besides HS^- other sulfidic compounds such as metal sulfides could serve as a sulfide source for the sulfidation of AgNP. In presence of other chalcophile metals like Cu or Zn, HS^- precipitates as CuS and ZnS. Metal sulfides are more resistant toward oxidation than HS^-, with half-life times of days to weeks (k < 10^{-4} min^{-1}). They have been found in oxic surface waters, mostly in urban areas and close to WWTP, hence, they could serve as a sulfide source in the absence of HS^- (Priadi et al. 2012, Rozan et al. 2000).

Ag_2S may persist under oxic conditions for an extended period of time, albeit, it is not in its thermodynamic equilibrium under such conditions (Levard et al. 2011). Additionally, already partial sulfidation of AgNP was shown to reduce the toxic-

ity by several orders of magnitude (Levard et al. 2013a). Therefore, sulfidation can significantly influence the environmental risk assessment of AgNP and is currently considered as of great interest (Peijnenburg et al. 2015).

1.5 Modelling of Transformations

The measured change of the AgNP speciation over time can then further be described by a kinetic model. Applying a model to the experimental data can be useful to make predictions about the speciation of AgNP in the environment. Models for nanoparticle transformations can range from mechanistic to empirical type, which then further can have varying complexity. Empirical models can have any mathematical form which is optimized to a given dataset. Mechanistic models on the other hand are based on physical or chemical processes. However, in reality many applied models are in-between the two types. To date many environmental transformation rates of nanoparticles are based on pseudo first-order kinetics:

$$c = c_0 \times e^{-kt} \qquad \text{Eq. 1.1}$$

where t is the time, k is the rate coefficient, c_0 is the initial concentration of reactant and c is the concentration at time t. The rate of the reaction is limited by a chemical reaction step (*e.g.* oxygen transfer). The model is only dependent on the decline of one reactant (c) which can also be a valid simplification if the other reactants are in excess. The rate coefficient k has the unit per time and can be empirically expanded to include further parameters which influence the rate such as the particle size (Zhang et al. 2011).

However, these classical solution chemistry based kinetic models (*e.g.* first- and second-order kinetics) have their limitations with respect to reacting solids. Solid-state reactions are often not chemically but physically limited due to mass transport / diffusion, hence, other models have to be used. One of these kinetic models is the parabolic rate law (Eq. 1.2), which is especially suitable for diffusion controlled corrosion reactions.

$$l^2 = k \times t \qquad \text{Eq. 1.2}$$

The diffusion length l squared is linearly increasing with time t multiplied by the rate coefficient k. The reaction slows down with increasing thickness of the diffusion layer. The rate coefficient has the unit of the distance in square per time. The parabolic rate law for solid-state kinetics has first been proposed by Jander (1927) and since then has successfully been applied to corrosion reactions. The model has been further improved to account for many factors influencing the corrosion process and, furthermore, was modified to also describe thin film oxidation reactions

in the nanometer range (Anderson and Tracy 2014, Cabrera and Mott 1949). However, so far the parabolic rate law has not yet been used to describe environmental transformations of nanoparticles.

The model with its parameter describing the transformation kinetics can then further be applied to predict the transformation of AgNP in larger scale models such as wastewater treatment or environmental fate models. These models combine a wide variety of processes such as transport, agglomeration and transformations (Barton et al. 2015, Praetorius et al. 2012).

1.6 Urban Wastewater and Water System

Mass-flow studies have shown that one of the main pathways of AgNP reaching the environment is through the urban wastewater system (Blaser et al. 2008, Gottschalk et al. 2009, Sun et al. 2014). Hence, it is important to understand the fate of nano-Ag in the urban wastewater system, which roughly consists of a sewer and some type of wastewater treatment plant (WWTP). The system has both oxic and anoxic parts where the environmental conditions change from oxidizing to reducing. Thus, the conditions are ideal for the sulfidation of AgNP and other Ag species (*e.g.* Ag^+, AgCl) released to the wastewater. In the sewer, the AgNP are efficiently transported with the wastewater and there is no substantial loss due to sorption of AgNP to the biofilm or sewer walls. Moreover, the sulfidation of the AgNP already starts in the sewer system (Kaegi et al. 2013, Kaegi et al. 2015) and reaches complete or near-complete sulfidation during the wastewater treatment (Doolette et al. 2013, Kaegi et al. 2011). In the WWTP about 95 % of the AgNP are removed from the water to the surplus sludge. Several studies have shown that the removal efficiency corresponds to the percentage of total suspended solids (TSS) removed by the plant (Doolette et al. 2013, Hendren et al. 2013, Kaegi et al. 2011, Shafer et al. 1998). Therefore, the AgNP are efficiently attached to the wastewater flocks and removed by sedimentation. The surplus sludge is treated under anaerobic conditions to harvest energy (production of methane), before the sludge is incinerated or applied in agriculture as fertilizer. A possible remaining fraction of metallic AgNP from the wastewater treatment is completely sulfidized during the anaerobic digestion (Lombi et al. 2013). One study found nanosized Ag_2S particles in the final sludge of a full scale WWTP most likely originating from either soluble Ag or AgNP species (Kim et al. 2010).

Approximately 5 % of dominantly sulfidized AgNP pass the WWTP together with many organic micropollutants and reach the surface waters which may have negative impacts on the aquatic environment of receiving waters. Ozonation and powdered activated carbon filtration of WWTP effluent are two suggested processes to mitigate the ecological impact of organic micropollutants (Joss et al. 2008). In Switzerland a decision has been taken to upgrade about 100 WWTP with an ad-

ditional treatment stage (ozone or powdered activated carbon) and similar discussions are also ongoing in other countries (*e.g.* Germany) (Eggen et al. 2014). Besides the beneficial removal of organic micropollutants, ozone can also affect inorganic materials (such as Ag_2S) that are sensitive to oxidation (von Sonntag and von Gunten 2012). However, there is yet no knowledge about the behavior of suspended inorganic matter during the ozone treatment of WWTP effluent.

1.7 Scope and Layout of the Thesis

Transformations of AgNP in the aquatic environment can cause significant changes in toxicity. Therefore, it is crucial to understand environmental transformations to assess any possible ecotoxicological risk that may occur associated with the release of AgNP to the environment. Currently there is a lack of information on the transformation mechanisms and kinetics of AgNP in the urban urban wastewater and water system. Within all possible transformations, sulfidation is a key process which alters the behavior of the AgNP and significantly lowers the toxicity. Sulfidation was shown to take place in the urban wastewater system, which also is the primary target of AgNP released from consumer products. The first aim of this thesis was, thus, to systematically investigate the sulfidation of AgNP under environmental conditions and to determine the reaction rates. To reduce the possibility of side reactions interfering with the sulfidation kinetics and due to analytical limitations, experiments were conducted in clean laboratory systems.

The introduction of new technologies to process wastewater such as ozonation of WWTP effluent has the potential to further change the speciation of Ag and may have negative side effects on the effluent water quality. Therefore, the second aim of this thesis was to study the impact of ozonation of WWTP effluent on the sulfidized AgNP. The following topics were investigated in detail:

Effect of Humic Acid on the Kinetics of Silver Nanoparticle Sulfidation (Chapter 2)

Bisulfide (HS^-) is the most readily available sulfide species for the sulfidation of AgNP and especially in the urban wastewater system it is present in excess to AgNP concentrations. As most of the AgNP are estimated to be released to the urban wastewater, the reaction of AgNP with HS^- is an important environmental transformation pathway. The following research questions were investigated:

- What is the rate of the sulfidation and how is it influenced by HA?
- How can the sulfidation rate of AgNP with HS^- be described by a kinetic model?
- How does the sulfidation of AgNP progress (*e.g.* via core-shell formation)?

The sulfidation kinetics and mechanisms of AgNP with HS^- and the influence of HA was investigated. The kinetics were assessed by X-ray absorption spectroscopy

(XAS) and mechanistic insights were elaborated with the use of analytical transmission electron microscopy (TEM).

Sulfidation Kinetics of Silver Nanoparticle Reacted with Metal Sulfide (Chapter 3)

In oxic waters, especially surface waters, HS^- is absent due to its oxidation with O_2. However, metal sulfides are a more persistent source of sulfides and could be capable of sulfidizing AgNP even in oxic surface waters. The investigated research questions were:

- To which extent can different type of metal sulfides be a sulfide source for the sulfidation of AgNP?
- What is the influence of AgNP size and metal sulfide type on the sulfidation rate?
- What are the implications for the urban surface waters?

The sulfidation kinetics of AgNP with CuS and ZnS were established with respect to AgNP size and metal sulfide type and concentration. Furthermore, implications for the surface waters were estimated.

Effect of Ozone Treatment on Nano-Sized Silver Sulfide in Wastewater Effluent (Chapter 4)

In Switzerland approximately 100 WWTP will be upgraded with an additional treatment step to mitigate the release of micropollutants to the receiving waters. One of the possible treatment methods is the ozonation of effluent water. However, the WWTP effluent may also contain up to 5 % of the total load of AgNP. Based on the literature these AgNP will most likely be sulfidized to nano-Ag_2S before they reach the ozone treatment. Ozone is a strong oxidant and it is likely to oxidize nano-Ag_2S. Thus, the investigated research questions were:

- Is nano-Ag_2S oxidized by ozone and what is the ozone consumption per Ag_2S?
- How fast is the overall reaction rate and is it likely to occur during the ozonation of effluent water?
- How does the ozonation influence the short-term toxicity of the Ag?

The ozone demand of the sulfide oxidation was determined and the reaction kinetics were established. The formation of new Ag species and the reactivity of nano-Ag_2S was tested in real WWTP effluent and assessed by XAS and analytical TEM. Furthermore, the change of short-term toxicity was assessed using the green algae *Chlamydomonas reinhardtii*.

Chapter 5 presents the conclusions of the thesis and an outlook including open research questions in this field are provided.

References

Akaighe, N., Maccuspie, R.I., Navarro, D.A., Aga, D.S., Banerjee, S., Sohn, M. and Sharma, V.K. (2011) Humic acid-induced silver nanoparticle formation under environmentally relevant conditions. Environ Sci Technol 45(9), 3895-3901.

Anderson, B.D. and Tracy, J.B. (2014) Nanoparticle conversion chemistry: Kirkendall effect, galvanic exchange, and anion exchange. Nanoscale 6(21), 12195-12216.

Asharani, P.V., Lian Wu, Y., Gong, Z. and Valiyaveettil, S. (2008) Toxicity of silver nanoparticles in zebrafish models. Nanotechnology 19(25), 255102.

Barton, L.E., Auffan, M., Durenkamp, M., McGrath, S., Bottero, J.-Y. and Wiesner, M.R. (2015) Monte Carlo simulations of the transformation and removal of Ag, TiO2, and ZnO nanoparticles in wastewater treatment and land application of biosolids. SciTotal Environ 511, 535-543.

Blaser, S.A., Scheringer, M., MacLeod, M. and Hungerbühler, K. (2008) Estimation of cumulative aquatic exposure and risk due to silver: Contribution of nano-functionalized plastics and textiles. Sci Total Environ 390(2–3), 396-409.

Cabrera, N. and Mott, N.F. (1949) Theory of the oxidation of metals. Prog Phys 12(1), 163.

Chen, H., Roco, M., Son, J., Jiang, S., Larson, C. and Gao, Q. (2013) Global nanotechnology development from 1991 to 2012: patents, scientific publications, and effect of NSF funding. Journal of Nanoparticle Research 15(9), 1-21.

Chen, K.Y. and Morris, J.C. (1972) Kinetics of oxidation of aqueous sulfide by oxygen. Environ Sci Technol 6(6), 529-537.

Choi, O. and Hu, Z. (2008) Size dependent and reactive oxygen species related nanosilver toxicity to nitrifying bacteria. Environ Sci Technol 42(12), 4583-4588.

Dobias, J. and Bernier-Latmani, R. (2013) Silver Release from Silver Nanoparticles in Natural Waters. Environ Sci Technol 47(9), 4140-4146.

Doolette, C., McLaughlin, M., Kirby, J., Batstone, D., Harris, H., Ge, H. and Cornelis, G. (2013) Transformation of PVP coated silver nanoparticles in a simulated wastewater treatment process and the effect on microbial communities. Chemistry Central Journal 7(1), 1-18.

Eggen, R.I.L., Hollender, J., Joss, A., Schärer, M. and Stamm, C. (2014) Reducing the Discharge of Micropollutants in the Aquatic Environment: The Benefits of Upgrading Wastewater Treatment Plants. Environ Sci Technol 48(14), 7683-7689.

Fabrega, J., Fawcett, S.R., Renshaw, J.C. and Lead, J.R. (2009) Silver nanoparticle impact on bacterial growth: effect of pH, concentration, and organic matter. Environ Sci Technol 43(19), 7285-7290.

Freestone, I., Meeks, N., Sax, M. and Higgitt, C. (2007) The Lycurgus Cup - A Roman nanotechnology. Gold Bulletin 40(4), 270-277.

Gao, J., Powers, K., Wang, Y., Zhou, H., Roberts, S.M., Moudgil, B.M., Koopman, B. and Barber, D.S. (2012) Influence of Suwannee River humic acid on particle properties and toxicity of silver nanoparticles. Chemosphere 89(1), 96-101.

Gottschalk, F., Sonderer, T., Scholz, R.W. and Nowack, B. (2009) Modeled environmental concentrations of engineered nanomaterials (TiO(2), ZnO, Ag, CNT, Fullerenes) for different regions. Environ Sci Technol 43(24), 9216-9222.

Gramp, J.P., Bigham, J.M., Sasaki, K. and Tuovinen, O.H. (2007) Formation of Ni- and Zn-sulfides in cultures of sulfate-reducing bacteria. Geomicrobiology Journal 24(7-8), 609-614.

Gramp, J.P., Sasaki, K., Bigham, J.M., Karnachuk, O.V. and Tuovinen, O.H. (2006) Formation of covellite (CuS) under biological sulfate-reducing conditions. Geomicrobiology Journal 23(8), 613-619.

Gunsolus, I.L., Mousavi, M.P.S., Hussein, K., Bühlmann, P. and Haynes, C.L. (2015) Effects of Humic and Fulvic Acids on Silver Nanoparticle Stability, Dissolution, and Toxicity. Environ Sci Technol.

Hao, O.J., Chen, J.M., Huang, L. and Buglass, R.L. (1996) Sulfate-reducing bacteria. Critical Reviews in Environmental Science and Technology 26(2), 155-187.

Haynes, W.M. (2014) CRC Handbook of Chemistry and Physics, CRC Press, Boca Raton, Fla.

Hendren, C.O., Badireddy, A.R., Casman, E. and Wiesner, M.R. (2013) Modeling nanomaterial fate in wastewater treatment: Monte Carlo simulation of silver nanoparticles (nano-Ag). Sci Total Environ 449, 418-425.

Ivanova, O.S. and Zamborini, F.P. (2010) Size-dependent electrochemical oxidation of silver nanoparticles. J Am Chem Soc 132(1), 70-72.

Jander, W. (1927) Reaktionen im festen Zustande bei höheren Temperaturen. Reaktionsgeschwindigkeiten endotherm verlaufender Umsetzungen. Zeitschrift für anorganische und allgemeine Chemie 163(1), 1-30.

Joss, A., Siegrist, H. and Ternes, T.A. (2008) Are we about to upgrade wastewater treatment for removing organic micropollutants? Water Science & Technology 57(2), 251-255.

Kaegi, R., Voegelin, A., Ort, C., Sinnet, B., Thalmann, B., Krismer, J., Hagendorfer, H., Elumelu, M. and Mueller, E. (2013) Fate and transformation of silver nanoparticles in urban wastewater systems. Water Res 47(12), 3866-3877.

Kaegi, R., Voegelin, A., Sinnet, B., Zuleeg, S., Hagendorfer, H., Burkhardt, M. and Siegrist, H. (2011) Behavior of metallic silver nanoparticles in a pilot wastewater treatment plant. Environ Sci Technol 45(9), 3902-3908.

Kaegi, R., Voegelin, A., Sinnet, B., Zuleeg, S., Siegrist, H. and Burkhardt, M. (2015) Transformation of AgCl nanoparticles in a sewer system - A field study. Sci Total Environ (0).

Kamyshny, A., Jr., Zilberbrand, M., Ekeltchik, I., Voitsekovski, T., Gun, J. and Lev, O. (2008) Speciation of Polysulfides and Zerovalent Sulfur in Sulfide-rich Water Wells in Southern and Central Israel. Aquatic Geochemistry 14(2), 171-192.

Keller, A., McFerran, S., Lazareva, A. and Suh, S. (2013) Global life cycle releases of engineered nanomaterials. Journal of Nanoparticle Research 15(6), 1-17.

Kim, B., Park, C.-S., Murayama, M. and Hochella, M.F. (2010) Discovery and Characterization of Silver Sulfide Nanoparticles in Final Sewage Sludge Products. Environ Sci Technol 44(19), 7509-7514.

Kim, D., Jeong, S. and Moon, J. (2006) Synthesis of silver nanoparticles using the polyol process and the influence of precursor injection. Nanotechnology 17(16), 4019.

Kittler, S., Greulich, C., Diendorf, J., Koller, M. and Epple, M. (2010) Toxicity of Silver Nanoparticles Increases during Storage Because of Slow Dissolution under Release of Silver Ions. Chemistry of Materials 22(16), 4548-4554.

Levard, C., Hotze, E.M., Colman, B.P., Dale, A.L., Truong, L., Yang, X.Y., Bone, A.J., Brown, G.E., Jr., Tanguay, R.L., Di Giulio, R.T., Bernhardt, E.S., Meyer, J.N., Wiesner, M.R. and Lowry, G.V. (2013a) Sulfidation of silver nanoparticles: natural antidote to their toxicity. Environ Sci Technol 47(23), 13440-13448.

Levard, C., Hotze, E.M., Lowry, G.V. and Brown, G.E., Jr. (2012) Environmental transformations of silver nanoparticles: impact on stability and toxicity. Environ Sci Technol 46(13), 6900-6914.

Levard, C., Mitra, S., Yang, T., Jew, A.D., Badireddy, A.R., Lowry, G.V. and Brown, G.E., Jr. (2013b) Effect of chloride on the dissolution rate of silver nanoparticles and toxicity to E. coli. Environ Sci Technol 47(11), 5738-5745.

Levard, C., Reinsch, B.C., Michel, F.M., Oumahi, C., Lowry, G.V. and Brown, G.E. (2011) Sulfidation processes of PVP-coated silver nanoparticles in aqueous solution: impact on dissolution rate. Environ Sci Technol 45(12), 5260-5266.

Liu, J. and Hurt, R.H. (2010) Ion release kinetics and particle persistence in aqueous nano-silver colloids. Environ Sci Technol 44(6), 2169-2175.

Liu, J., Pennell, K.G. and Hurt, R.H. (2011) Kinetics and mechanisms of nanosilver oxysulfidation. Environ Sci Technol 45(17), 7345-7353.

Lombi, E., Donner, E., Taheri, S., Tavakkoli, E., Jämting, Å.K., McClure, S., Naidu, R., Miller, B.W., Scheckel, K.G. and Vasilev, K. (2013) Transformation of four silver/silver chloride nanoparticles during anaerobic treatment of wastewater and post-processing of sewage sludge. Environmental Pollution 176, 193-197.

Louie, S.M., Tilton, R.D. and Lowry, G.V. (2013) Effects of Molecular Weight Distribution and Chemical Properties of Natural Organic Matter on Gold Nanoparticle Aggregation. Environ Sci Technol 47(9), 4245-4254.

Lowry, G.V., Gregory, K.B., Apte, S.C. and Lead, J.R. (2012) Transformations of Nanomaterials in the Environment. Environ Sci Technol 46(13), 6893-6899.

Lu, W., Senapati, D., Wang, S., Tovmachenko, O., Singh, A.K., Yu, H. and Ray, P.C. (2010) Effect of surface coating on the toxicity of silver nanomaterials on human skin keratinocytes. Chemical Physics Letters 487(1–3), 92-96.

Luther, G.W., 3rd, Findlay, A.J., Macdonald, D.J., Owings, S.M., Hanson, T.E., Beinart, R.A. and Girguis, P.R. (2011) Thermodynamics and kinetics of sulfide oxidation by oxygen: a look at inorganically controlled reactions and biologically mediated processes in the environment. Frontiers in Microbiology 2.

Ma, R., Levard, C., Marinakos, S.M., Cheng, Y., Liu, J., Michel, F.M., Brown, G.E. and Lowry, G.V. (2012) Size-controlled dissolution of organic-coated silver nanoparticles. Environ Sci Technol 46(2), 752-759.

Meyer, J.N., Lord, C.A., Yang, X.Y., Turner, E.A., Badireddy, A.R., Marinakos, S.M., Chilkoti, A., Wiesner, M.R. and Auffan, M. (2010) Intracellular uptake and associated toxicity of silver nanoparticles in Caenorhabditis elegans. Aquatic Toxicology 100(2), 140-150.

Mueller, N.C. and Nowack, B. (2008) Exposure modeling of engineered nanoparticles in the environment. Environ Sci Technol 42(12), 4447-4453.

Navarro, E., Baun, A., Behra, R., Hartmann, N.B., Filser, J., Miao, A.-J., Quigg, A., Santschi, P.H. and Sigg, L. (2008a) Environmental behavior and ecotoxicity of engineered nanoparticles to algae, plants, and fungi. Ecotoxicology 17(5), 372-386.

Navarro, E., Piccapietra, F., Wagner, B., Marconi, F., Kaegi, R., Odzak, N., Sigg, L. and Behra, R. (2008b) Toxicity of Silver Nanoparticles to Chlamydomonas reinhardtii. Environ Sci Technol 42(23), 8959-8964.

Nielsen, P.H., Raunkjær, K. and Hvitved-Jacobsen, T. (1998) Sulfide production and wastewater quality in pressure mains. Water Science and Technology 37(1), 97-104.

Ostermeyer, A.-K., Kostigen Mumuper, C., Semprini, L. and Radniecki, T. (2013) Influence of Bovine Serum Albumin and Alginate on Silver Nanoparticle Dissolution and Toxicity to Nitrosomonas europaea. Environ Sci Technol 47(24), 14403-14410.

Peijnenburg, W.J.G.M., Baalousha, M., Chen, J., Chaudry, Q., Von Der Kammer, F., Kuhlbusch, T.A.J., Lead, J., Nickel, C., Quik, J.T.K., Renker, M., Wang, Z. and Koelmans, A.A. (2015) A review of the properties and processes determining the fate of engineered nanomaterials in the aquatic environment. Critical Reviews in Environmental Science and Technology, 00-00.

Peretyazhko, T., Zhang, Q. and Colvin, V.L. (2014) Size-Controlled Dissolution of Silver Nanoparticles at Neutral and Acidic pH Conditions: Kinetics and Size Changes. Environ Sci Technol.

Praetorius, A., Scheringer, M. and Hungerbühler, K. (2012) Development of Environmental Fate Models for Engineered Nanoparticles—A Case Study of TiO2 Nanoparticles in the Rhine River. Environ Sci Technol 46(12), 6705-6713.

Priadi, C., Le Pape, P., Morin, G., Ayrault, S., Maillot, F., Juillot, F., Hochreutener, R., Llorens, I., Testemale, D., Proux, O. and Brown, G.E. (2012) X-ray Absorption Fine Structure Evidence for Amorphous Zinc Sulfide as a Major Zinc Species in Suspended Matter from the Seine River Downstream of Paris, Ile-de-France, France. Environ Sci Technol 46(7), 3712-3720.

Ratte, H.T. (1999) Bioaccumulation and toxicity of silver compounds: A review. Environmental Toxicology and Chemistry 18(1), 89-108.

Rozan, T.F., Lassman, M.E., Ridge, D.P. and Luther, G.W. (2000) Evidence for iron, copper and zinc complexation as multinuclear sulphide clusters in oxic rivers. Nature 406(6798), 879-882.

Shafer, M.M., Overdier, J.T. and Armstong, D.E. (1998) Removal, partitioning, and fate of silver and other metals in wastewater treatment plants and effluent-receiving streams. Environmental Toxicology and Chemistry 17(4), 630-641.

Sondi, I. and Salopek-Sondi, B. (2004) Silver nanoparticles as antimicrobial agent: a case study on E-coli as a model for Gram-negative bacteria. Journal of Colloid and Interface Science 275(1), 177-182.

Sotiriou, G.A. and Pratsinis, S.E. (2010) Antibacterial Activity of Nanosilver Ions and Particles. Environ Sci Technol 44(14), 5649-5654.

Stumm, W. and Morgan, J.J. (1981) Aquatic chemistry, Wiley, New-York.

Sun, T.Y., Gottschalk, F., Hungerbühler, K. and Nowack, B. (2014) Comprehensive probabilistic modelling of environmental emissions of engineered nanomaterials. Environmental Pollution 185(0), 69-76.

Usepa (2007) EPA Nanotechnology White Paper, USEPA.

von Sonntag, C. and von Gunten, U. (2012) Chemistry of Ozone in Water and Wastewater Treatment, IWA Publishing.

Yin, L., Cheng, Y., Espinasse, B., Colman, B.P., Auffan, M., Wiesner, M., Rose, J., Liu, J. and Bernhardt, E.S. (2011) More than the ions: the effects of silver nanoparticles on Lolium multiflorum. Environ Sci Technol 45(6), 2360-2367.

Yin, Y., Shen, M., Tan, Z., Yu, S., Liu, J.-f. and Jiang, G. (2015) Particle Coating-dependent Interaction of Molecular Weight Fractionated Natural Organic Matter: Impacts on the Aggregation of Silver Nanoparticles. Environ Sci Technol.

Zhang, W., Yao, Y., Sullivan, N. and Chen, Y. (2011) Modeling the primary size effects of citrate-coated silver nanoparticles on their ion release kinetics. Environ Sci Technol 45(10), 4422-4428.

2. Effect of Humic Acid on the Kinetics of Silver Nanoparticle Sulfidation

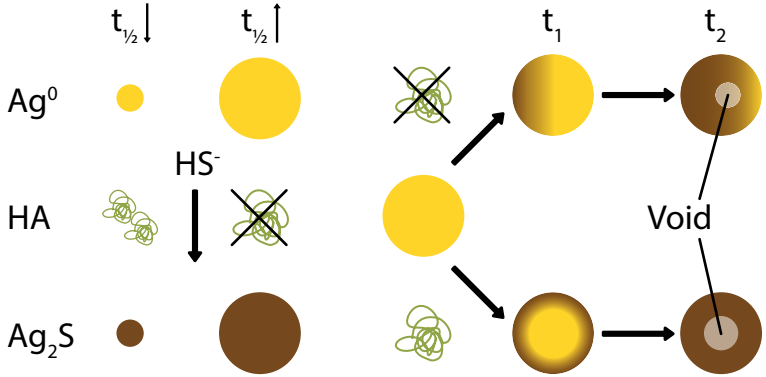

Submitted to Environmental Science: Nano
Basilius Thalmann[a, b, c, d], Andreas Voegelin[d], Eberhard Morgenroth[d] and Ralf Kaegi[a, b, c, d]

[a] Study concept and design; [b] Acquisition, analysis and interpretation of data; [c] Drafting of manuscript; [d] Critical revision

2.1 Abstract

The sulfidation of metallic silver nanoparticles (AgNP) observed in urban wastewater systems and in natural waters reduces their toxicity by several orders of magnitude. However, the reaction rate of this transformation is only poorly understood and the influence of humic acid (HA) on AgNP sulfidation has not been studied to date. We therefore investigate the sulfidation kinetics of AgNP reacted with bisulfide (HS^-) in the absence and presence of HA and evaluate different kinetic models to describe the observed reaction kinetics.

Citrate-stabilized AgNP of different sizes (20 – 200 nm) were reacted with an excess of HS^- in the absence of HA as well as at HA concentrations ranging from 50 to 1000 mg L^{-1}. The extent of AgNP sulfidation after selected reaction times was determined by X-ray absorption spectroscopy (XAS). The overall sulfidation rate increased with decreasing AgNP size and increasing HA concentration. The sulfidation rate of the AgNP was best described by a diffusion-limited solid-state reaction model (parabolic rate law). The corresponding half-life times of the AgNP ranged from minutes to hours. The increase of the sulfidation rate with increasing HA concentration may be explained by the adsorption of HA onto the AgNP surface facilitating the access of HS^- to the particle surface. Results from analytical transmission electron microscopy suggest that the AgNP sulfidized asymmetrically in the absence of HA. In the presence of HA, initially formed concentric core-shell Ag^0-Ag_2S structures developed into hollow Ag_2S nanoparticles with increasing reaction time, possibly via the Kirkendall effect.

2.2 Introduction

Silver nanoparticles (AgNP) are widely applied to consumer products (*e.g.,* textiles and cosmetics) (Woodrow Wilson 2015), with the intention to slowly release antimicrobial active Ag^+ (Ratte 1999, Russell and Hugo 1994). During the use and the washing of such products, AgNP can detach from the host material (Benn et al. 2010, Farkas et al. 2011, Geranio et al. 2009) and may reach the aquatic environment causing environmental concern (Gottschalk et al. 2009). Mass flow analysis revealed, that the largest fraction of AgNP released will be discharged into urban wastewater systems (Sun et al. 2014) and about 5% will pass the wastewater treatment plants and reach surface waters (Kaegi et al. 2011).

Released AgNP will interact with various constituents such as natural organic matter (NOM) present in the aquatic environment. Humic acid (HA), a part of NOM, was shown to increase the colloidal stability of AgNP due to the attachment of HA onto the particles surface (Yin et al. 2015). Additionally, the adsorption of HA onto the AgNP surface can reduce the toxicity of the AgNP (Gunsolus et al. 2015).

The environmentally most important AgNP transformations are the dissolution of AgNP and the formation of Ag_2S, AgCl or Ag complexes with organics. In the presence of HA and light, the formation of smaller AgNP has been reported (Akaighe et al. 2011, Manoharan et al. 2014, Maurer et al. 2012). Dissolution is dependent on the size and the coating of the AgNP in addition to pH and dissolved molecular oxygen (Liu and Hurt 2010, Ma et al. 2012, Peretyazhko et al. 2014, Zhang et al. 2011). In chloride-rich environments, the dissolution of AgNP is followed by the precipitation of AgCl or the formation of soluble chloride complexes (Levard et al. 2013b). In the presence of sulfides, the formation of Ag_2S is dominant due to its low solubility product (Haynes et al. 2014). In sulfidation experiments, HS^- reacting with AgNP decreased faster with decreasing particle diameter and in the presence of HA, but these qualitative observations were not explored in more detail (Liu et al. 2011).

In urban wastewater the sulfidation of AgNP to Ag_2S starts in the sewer system (Brunetti et al. 2015, Kaegi et al. 2013) and continues in the wastewater treatment plant due to elevated HS^- concentrations (Doolette et al. 2013, Impellitteri et al. 2013, Kaegi et al. 2011, Ma et al. 2013, Nielsen et al. 1998). Within typical hydraulic residence times in the urban wastewater system of ~24 h, metallic AgNP get almost completely sulfidized. The sulfidation of AgNP has also been reported in freshwater wetland sediment (Lowry et al. 2012). We recently showed that AgNP sulfidation also occurs in oxic surface waters by reaction with metal sulfides such as ZnS and CuS with lower thermodynamic stability than Ag_2S (Thalmann et al. 2014). The toxicity of very poorly soluble Ag_2S is several orders of magnitude lower than the

toxicity of soluble Ag salts and the oxidation of Ag_2S in oxic waters proceeds rather slowly (Levard et al. 2013b, Navarro et al. 2008, Reinsch et al. 2012, Thalmann et al. 2015). Furthermore, substantial amounts of HA are present in wastewater, as up to 85 mg organic C per g sewage sludge have been reported (Réveillé et al. 2003). Despite the overarching importance of the sulfidation of AgNP and the ubiquitous presence of HA, the dependence of the sulfidation rates on the AgNP size and the HA concentrations is only poorly understood (Kent et al. 2014, Levard et al. 2013a, Levard et al. 2011, Liu et al. 2011, Thalmann et al. 2014).

The objectives of this study were, therefore, to investigate the sulfidation kinetics and mechanism of AgNP reacting with HS^- under oxic conditions and to determine the influence of HA on the sulfidation rates and mechanisms. We investigated the effects of AgNP (nominal) size (20, 40, 100 and 200 nm) and HA concentrations (0, 50, 250, 1000 $mg_{HA}\ L^{-1}$) on the sulfidation rates. The reaction progress was monitored by measuring the Ag speciation at selected reaction times using X-ray absorption spectroscopy (XAS). We evaluated four different kinetic models to best describe the sulfidation kinetics. Further insights into the reaction mechanism were obtained by transmission electron microscopy (TEM) analysis of partially and fully sulfidized AgNP.

2.3 Materials and Methods

Starting Materials

Citrate stabilized AgNP (20, 40, 100 and 200 nm in diameter; Nanocomposix, 1000 mg_{Ag} L^{-1}, BioPure, CA, USA) were used for all experiments. The particles were characterized using transmission electron microscopy (TEM), dynamic light scattering (DLS), phase analysis light scattering (PALS) and UV/Vis spectroscopy. The zeta potential was calculated from the electrophoretic mobility (PALS) using the Smoluchowski approximation. DLS and electrophoretic mobility measurements were performed with a Zetasizer (NanoZS, Malvern Instruments, UK). The plasmon resonance was recorded with a UV/Vis-spectrometer (Cary 100, Varian). The results are given in the supporting information (SI) and are in good agreement with the data provided by the supplier (Figure A.1 and Figure A.2, Table A.1).

For the sulfidation experiments, 56.4 mg of sodium hydrogen sulfide (NaHS, Alfa Aesar) were dissolved in 10 mL deionized water (doubly deionized (DDI) water was used in all experiments; Millipore, 18.2 MΩ cm) to obtain a bisulfide (HS^-) stock solution of ~100 mM. The HS^- concentration (100.4 mM) was determined iodometrically (according to Eaton et al. (2005)). In brief, 1 mL of lugol's solution was mixed with 50 mL of water and 20 µL stock solution followed by the addition of 1 mL of starch solution (10 g L^{-1}). This solution was titrated with thiosulfate (3.26 mM) until it became colorless.

Humic acid (HA, Sigma Aldrich, Lot: #STBD5313V, technical grade) was used as received. A stock solution was produced by dissolving 70 mg HA in 50 mL DDI water. The iron concentration of the HA was 254 $mmol_{Fe}$ Kg_{HA}^{-1} (measured by inductively coupled plasma optical emission spectroscopy (ICP-OES) after acid digestion of 100 µL HA solution with 1 mL of HNO_3 (Ultrapure 60%, Merck, DE) and 100 µL H_2O_2 (30%) in an UltraClave3 (MLS GmbH)).

Methods

AgNP Sulfidation Kinetic Experiments

The kinetics of the reaction of AgNP with HS^- and the influence of HA on the sulfidation rates were studied by mixing 20 µL of AgNP (final concentration: 100 ppm, 0.93 mM) with 175 µL buffer (50 mM, HEPES, pH 7.5) containing variable amounts of HA (0, 50, 250 or 1000 mg_{HA} L^{-1}) in a 500 µL Eppendorf tube. The sulfidation reaction was initiated by adding 5 µL of HS^- stock solution (2.5 mM HS^-). After selected reaction times the suspension was pipetted directly into the XAS sample holder and immediately frozen in liquid nitrogen to quench the reaction. Frozen samples were stored in liquid nitrogen until analyzed at the synchrotron (Table A.2 summary of experiments conducted).

Interaction of HA with AgNP and HS^-

The adsorption of HA to the AgNP was studied by mixing 30 µL AgNP stock solution (20, 40, 100 and 200 nm in diameter) with 270 µL of buffered HA mixture (50 mM HEPES, pH 7.5; 0, 25, 50, 100, 200, 400 or 800 $mg_{HA}\ L^{-1}$) and measuring the hydrodynamic diameter of the particles with DLS using a micro quartz cuvette (Portmann Instruments AG, CH). Additionally, the hydrodynamic diameter was recorded over 45 min for 20-nm AgNP with 0, 50 and 250 $mg_{HA}\ L^{-1}$ in the presence of 2.5 mM HS^-.

The interaction of HA with HS^- was studied by reacting specific amounts of HS^- (1 - 4.5 mM) with a buffered solution (pH = 7.5, 50 mM HEPES) containing 250 $mg_{HA}\ L^{-1}$ in 1.5 mL Eppendorf tubes with minimal head space. An aliquot of 100 µL was used to determine the initial HS^- concentration in every vial. The tubes were closed and sealed with Parafilm and the HA was separated by centrifugation (18`000 g, 60 min, Mikro 220R, Hettich Zentrifugen) at the end of the experiments. Additional experiments were conducted with 250 $mg_{HA}\ L^{-1}$ and 2.3 mM HS^- without centrifugation for the same time period (60 min). The HS^- concentration in the supernatant / bulk solution was determined according to the methylene blue method (4500-S^{2-}), as it is very selective to S^{-2} (Eaton et al. 2005). In brief, 100 µL of sample was mixed with 0.9 mL of DDI water and 0.1 mL of N,N-Dimethylbenzene-1,4-diamine (337.5 mg (Sigma-Aldrich, CH) dissolved in 50 mL 49% H_2SO_4, 50 mM). This solution was reacted with 30 µL of an iron(III) chloride solution (9 M, $FeCl_3$,Sigma-Aldrich, CH) for 4 min, followed by the addition of 0.32 mL of diammonium hydrogen phosphate (3.8 M, $(NH_3)_2HPO_4$, Sigma-Aldrich, CH). The absorption peak maximum at 605 nm of the stoichiometrically formed dye methylene blue was measured with a photo spectrometer and the concentration was calculated using the extinction coefficient of ε = 132000 cm M^{-1} (Cenens and Schoonheydt 1988).

Ag K-Edge X-ray Absorption Spectroscopy (XAS)

XAS was performed at the Ag K-edge (25'514 eV) at the Dutch Belgian Beamline (DUBBLE, BM01B) at the European Synchrotron Radiation Facility (ESRF, Grenoble, France). A closed-cycle He-cryostat adjusted to 80 K (DUBBLE) was used to cool the samples. The reference samples Ag0 (metallic foil) and Ag2S (acanthite) were measured in transmission mode. The frozen samples were measured with a 9-element monolithic Ge fluorescence detector (Canberra, CT, USA).

Athena (Ravel and Newville 2005) was used to process the X-ray absorption near-edge structure (XANES) and extended X-ray absorption fine structure (EXAFS) spectra and to quantify the metallic and the sulfidic fractions by linear combination fitting (LCF). E_0 was set to 25'514 eV and a first-order polynomial fit to the data from 25'414 to 25'454 eV was subtracted from the raw data. A second-order polynomial fit to the data from 25'554 to 25'814 eV was used to normalize the edge-

jump at E_0 to unity and to flatten the spectrum. LCF analysis of the XANES spectra was performed over the energy-range from 25'494 to 25'814 eV, and LCF analysis of the EXAFS spectra over the k-range from 2.5 to 9 $Å^{-1}$. The individual fractions of Ag^0 and Ag_2S were constrained to values between 0 and 1, the sum was not constrained. The fractions of Ag^0 derived from the LCF analysis of the XANES and EXAFS data were averaged and are reported together with the respective standard deviations.

Transmission Electron Microscopy

Pristine, partially and fully sulfidized AgNP were characterized with a scanning transmission electron microscope (STEM, HD-2700-Cs, Hitachi, Japan). Samples for TEM analyses were prepared by either drop-on-grid deposition (Lacey-carbon Cu, Okenshoji Co. LTD, Japan) or direct on-grid centrifugation using carbon-coated copper grids (Quantifoil, DE) (Mavrocordatos et al. 1994). Images were recorded using either a bright field (BF) or a high-angular annular dark field (HAADF) detector. High resolution images were processed using Digital Micrograph (v.1.85, Gatan). Elemental analysis of individual particles was performed using an energy dispersive X-ray detector (EDX) and the spectra were recorded and processed using Digital Micrograph.

2.4 Results and Discussion

Sulfidation Kinetics of AgNP

A multi-factorial design (Table A.2) was used to investigate the sulfidation kinetics of AgNP with HS^- in the presence / absence of HA in oxic water. In time resolved experiments AgNP (20, 40, 100, 200 nm) were reacted with HS^- (2.5 mM, HS^- in fivefold excess compared to Ag) in the presence of HA (0, 50, 250, 1000 $mg_{HA}\ L^{-1}$) for up to 60 min and the reaction progress was monitored by determining the sulfidic and the metallic fraction of the suspension using Ag K-edge XAS. The recorded spectra and the corresponding LCF results for XANES (Figure A.3) and EXAFS (Figure A.4) analysis are given in the supporting information (Appendix A, Table A.3). In all experiments, the metallic fraction steadily decreased with increasing reaction time and the decrease was faster for smaller particles (Figure 2.1, Table A.3). After 15 min reaction (1000 $mg_{HA}\ L^{-1}$) the 20- and 40-nm AgNP were almost completely sulfidized, whereas the 100- and 200-nm were still to 20 and 30 % metallic (Figure 2.1A). An increasing sulfidation rate (faster decrease of the metallic fraction) was observed for increasing HA concentrations at constant particle size (Figure 2.1B). After 15 min reaction time, the metallic fraction of the 20-nm AgNP decreased from 43% (absence of HA) over 27% (50 $mg_{HA}\ L^{-1}$) and 10% (250 $mg_{HA}\ L^{-1}$) and was completed in the presence of 1000 $mg_{HA}\ L^{-1}$.

Four different models were evaluated to describe the sulfidation kinetics of AgNP: (i) A parabolic rate model originally proposed by Jander (1927) (parabolic rate model, Eq. 2.1), which has previously been applied to describe the diffusion-limited solid state reaction of Ag^0 and Sulfur at elevated temperatures (Bartkowicz and Stokłosa 1987, Strafford 1969). (ii) A pseudo first-order rate model which has been used to describe the sulfidation kinetics of AgNP (FO model, Eq. 2.2) (Liu et al. 2011). (iii) A shrinking core model where the reaction progress is limited by diffusion through an outer, reacted (ash) layer (Ash model, Eq. 2.3) (Levenspiel 1999). (iv) A shrinking core model limited by the chemical reaction at the reactive surface of the shrinking core (Chem model, Eq. 2.4) (Levenspiel 1999):

$$F = (1 - \sqrt{\frac{k}{r^2} \times t})^3 \qquad \text{Eq. 2.1}$$

$$F = e^{-k \times t} \qquad \text{Eq. 2.2}$$

$$1 - 3F^{2/3} + 2F = \frac{k}{r^2} \times t \qquad \text{Eq. 2.3}$$

$$1 - F^{1/3} = \frac{k}{r} \times t \qquad \text{Eq. 2.4}$$

F is the metallic Ag fraction (determined by XAS), r is the radius of the AgNP (determined by TEM), k is the rate constant and t is the time. All four models were fitted to the measured data using the non-linear regression package (nls2) for the statistic program R (Team 2012).

Results of two selected time series (40 and 200 nm with 1000 mg_{HA} L^{-1}) are given for each model in Figure 2.2. Qualitatively, the parabolic rate and the FO model fit-

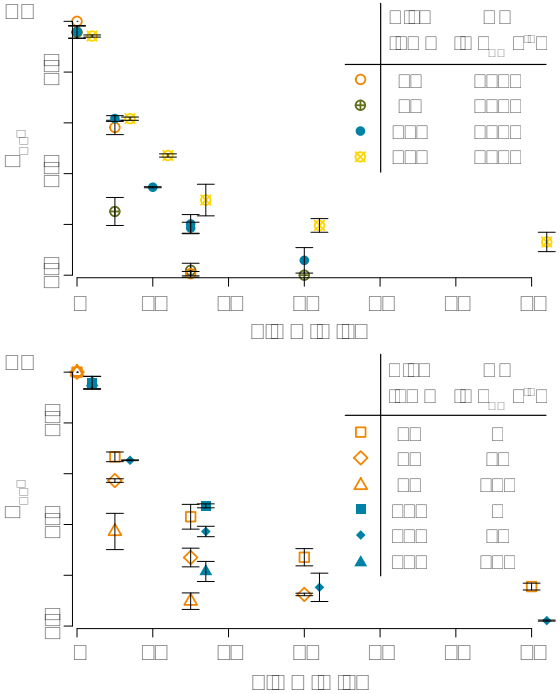

Figure 2.1: Average metallic Ag^0 fraction from LCF (XANES and EXAFS) against time for different experiments (error bars = 1σ, derived from average of XANES and EXAFS Ag^0 fraction, Table A.3). The legend is given as inset. For better readability the data of the 200-nm AgNP have been shifted by plus 2 min. **A:** Different AgNP sizes at 1000 mg_{HA} L^{-1}, **B:** different HA concentrations (0, 50 and 250 mg_{HA} L^{-1}) for experiments with 20 and 100 nm AgNP. For better readability the data of the 100-nm AgNP have been shifted by plus 2 min.

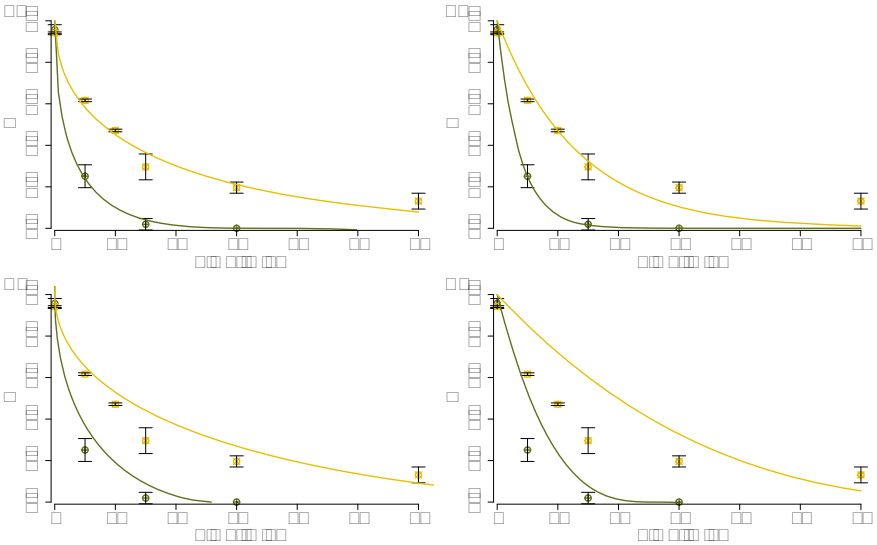

Figure 2.2: Comparison of the four different reaction models (**A**: parabolic rate model (Eq. 2.1), **B**: Pseudo-First-Order model (Eq. 2.2), **C**: Ash model (Eq. 2.3), **D**: Chem model (Eq. 2.4)) for two data series (green: 40-nm AgNP, yellow: 200-nm AgNP; both with 1000 mg_{HA} L^{-1}). Solid lines represent model fits derived from non-linear regressions to the experimental data.

ted the data better than the two other models. When comparing the model fits for the sulfidation of the 200-nm AgNP the parabolic rate model seemed to reproduce the measured data more closely than the FO model. The residual sum of squares (RSS) from each fitted data series was summed to compare the overall fit quality of the individual models. The Chem and Ash model had the highest values (0.70 and 0.44) followed by the FO model (0.19) and the parabolic rate model had the lowest value (0.15) indicating the best fit quality. Thus, qualitative visual inspection and the sum of RSS both suggested that the parabolic rate model was best suited to describe the sulfidation kinetics of AgNP (results of the model with the data is given in Figure A.6 and Table A.4). The experiment conducted with 20-nm AgNP in the presence 1000 mg_{HA} L^{-1} over 5 minutes showed an unusual high metallic fraction, which was considerably higher than that the metallic fraction obtained for the 40 nm AgNP for the same treatment (Figure 2.1A). This high metallic fraction resulted in a substantial discrepancy between the model fit and the measured data for the 20-nm AgNP in the presence of 1000 mg_{HA} L^{-1} (Figure A.6A). As a consequence, a lower sulfidation rate was derived for the 20-nm AgNP compared

to the 40-nm AgNP in the presence of 1000 mg_{HA} L^{-1} (Figure A.6A). However, this apparently lower reaction rate is most probably due to an artifact in the experiment with 20-nm AgNP in the presence of 1000 mg_{HA} L^{-1} over 5 min (*e.g.,* incomplete mixing of the AgNP with HA).

The parabolic rate model implies that the reaction is diffusion-limited and dependent on the diffusion gradient of the diffusing element (given that sufficient HS^- for the complete sulfidation of the AgNP is available). In the following, the rate coefficients derived from the parabolic rate model are evaluated in more detail with respect to the effects of nanoparticles size and HA concentration on sulfidation kinetics and mechanism.

In Figure 2.3 the sulfidation rate coefficients (*k*) derived from the parabolic rate model are plotted against the HA concentration normalized to the total AgNP surface (HA_{norm}, assuming ideal spherical particles). The rate coefficients increased almost linearly with increasing HA_{norm}, except for the rate coefficients of 100-nm AgNP reacted with 0, 50 and 250 mg_{HA} L^{-1}, which had significantly higher *k* values. The *k* values for 100-nm AgNP reacted in the presence of 0 and 250 mg_{HA} L^{-1} were derived from only one time point (15 min) and are thus associated with a considerably higher uncertainty.

Possible explanations for the increasing rate constants with increasing HA_{norm} are (i) the stabilizing effect of HA preventing AgNP agglomeration and (ii) the replacement of citrate coating with HA leading to a larger AgNP surface area available for the sulfidation reaction, due to the presence of HS^- within the HA. The first hypothesis (i) was tested by measuring the hydrodynamic diameter of 20-nm AgNP (0, 50 or 250 mg_{HA} L^{-1}) during the reaction with HS^- over ~45 min (Figure

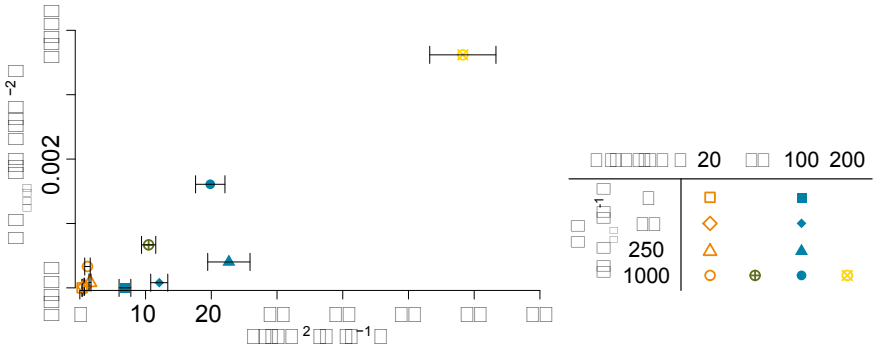

Figure 2.3: HA concentration divided by the total AgNP surface (HA_{norm}) against sulfidation rates (k) derived from the parabolic rate model (k values are given in Table A.4 , error bars = 1σ).

A.7). In the absence of HA, the diameter increased from 32 to 42 nm and sedimentation was observed, indicating that agglomeration of AgNP induced by the sulfidation with HS^- occurred. In presence of HA, however, the diameter only increased by 2-4 nm regardless of the HA concentration. Thus, the stabilizing effect of HA may be responsible for an initial increase of the sulfidation rates (difference between absence and presence of HA), but with increasing HA concentrations no further stabilizing effect was observed. The increased reaction rates can thus not exclusively be explained with the colloidal stabilization of the AgNP by the HA.

To investigate the second hypothesis (ii) – replacement of citrate by HA bringing HS^- in close contact with the AgNP surface – we studied the interaction of HA with AgNP and HA with HS^-.

Interaction of HA with AgNP

The hydrodynamic diameter of the AgNP in the presence of selected amounts of HA was measured by DLS (Table 2.1). The diameter of the 20-nm AgNP slightly decreased with the addition of 25 mg_{HA} L^{-1} HA concentration but then steadily increased with increasing HA concentration to a maximum of 79 nm. The polydispersity index (PDI) followed the same trend with an initial slight decrease from 0.29 to 0.21 followed by a steady increase up to 0.836. However, the highest values might be unreliable due to the very high PDI of up to 0.84 (Table 2.1). Comparable results were obtained for experiments conducted with the 40-nm and the 100-nm AgNP, where the diameter increased to 63 nm and 117.7 nm with a PDI of 0.414 and

Table 2.1: Hydrodynamic Diameter of AgNP (100 ppm) with Different Concentrations of HA at pH 7.5.

AgNP diameter [nm][1] (PDI)[2]	0 mg_{HA} L^{-1}	25 mg_{HA} L^{-1}	50 mg_{HA} L^{-1}	100 mg_{HA} L^{-1}	200 mg_{HA} L^{-1}	400 mg_{HA} L^{-1}	800 mg_{HA} L^{-1}
20	29.3 (0.29)	27.3 (0.21)	27.7 (0.22)	31.1 (0.32)	37.9 (0.40)	55.8 (0.74)	79.1 (0.84)
40	39.4 (0.19)	38.4 (0.19)	39.8 (0.20)	40.3 (0.21)	43.3 (0.24)	49.6 (0.35)	63.3 (0.41)
100	103.7 (0.22)	98.6 (0.15)	96.3 (0.12)	98.2 (0.13)	108.1 (0.16)	116.2 (0.17)	117.7 (0.22)
200	228.8 (0.23)	254.3 (0.25)	233.2 (0.18)	242.4 (0.20)	233.9 (0.18)	213.4 (0.17)	235.8 (0.32)

[1] The data refer to number weighted particle size distributions using the cumulant method.

[2] PDI = Polydispersity Index

0.218 respectively. The hydrodynamic diameter of the 200-nm AgNP did not follow any consistent trend. The relative change in size for the 200-nm AgNP is expected to be even smaller than for the 100-nm AgNP and, therefore, may not be detectable with DLS anymore.

The initial decrease of the PDI indicates that the AgNP were stabilized by HA (and possibly disaggregated to some extent), leading to a more mono-disperse suspension, which also has been previously observed by other researchers (Gunsolus et al. 2015, Louie et al. 2015, Louie et al. 2013). The particle diameter mostly remained within 10% of the original value (determined in the absence of HA) for polydispersity index smaller than 0.3. Higher PDI where mainly observed at high HA concentrations and resulted in larger particle sizes. However, DLS results with a PDI >0.3 are difficult to interpret and are thus excluded from the discussion. Furthermore, additional measurements confirmed, that the particle size remained constant over 60 min, indicating a high colloidal stability of the suspensions. We did not observe a decreasing particle size with time as previously reported (Manoharan et al. 2014). This apparent discrepancy can most likely be explained by the considerably shorter run times in our experiments (1 h) compared to the aforementioned study (24 h).

Although our DLS measurements did not allow us to assess whether citrate was displaced from the surface of the AgNP, it is generally assumed that citrate is only weakly bound to the AgNP surface. The stronger interaction of the AgNP surface with NOM, especially with sulfur and nitrogen groups in the form of thiols and amines, will lead to the displacement of citrate by NOM as suggested by Gunsolus et al. (2015). Furthermore, the high molecular weight fraction extracted from a specific NOM source was shown to have stronger interactions with citrate coated AuNP compared to the lighter weight fraction (Louie et al. 2015, Louie et al. 2013). Thus, we assume that especially the heavy weight fraction of the NOM would displace the citrate from the AgNP surface, which would be in favor of hypothesis (ii). Whether the sorption of HA to the surface could increase the HS^- concentration at the AgNP surface was therefore investigated in additional experiments.

Interaction of HA with HS^-

Different concentrations of HS^- were mixed with 250 mg_{HA} L^{-1}, followed by a centrifugal separation of the HA for 60 min. The HS^- concentration was measured in the supernatant. The HS^- associated with the HA, and thus removed by centrifugation, divided by the total HA concentration (q) was plotted against the free HS^- concentration measured in the supernatant (C, Figure 2.4). A Freundlich sorption isotherm was fitted to the data (Eq. 2.5):

$$q = l \times C^n \qquad \text{Eq. 2.5}$$

The two constants l and n where 0.00404(2) and 0.64(6) respectively (a standard

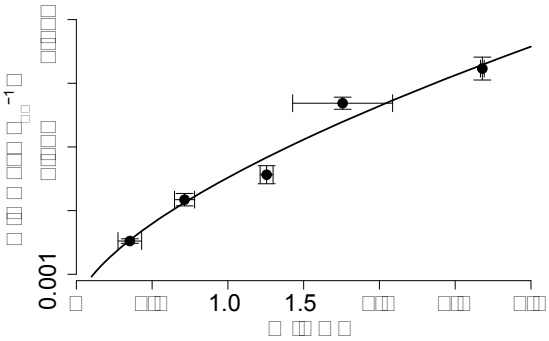

Figure 2.4: Adsorbed HS^- on HA (q) versus HS^- in solution (C) (for both values error bars (1σ), derived from duplicate experiments). Sorption of HS^- on HA follows a Freundlich isotherm (solid line, Eq. 2.5).

error of 1σ is given in brackets referring to the last digit). The sorption capacity of HA for metal cations is in the range of 0.1-0.2 μmol $mgHA^{-1}$ (Kerndorff and Schnitzer 1980), which is substantially lower compared to the observed sorption capacity of up to 7 μmol mg_{HA} for HS^-. These high (apparent) sorption capacities may be explained by an oxidative loss of HS^-, as it was recently shown that HS^- can react with HA to form higher oxidized sulfur species.(Yu et al. 2015) However, the methylene blue method is specific to sulfides (Small and Hintelmann 2007) and in experiments, where the HA was not separated by centrifugation, we did not observe a significant decrease of HS^- over the time period of 60 min, and thus, the oxidative loss of HS^- can be excluded. Alternatively, a fraction of HS^- may have reacted with metals present in the HA and thus, may have precipitated as metal sulfides and removed during the centrifugation. Also this can be excluded, as ICP-OES measurement of the HA revealed only very small amounts of Fe (0.254 μmol_{Fe} mg_{HA}^{-1}), which could only explain a loss of 63.5 μmol of HS^- or 13% of the observed loss after centrifugation. Therefore, we speculate that due to the lower pKa of HA compared to HS^-, the HS^- becomes protonated within the Donnan volume to form H_2S which may be sorbed to non-polar groups of the HA. The replacement of the citrate with HA and the sorption of HS^- to HA may thus bring the sulfide close to the AgNP surface and could explain the increased sulfidation rates observed with increasing HA concentrations.

Microscopic Insights into the Sulfidation Mechanism

To study the mechanism of AgNP sulfidation in more detail, analytical STEM analyses were performed. Samples were collected from partially and fully sulfidized 20 and 100-nm AgNP after specific reaction times (5 and 45 min for 20-nm and 5 and 15 min or 4 h for 100-nm AgNP) in the absence and presence of HA (250 mg_{HA} L^{-1} for 20-nm and 1000 mg_{HA} L^{-1} for 100-nm particles, Figure 2.5, Table A.2).

During sulfidation, the 20-nm AgNP aggregated to form larger colloids, as already suggested by the DLS experiments, but the primary particles preserved their shapes and remained spherical. In the absence of HA and after 5 min, HAADF images of the 20-nm AgNP revealed a bright, spherical area with an adjacent grey sickle-shaped part. EDX analysis revealed that the bright part corresponded to metallic Ag and the grey areas represented Ag_2S (Figure 2.5i, A, B). With increasing reaction time, the Ag_2S increasingly replaced the metallic Ag resulting in mostly light-grey, spherical particles (Figure 2.5iii).

In the presence of 250 mg_{HA} L^{-1} and after 5 min reaction time, the metallic Ag (bright areas) was concentrically surrounded by a grey (Ag_2S) shell, forming core-shell type structures (Figure 2.5ii, high resolution TEM image Figure A.8). After 45 min reaction time, the contrast of the core-shell structures was reversed and a dark core was often surrounded by a light-grey shell. EDX analysis of the core and the shell revealed that both parts consisted of Ag_2S (Figure 2.5iv, C, D).

For the 100-nm AgNP and in the absence of HA, the sulfidation resulted in similar structures as observed for the 20-nm AgNP (Figure 2.5v and vii). However, in the presence of 1000 mg_{HA} L^{-1}, the 100-nm AgNP developed more heterogeneous structures than without HA, with a distinct surface structure, probably representing adsorbed HA (Figure A.9). Furthermore, we observed the reduction of freshly sulfidized AgNP to metallic Ag under the electron beam within a minute (Figure 2.5vi, a time sequence over one minute revealing the formation of metallic Ag under the electron beam is provided in Appendix A, Figure A.10). Well crystalline Ag_2S particles are very stable under the electron beam as demonstrated by lattices fringes in high-resolution images (HR-TEM) (Levard et al. 2011, Thalmann et al. 2015). Therefore, we speculate, that the presence of large amounts of HA (1000 mg L^{-1}) interfered with the formation of well crystalline Ag_2S nano particles and resulted in poorly crystalline Ag_2S which was unstable under the electron beam. For the 100-nm AgNP, larger and in some cases even multiple dark spots were observed within a single particle (Figure 2.5vii an viii).

The dark spots in the center of the sulfidized AgNP observed in Figure 2.5 could therefore be explained by either different elemental compositions (*e.g.,* lighter elements concentrated in the center) or by a reduced thickness (Utsunomiya and Ewing 2003). Elemental analysis of the central dark spots revealed the same elemental distribution as for the rim of the particles. Therefore, the contrast observed on the

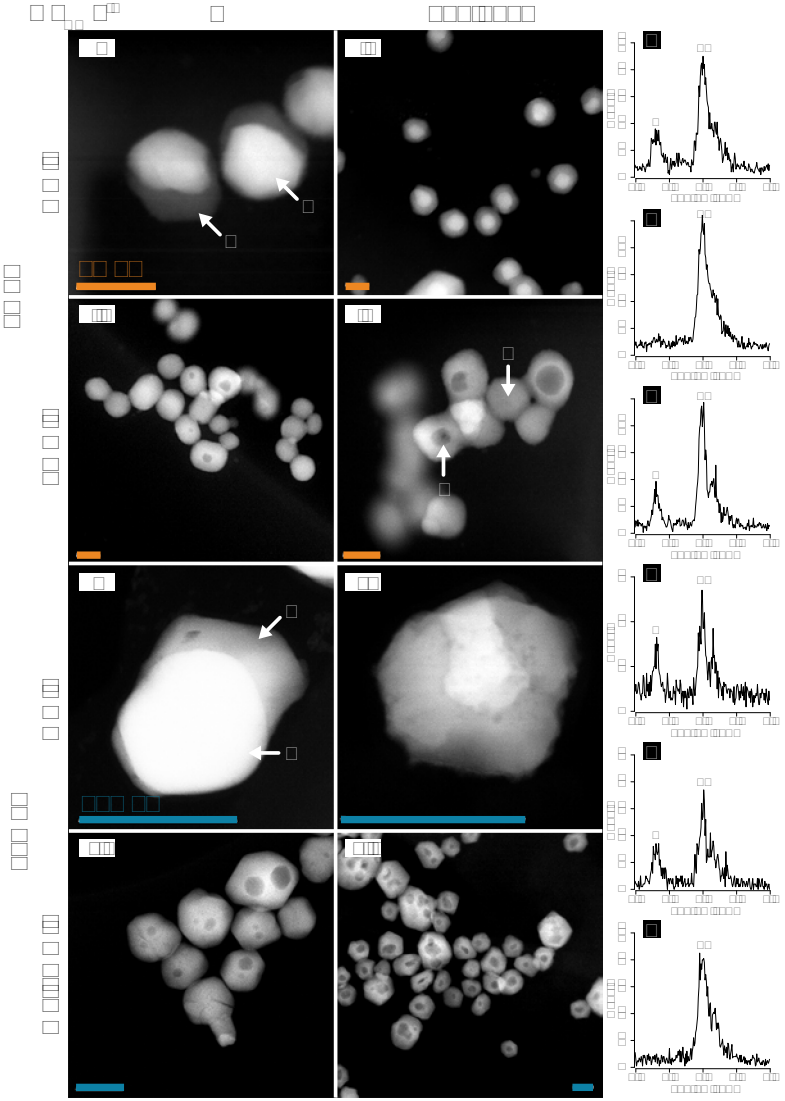

Figure 2.5: HAADF images of partially to fully sulfidized 20- and 100-nm AgNP in the absence and presence of HA (250 or 1000 mg^{HA} L^{-1} for 20 and 100 nm AgNP, respectively) after 5, 15 and 45 min or 4 h (vii: 100 nm and 0 mg^{HA} L^{-1}) reaction time (orange bars are 20 nm (i-iv), blue bars are 100 nm (v-viii)). EDX spectra (right side, A - F) corresponding to specific locations in i, iv, and v are indicated by arrows.

HAADF image can only be explained by a thickness contrast. Additional secondary electron images (SE), probing the topography of the particles revealed that the sulfidized particles remained spherical (Figure A.11). Therefore, the central dark spots observed in the HAADF images can only be explained by a central cavity.

The formation of hollow nanoparticles is well known in material science (Anderson and Tracy 2014, Tang and Ouyang 2007, Wang et al. 2013) and recently has also been described in environmental systems (Weber et al. 2009). The formation of central voids can be explained by different diffusion coefficients of two counter-diffusing species across an interfacial layer, which is compensated by the (inward) diffusion of vacancies. When the concentration of the vacancies that migrated into the center of the particle reaches a certain threshold value, the vacancies collapse into a central cavity. This phenomena is known as Kirkendall-effect (Wang et al. 2013) and has been used to synthesize hollow Ag_2Se nanoparticles in organic solvents (Tang and Ouyang 2007). We observed the formation of Kirkendall voids during the sulfidation of AgNP in oxic water, at room temperature and more prominently in the presence of HA. Furthermore, the 100-nm AgNP also had multiple voids within one particle, most likely due to the polycrystalline nature of larger AgNP. Similar core-shell structures as reported in this study may also have been observed by Impellitteri et al. (2013) (Figure 3A and 4A in their publication) for AgNP that were sulfidized in real wastewater samples, indicating that Kirkendall-like core-shell structures may also form in real wastewater. The occurrence of hollow AgNP may therefore be indicative for the release of (engineered) AgNP into the wastewater.

In the Ag(0) – S(-II) system, presumably a thin layer of Ag_2S initially forms and Ag diffuses faster through the Ag_2S than S, which was previously also reported for bulk Ag(0) with S(0) at elevated temperatures (220° C) (Strafford 1969). These observations are in line with the parabolic rate model which is based on the assumption of diffusion limitation.

Furthermore, TEM analysis revealed, that in the absence of HA the sulfidation of AgNP mostly started from one side of the particle, whereas in the presence of HA the sulfidation resulted in more symmetrical core-shell structures. We hypothesize, that citrate was preventing the even sulfidation of the AgNP and the replacement of citrate with HA increased the reaction rate as an increased area of the particle surface was available for sulfidation, resulting in the observed core-shell structures. This hypothesis is also supported by the formation of larger and central Kirkendall voids that were generally observed in the presence of HA (20-nm AgNP). The 'asymmetrical' sulfidation observed in the absence of HA favors the formation of voids which are either off center or completely lost at the surface of the particles.

Results from the TEM investigations are thus in line with the hypothesis that the replacement of citrate coating with HA increases the AgNP surface area available for the sulfidation. In addition, the adsorption of HS^- within HA brings the HS^- close to the AgNP surface and thus facilitates the sulfidation. The combination of both effects eventually led to increased sulfidation rates with increasing HA_{norm} (Figure 2.3). The diffusion of S and Ag along subgrain boundaries (Thalmann et al. 2014) resulting in the formation of more heterogeneous structures observed for larger, poly-crystalline AgNP additionally increases the complexity of the sulfidation pathways of AgNP.

2.5 Conclusions

The results of this study demonstrate that HA increases the sulfidation rates of AgNP. The half-life time ($t_{1/2}$, were 50 % of the total Ag was transformed to Ag_2S) of AgNP was decreasing from 12 to 1 min with an increase of the HA concentration from 0 and 1000 mg_{HA} L^{-1} for the 20-nm AgNP. Based on the results from the current study, it is likely that the sulfidation of AgNP in the presence of HA is substantially accelerated and completed within one hour or less. The sulfidation of AgNP in the presence of HA initially led to the formation of core (Ag^0) – shell (Ag_2S) particles that transformed into hollow – Ag_2S particles via the Kirkendall effect.

Furthermore, we found that the sulfidation kinetics are best described by a parabolic rate model, which implies that neither the overall Ag nor the HS^- concentration influence the sulfidation rate. Therefore, in the presence of sufficient amounts of HS^- to completely sulfidize all AgNP (which should be the case in urban wastewater systems) (Gottschalk et al. 2010, Nielsen et al. 1998) the half-life time of AgNP can be estimated based on their size and the concentrating of the HA in the respective water. The sulfidation of polycrystalline AgNP (100 nm) resulted in Ag_2S particles that quickly degraded under the electron beam, in contrast to well-crystalline Ag_2S formed in the absence of organics. This might indicate that Ag_2S formed by sulfidation of Ag in the presence of HA is more reactive than Ag_2S formed in the HA-free systems. Further work is required to evaluate this hypothesis and its potential implications for the assessment of the fate and impact of Ag in environmental systems.

Acknowledgements

We acknowledge the Electron Microscopy Centers at ETH Zurich (EMEZ, Zurich, Switzerland) and at Empa (Swiss Federal Institute for Materials Science and Technology, Duebendorf, Switzerland) for providing access to the microscopes. The Swiss Norwegian Beamline at the European Synchrotron Radiation Facility (SNBL, ESRF, Grenoble, France) is acknowledged for the allocation of beamtime. We thank Dipanjan Banerjee for support at the Dutch Belgian Beamline (DUBBLE) at ESRF. This work is part of the project "Behavior of silver nanoparticles in a wastewater treatment plant" within the Swiss National Research Program NRP 64 "Opportunities and Risks of Nanomaterials". Additionally, we would like to thank Brian Sinnet for the support in the laboratories at Eawag.

References

Akaighe, N., Maccuspie, R.I., Navarro, D.A., Aga, D.S., Banerjee, S., Sohn, M. and Sharma, V.K. (2011) Humic acid-induced silver nanoparticle formation under environmentally relevant conditions. Environ Sci Technol 45(9), 3895-3901.

Anderson, B.D. and Tracy, J.B. (2014) Nanoparticle conversion chemistry: Kirkendall effect, galvanic exchange, and anion exchange. Nanoscale 6(21), 12195-12216.

Bartkowicz, I. and Stokłosa, A. (1987) The effect of reactions at the metal/sulfide scale interface on the silver sulfidation kinetics. Solid State Ionics 24(1), 45-49.

Benn, T., Cavanagh, B., Hristovski, K., Posner, J.D. and Westerhoff, P. (2010) The Release of Nanosilver from Consumer Products Used in the Home Supplemental data file available online for this article. J. Environ. Qual. 39(6), 1875-1882.

Brunetti, G., Donner, E., Laera, G., Sekine, R., Scheckel, K.G., Khaksar, M., Vasilev, K., De Mastro, G. and Lombi, E. (2015) Fate of zinc and silver engineered nanoparticles in sewerage networks. Water Research 77(0), 72-84.

Cenens, J. and Schoonheydt, R.A. (1988) Visible spectroscopy of methylene blue on hectorite, laponite B, and barasym in aqueous suspension. Clays and Clay Minerals 36(3), 214-224.

Doolette, C., McLaughlin, M., Kirby, J., Batstone, D., Harris, H., Ge, H. and Cornelis, G. (2013) Transformation of PVP coated silver nanoparticles in a simulated wastewater treatment process and the effect on microbial communities. Chemistry Central Journal 7(1), 1-18.

Eaton, A.D., Franson, M.A.H., Association, A.P.H., Association, A.W.W. and Federation, W.E. (2005) Standard Methods for the Examination of Water & Wastewater, American Public Health Association.

Farkas, J., Peter, H., Christian, P., Gallego Urrea, J.A., Hassellov, M., Tuoriniemi, J., Gustafsson, S., Olsson, E., Hylland, K. and Thomas, K.V. (2011) Characterization of the effluent from a nanosilver producing washing machine. Environ Int 37(6), 1057-1062.

Geranio, L., Heuberger, M. and Nowack, B. (2009) The behavior of silver nanotextiles during washing. Environ Sci Technol 43(21), 8113-8118.

Gottschalk, F., Sonderer, T., Scholz, R.W. and Nowack, B. (2009) Modeled environmental concentrations of engineered nanomaterials (TiO(2), ZnO, Ag, CNT, Fullerenes) for different regions. Environ Sci Technol 43(24), 9216-9222.

Gottschalk, F., Sonderer, T., Scholz, R.W. and Nowack, B. (2010) Possibilities and limitations of modeling environmental exposure to engineered nanomaterials by probabilistic material flow analysis. Environmental Toxicology and Chemistry 29(5), 1036-1048.

Gunsolus, I.L., Mousavi, M.P.S., Hussein, K., Bühlmann, P. and Haynes, C.L. (2015) Effects of Humic and Fulvic Acids on Silver Nanoparticle Stability, Dissolution, and Toxicity. Environ Sci Technol.

Haynes, W.M. (2014) CRC Handbook of Chemistry and Physics, CRC Press, Boca Raton, Fla.

Impellitteri, C.A., Harmon, S., Silva, R.G., Miller, B.W., Scheckel, K.G., Luxton, T.P., Schupp, D. and Panguluri, S. (2013) Transformation of silver nanoparticles in fresh, aged, and incinerated biosolids. Water Research 47(12), 3878-3886.

Jander, W. (1927) Reaktionen im festen Zustande bei höheren Temperaturen. Reaktionsgeschwindigkeiten endotherm verlaufender Umsetzungen. Zeitschrift für anorganische und allgemeine Chemie 163(1), 1-30.

Kaegi, R., Voegelin, A., Ort, C., Sinnet, B., Thalmann, B., Krismer, J., Hagendorfer, H., Elumelu, M. and Mueller, E. (2013) Fate and transformation of silver nanoparticles in urban wastewater systems. Water Res 47(12), 3866-3877.

Kaegi, R., Voegelin, A., Sinnet, B., Zuleeg, S., Hagendorfer, H., Burkhardt, M. and Siegrist, H. (2011) Behavior of metallic silver nanoparticles in a pilot wastewater treatment plant. Environ Sci Technol 45(9), 3902-3908.

Kent, R.D., Oser, J.G. and Vikesland, P.J. (2014) Controlled evaluation of silver nanoparticle sulfidation in a full-scale wastewater treatment plant. Environ Sci Technol 48(15), 8564-8572.

Kerndorff, H. and Schnitzer, M. (1980) Sorption of metals on humic acid. Geochimica et Cosmochimica Acta 44(11), 1701-1708.

Levard, C., Hotze, E.M., Colman, B.P., Dale, A.L., Truong, L., Yang, X.Y., Bone, A.J., Brown, G.E., Jr., Tanguay, R.L., Di Giulio, R.T., Bernhardt, E.S., Meyer, J.N., Wiesner, M.R. and Lowry, G.V. (2013a) Sulfidation of silver nanoparticles: natural antidote to their toxicity. Environ Sci Technol 47(23), 13440-13448.

Levard, C., Mitra, S., Yang, T., Jew, A.D., Badireddy, A.R., Lowry, G.V. and Brown, G.E., Jr. (2013b) Effect of chloride on the dissolution rate of silver nanoparticles and toxicity to E. coli. Environ Sci Technol 47(11), 5738-5745.

Levard, C., Reinsch, B.C., Michel, F.M., Oumahi, C., Lowry, G.V. and Brown, G.E. (2011) Sulfidation processes of PVP-coated silver nanoparticles in aqueous solution: impact on dissolution rate. Environ Sci Technol 45(12), 5260-5266.

Levenspiel, O. (1999) Chemical reaction engineering. Industrial & engineering chemistry research 38(11), 4140-4143.

Liu, J. and Hurt, R.H. (2010) Ion release kinetics and particle persistence in aqueous nano-silver colloids. Environ Sci Technol 44(6), 2169-2175.

Liu, J., Pennell, K.G. and Hurt, R.H. (2011) Kinetics and mechanisms of nanosilver oxysulfidation. Environ Sci Technol 45(17), 7345-7353.

Louie, S.M., Spielman-Sun, E.R., Small, M.J., Tilton, R.D. and Lowry, G.V. (2015) Correlation of the Physicochemical Properties of Natural Organic Matter Samples from Different Sources to Their Effects on Gold Nanoparticle Aggregation in Monovalent Electrolyte. Environ Sci Technol 49(4), 2188-2198.

Louie, S.M., Tilton, R.D. and Lowry, G.V. (2013) Effects of Molecular Weight Distribution and Chemical Properties of Natural Organic Matter on Gold Nanoparticle Aggregation. Environ Sci Technol 47(9), 4245-4254.

Lowry, G.V., Espinasse, B.P., Badireddy, A.R., Richardson, C.J., Reinsch, B.C., Bryant, L.D., Bone, A.J., Deonarine, A., Chae, S., Therezien, M., Colman, B.P., Hsu-Kim, H., Bernhardt, E.S., Matson, C.W. and Wiesner, M.R. (2012) Long-term transformation and fate of manufactured ag nanoparticles in a simulated large scale freshwater emergent wetland. Environ Sci Technol 46(13), 7027-7036.

Ma, R., Levard, C., Judy, J.D., Unrine, J.M., Durenkamp, M., Martin, B., Jefferson, B. and Lowry, G.V. (2013) Fate of zinc oxide and silver nanoparticles in a pilot waste water treatment plant and in processed biosolids. Environ Sci Technol.

Ma, R., Levard, C., Marinakos, S.M., Cheng, Y., Liu, J., Michel, F.M., Brown, G.E. and Lowry, G.V. (2012) Size-controlled dissolution of organic-coated silver nanoparticles. Environ Sci Technol 46(2), 752-759.

Manoharan, V., Ravindran, A. and Anjali, C.H. (2014) Mechanistic Insights into Interaction of Humic Acid with Silver Nanoparticles. Cell Biochemistry and Biophysics 68(1), 127-131.

Maurer, F., Christl, I., Hoffmann, M. and Kretzschmar, R. (2012) Reduction and Reoxidation of Humic Acid: Influence on Speciation of Cadmium and Silver. Environ Sci Technol 46(16), 8808-8816.

Mavrocordatos, D., Lienemann, C.-P. and Perret, D. (1994) Energy filtered transmission electron microscopy for the physico-chemical characterization of aquatic submicron colloids. Microchimica Acta 117(1-2), 39-47.

Navarro, E., Piccapietra, F., Wagner, B., Marconi, F., Kaegi, R., Odzak, N., Sigg, L. and Behra, R. (2008) Toxicity of Silver Nanoparticles to Chlamydomonas reinhardtii. Environ Sci Technol 42(23), 8959-8964.

Nielsen, P.H., Raunkjær, K. and Hvitved-Jacobsen, T. (1998) Sulfide production and wastewater quality in pressure mains. Water Science and Technology 37(1), 97-104.

Peretyazhko, T., Zhang, Q. and Colvin, V.L. (2014) Size-Controlled Dissolution of Silver Nanoparticles at Neutral and Acidic pH Conditions: Kinetics and Size Changes. Environ Sci Technol.

Ratte, H.T. (1999) Bioaccumulation and toxicity of silver compounds: A review. Environmental Toxicology and Chemistry 18(1), 89-108.

Ravel, B. and Newville, M. (2005) ATHENA , ARTEMIS , HEPHAESTUS : data analysis for X-ray absorption spectroscopy using IFEFFIT. Journal of Synchrotron Radiation 12(4), 537-541.

Reinsch, B.C., Levard, C., Li, Z., Ma, R., Wise, A., Gregory, K.B., Brown, G.E., Jr. and Lowry, G.V. (2012) Sulfidation of silver nanoparticles decreases Escherichia coli growth inhibition. Environ Sci Technol 46(13), 6992-7000.

Réveillé, V., Mansuy, L., Jardé, É. and Garnier-Sillam, É. (2003) Characterisation of sewage sludge-derived organic matter: lipids and humic acids. Organic Geochemistry 34(4), 615-627.

Russell, A.D. and Hugo, W.B. (1994) Antimicrobial activity and action of silver. Prog Med Chem 31, 351-370.

Small, J. and Hintelmann, H. (2007) Methylene blue derivatization then LC–MS analysis for measurement of trace levels of sulfide in aquatic samples. Analytical and Bioanalytical Chemistry 387(8), 2881-2886.

Strafford, K.N. (1969) The sulphidation of metals and alloys. Metallurgical Reviews 14(1), 153-174.

Sun, T.Y., Gottschalk, F., Hungerbühler, K. and Nowack, B. (2014) Comprehensive probabilistic modelling of environmental emissions of engineered nanomaterials. Environmental Pollution 185(0), 69-76.

Tang, Y. and Ouyang, M. (2007) Tailoring properties and functionalities of metal nanoparticles through crystallinity engineering. Nat Mater 6(10), 754-759.

Team, R.C. (2012) R: A Language and Environment for Statistical Computing, R Foundation for Statictical Computing.

Thalmann, B., Voegelin, A., Sinnet, B., Morgenroth, E. and Kaegi, R. (2014) Sulfidation kinetics of silver nanoparticles reacted with metal sulfides. Environ Sci Technol 48(9), 4885-4892.

Thalmann, B., Voegelin, A., von Gunten, U., Behra, R., Morgenroth, E. and Kaegi, R. (2015) Effect of Ozone Treatment on Nano-Sized Silver Sulfide in Wastewater Effluent. Environ Sci Technol 49(18), 10911-10919.

Utsunomiya, S. and Ewing, R.C. (2003) Application of High-Angle Annular Dark Field Scanning Transmission Electron Microscopy, Scanning Transmission Electron Microscopy-Energy Dispersive X-ray Spectrometry, and Energy-Filtered Transmission Electron Microscopy to the Characterization of Nanoparticles in the Environment. Environ Sci Technol 37(4), 786-791.

Wang, W., Dahl, M. and Yin, Y. (2013) Hollow Nanocrystals through the Nanoscale Kirkendall Effect. Chemistry of Materials 25(8), 1179-1189.

Weber, F.-A., Voegelin, A., Kaegi, R. and Kretzschmar, R. (2009) Contaminant mobilization by metallic copper and metal sulphide colloids in flooded soil. Nature Geosci 2(4), 267-271.

Woodrow Wilson, I. (2015) Nanotechnology Consumer Products, Informa Healthcare.

Yin, Y., Shen, M., Tan, Z., Yu, S., Liu, J.-f. and Jiang, G. (2015) Particle Coating-dependent Interaction of Molecular Weight Fractionated Natural Organic Matter: Impacts on the Aggregation of Silver Nanoparticles. Environ Sci Technol.

Yu, Z.-G., Peiffer, S., Göttlicher, J. and Knorr, K.-H. (2015) Electron Transfer Budgets and Kinetics of Abiotic Oxidation and Incorporation of Aqueous Sulfide by Dissolved Organic Matter. Environ Sci Technol 49(9), 5441-5449.

Zhang, W., Yao, Y., Sullivan, N. and Chen, Y. (2011) Modeling the primary size effects of citrate-coated silver nanoparticles on their ion release kinetics. Environ Sci Technol 45(10), 4422-4428.

3. Sulfidation Kinetics of Silver Nanoparticles Reacted with Metal Sulfides

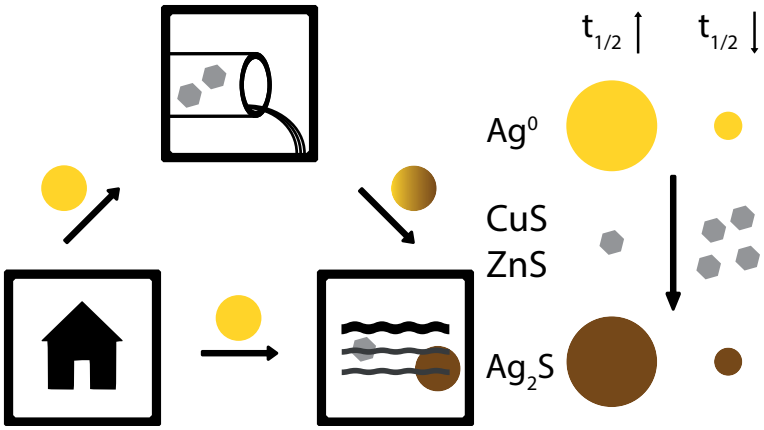

Published in Environmental Science & Technology, (DOI: 10.1021/es5003378)
Basilius Thalmann[a, b, c, d], Andreas Voegelin[d], Brian Sinnet[b], Eberhard Morgenroth[d] and Ralf Kaegi[a, b, c, d]

[a] Study concept and design; [b] Acquisition, analysis and interpretation of data; [c] Drafting of manuscript; [d] Critical revision

3.1 Abstract

Recent studies have documented that the sulfidation of silver nanoparticles (AgNP), possibly released to the environment from consumer products, occurs in anoxic zones of urban wastewater systems and that sulfidized AgNP exhibit dramatically reduced toxic effects. However, whether AgNP sulfidation also occurs under oxic conditions in the absence of bisulfide has not been addressed, yet. In this study we, therefore, investigated whether metal sulfides that are more resistant towards oxidation than free sulfide, could enable the sulfidation of AgNP under oxic conditions.

We reacted citrate-stabilized AgNP of different sizes (10 – 100 nm) with freshly precipitated and crystalline CuS and ZnS in oxygenated aqueous suspensions at pH 7.5. The extent of AgNP sulfidation was derived from the increase in dissolved Cu^{2+} or Zn^{2+} over time and linked with results from X-ray absorption spectroscopy (XAS) analysis of selected samples. The sulfidation of AgNP followed pseudo first-order kinetics, with rate coefficients increasing with decreasing AgNP diameter and increasing metal sulfide concentration and depending on the type (CuS and ZnS) and crystallinity of the reacting metal sulfide. Results from analytical electron microscopy revealed the formation of complex core-shell like sulfidation patterns that seemed to follow preexisting subgrain boundaries in the pristine AgNP. The kinetics of AgNP sulfidation observed in this study in combination with reported ZnS and CuS concentrations and predicted AgNP concentrations in wastewater and urban surface waters indicate that even under oxic conditions and in the absence of free sulfide, AgNP can be transformed into Ag_2S within a few hours to days by reaction with metal sulfides.

3.2 Introduction

Silver nanoparticles (AgNP) are widely used in consumer products (Woodrow Wilson 2015) due to the antimicrobial activity of dissolved Ag^+ (Ratte 1999, Russell and Hugo 1994). AgNP incorporated in textiles and cosmetics will be released during the use or the washing process (Benn et al. 2010, Benn and Westerhoff 2008, Farkas et al. 2011, Geranio et al. 2009) and thus may reach the aquatic environment. Therefore, AgNP are considered as engineered nanomaterials of high environmental concern (Gottschalk et al. 2009).

In the aquatic environment, AgNP are not stable under most conditions but will dissolve or transform into other species, most importantly AgCl and Ag_2S or complexes with dissolved organic matter. AgNP in surface waters are subject to oxidative dissolution (Dobias and Bernier-Latmani 2013). The kinetics of oxidative dissolution depends mainly on dissolved molecular oxygen, pH and natural organic matter (Kittler et al. 2010, Liu and Hurt 2010, Ma et al. 2012, Zhang et al. 2011). In the presence of high levels of chloride, AgNP dissolution is followed by the precipitation of AgCl(s) or the formation of soluble chloride complexes (Levard et al. 2013). However, under anoxic conditions (no O_2 present) in the presence of sulfides, Ag_2S is thermodynamically favored over AgCl and under oxic conditions, only minor fractions of Ag_2S dissolved over periods of months (Levard et al. 2011, Lombi et al. 2013). In urban wastewater systems, sulfidation of AgNP already starts during their transport in the sewer system (Kaegi et al. 2013) and will further proceed during wastewater treatment (Doolette et al. 2013, Impellitteri et al. 2013, Kaegi et al. 2011, Ma et al. 2013a).

The sulfidation of AgNP either proceeds via oxidative dissolution of Ag^0 to Ag^+ followed by precipitation of Ag_2S particles or as a direct heterogeneous transformation process at the AgNP surface (Liu et al. 2011). At elevated sulfide concentrations the direct heterogeneous sulfidation of AgNP is preferred and only minor amounts of new Ag_2S particles were formed in solution (Levard et al. 2011). Although Ag_2S may not be in thermodynamic equilibrium (for example after being discharged in surface waters (oxic and no free sulfide)), it may still persist for an extended amount of time, due to the very slow oxidation of Ag_2S in oxic environments. Therefore, the speciation of AgNP in surface waters may be governed by the reaction kinetics rather than by the thermodynamic equilibrium. The sulfidation of AgNP greatly decreases the release of $Ag^+_{(aq)}$ due to the limited solubility of Ag_2S which resulted in a substantially reduced growth inhibition of *Escherichia coli* (Reinsch et al. 2012). Transformation processes and especially sulfidation thus critically affect the toxicity of AgNP and need to be taken into account when assessing the environmental risk associated with the use and release of AgNP.

In anoxic zones of sewer systems and in wastewater treatment plants, sulfate-reducing bacteria drive the formation of sulfides (S(-II), dominantly bisulfide (HS^-) at pH values > 7) (Nielsen et al. 2008, Pomeroy and Bowlus 1946). Under oxic conditions, dissolved sulfide is not stable and is readily oxidized either abiotically or biotically (Luther et al. 2011). However, considerable levels of dissolved Cu and Zn in the wastewater (Page 1974, Stover et al. 1976) may efficiently scavenge dissolved sulfide by the formation of metal sulfides which can stabilize the S(-II) towards oxidation with dissolved O_2 (Sukola et al. 2005). Metal sulfides may thus serve as a pool of sulfide in oxic zones of urban wastewater systems or in surface waters that may be available for the reaction with Ag (Priadi et al. 2012, Rozan et al. 1999).

The objectives of this study were therefore to investigate the extent to which different metal sulfides can serve as a source of sulfide for the sulfidation of AgNP under oxic conditions and to assess the kinetics of the respective sulfidation reactions. We specifically addressed the effects of AgNP size (10, 20, 40, 70 or 100 nm), metal sulfide type (CuS or ZnS) and crystallinity on the sulfidation kinetics. For that purpose, we reacted AgNP with CuS or ZnS, monitored the release of Cu^{2+} or Zn^{2+} as a proxy for the metal sulfide reaction with AgNP, and quantified and characterized the sulfidized AgNP using X-ray absorption spectroscopy (XAS) and transmission electron microscopy (TEM).

3.3 Materials and Methods

Materials

All experiments were performed with commercially available, citrate stabilized AgNP (20 mg/L, Nanocomposix, CA, USA). The particles were characterized using TEM, dynamic light scattering (DLS) and UV-Vis spectroscopy. For DLS and electrophoretic mobility measurements, a Zetasizer (NanoZS, Malvern Instruments, UK) was used. The zeta potential was calculated from the electrophoretic mobility using the Smoluchowski approximation. Before DLS measurements, particle suspensions (10, 20 nm undiluted, 40 – 100 nm 1:5 diluted with buffer) were sonicated for 10 minutes in a sonication bath (38 W L^{-1}, Bioblock Scientific, CH). The plasmon resonance was recorded with a UV-Vis detector (Cary 1E, Varian, CH). The data are in close agreement with the information provided by the manufacturer (Table 3.1, Figure B.1).

Crystalline metal sulfides (MS_{cryst}) were bought from Alfa Aesar (CuS, 1317-40-4; ZnS, 1314-98-3; Ag_2S, 21548-73-2; >99.8%, MA, USA) and ground before use. Freshly precipitated metal sulfides (MS_{ppt}) were synthesized immediately before use by reacting 60 mM of dissolved zinc acetate or copper nitrate (>99%, Fluka, CH) in 50 mL of deionized water (doubly deionized (DDI) water was used in all experiments, Millipore, 18.2 MΩ cm) with 55 mM bisulfide. For that purpose, the respective amounts of Na_2S were added to the Cu- or Zn-containing solutions which were then vigorously shaken until the Na_2S crystals were completely dissolved. The precipitating metal sulfides were immediately separated by centrifugation (4300 rpm, 2400 g, 10 min, Megafuge 1.0, Heraeus AG, DE), washed with 50 mL water, centrifuged again, dried overnight at 40°C (FD53, Binder, CH) and ground to a fine powder using an agate mortar. The size of the metal sulfides (aggregates) was measured with DLS, after dispersing 1 mg in 10 mL of buffer and following the same sonication procedure as the AgNP suspensions (Table 3.1). In addition, the shape and morphology of the metal sulfides was assessed by electron microscopy (Figure B.3).

Ag sulfidation experiments

Time resolved AgNP sulfidation experiments were conducted in 10 mM TRIS (tris(hydroxymethyl)aminomethane, 99.8%, Sigma-Aldrich, CH) buffer adjusted to pH 7.5 with HNO_3. Seventy mL of the buffer solution were transferred into glass bottles and spiked with selected amounts of metal sulfides (40, 80, 130, 200 µM $CuS_{cryst/ppt}$ or $ZnS_{cryst/ppt}$) that were dispersed by sonication (10 min). Subsequently, 10 mL of sonicated (10 min) AgNP suspension (0.15 mM Ag; 10, 20, 40, 70, 100 nm) were added to reach an Ag concentration of 18.6 µM Ag (2 mg L^{-1}). This corresponded to molar S/Ag ratios of 2.2, 4.3, 7.0 and 10.8 for metal sulfide concentrations of 40, 80, 130 and 200 µM. The total Ag concentration in the starting suspensions

were measured by inductively coupled plasma mass spectrometry (ICP-MS) after acid digestion (1 mL of suspension digested with 1 mL HNO_3 (Ultrapure 60%, Merck, DE) in a microwave-assisted acid digestion system (UltraClave3, MLS GmbH), results are given in Table B.1). The reaction bottles were closed and wrapped in aluminum foil to prevent photo oxidation (Gorham et al. 2012). The suspensions were then vigorously stirred for the reaction period under oxic conditions at room temperature. The suspension was oxygen saturated as confirmed by O_2 measurements at the beginning and at the end of the experiment (O_2 probe, MicroTX3, PreSens, DE). Additional experiments were conducted with 40 µM metal sulfide (70 mL) spiked with 10 mL dissolved Ag^+ (0.15 mM $AgNO_3$ in water), resulting in a S/Ag ratio of 1.9.

During the sulfidation of AgNP with metal sulfides (MS), Zn^{2+} or Cu^{2+} cations (M^{2+}) are released into the solution according to Eq. 3.1.

$$2Ag_{(s)} + \frac{1}{2}O_{2(aq)} + 2H^{+}_{(aq)} + MS_{(s)} \rightarrow Ag_2S_{(S)} + H_2O_{(l)} + M^{2+}_{(aq)} \qquad \text{Eq. 3.1}$$

In order to derive the sulfidation rate laws, the dissolved M^{2+} concentration was measured at selected reaction times. Additional release of M^{2+} is due to oxidative-dissolution of the metal sulfides (Eq. 3.2).

$$MS + 2O_{2(aq)} \rightarrow SO^{2-}_4 + M^{2+}_{(aq)} \qquad \text{Eq. 3.2}$$

To correct for metal cation release by oxidative dissolution of the metal sulfide, additional blank experiments were conducted with the metal sulfides alone (40 µM) under otherwise identical conditions.

Dissolved Cu^{2+} and Zn^{2+} were measured spectrophotometrically using zincon (Merck, DE) as a complexing agent (Säbel et al. 2010). At each measurement time, 1.5 mL of suspension was withdrawn from the reaction vessel through the septum with a syringe, mixed with 15 µL of a zincon (10 mM) solution and 100 µL of TRIS buffer (1 M, pH 10) to adjust the pH to 9. Both Cu^{2+} and Zn^{2+} form a complex with zincon producing a distinct absorption peak (Cu^{2+}: 600 nm, Zn^{2+}: 620 nm) that was recorded on a UV-Vis spectrometer (Cary 1E, Varian, CH). The intensity of the absorption scales linearly with the metal cation concentration and a calibration curve was established by comparing the absorption intensity against the Zn-content that was determined by ICP-MS. Blank measurements without zincon were conducted in parallel for all samples to correct for interferences of the AgNP plasmon resonance and of the absorption of the metal sulfide dispersed in solution. A 2-cm quartz micro cuvette (Portmann Instruments, CH) was used for the UV-Vis measurements. The data were processed using the software code R (Team 2012).

Electron microscopy

The synthesized metal sulfide particles were characterized with a scanning electron microscope (SEM, Nova Nano-SEM 230, FEI, USA) equipped with an energy dispersive x-ray (EDX) analysis system (XMAX80, Oxford Inc., UK). Five mL of metal sulfide suspensions were filtered through Au-coated, 0.2-µm membrane filters (Nuclepore polycarbonate) and analyzed under either low vacuum conditions (0.5 mbar H_2O) at an acceleration voltage of 15 kV (for EDX analysis) or at high vacuum conditions at lower acceleration voltages (for imaging).

Samples obtained from experiments in TRIS buffer were affected by substantial carbon contamination during analysis in the TEM. Therefore, samples from replicated experiments in HEPES buffer (pH 7.5, 10 mM) were used for TEM investigations. These experiments were conducted in glass flasks in an overhead shaker with 100-nm AgNP and 40 µM ZnS_{ppt}. Spectrophotometric results of the Zn^{2+} release confirmed that the reaction kinetics were in line with results obtained in TRIS buffer. A sample for analysis by electron microscopy was collected at the time where roughly half of the Ag was sulfidized.

The pristine AgNP and the partially sulfidized 100-nm AgNP were studied with a scanning transmission electron microscope (STEM, HD-2700-Cs, Hitachi, Japan). Elemental analysis and elemental distribution maps were obtained with an EDX system attached to the microscope (EDAX, New Jersey, USA). Particles were deposited on plasma-cleaned TEM grids (Lacey-carbon Cu, Okenshoji Co. LTD, Japan) by either drawing a drop of suspension through the TEM grid using a paper tissue or by gently rotating the grid through the suspension. After particle deposition, the grids were washed in a drop of water. The grids were stored under N_2 atmosphere in the dark at a relative humidity < 20%.

X-ray diffraction (XRD)

The metal sulfides were characetrized by X-ray diffraction using Co Kα radiation (X'Pert Powder diffractometer with XCelerator detector, PANanlytical, Almelo, The Netherlands). Approximately 100 mg of metal sulfides were dispersed in 1 mL ethanol (analysis, Merck) and dried on a 27-mm diameter low-background Si slide. After evaporation of the solvent, XRD patterns were recorded from 5-95° 2-θ with a step-size of 0.0130° and a measurement time of 2 h per sample.

Ag K-edge X-ray absorption spectroscopy (XAS)

For XAS measurements, experiments with 10- and 100-nm AgNP were replicated in TRIS buffer. Samples were collected after partial sulfidation (0.5 to 1 day) and after 3 days. $NaNO_3$ (2 M, analysis, Merck) and cellulose (200 mg) were added to the reaction bottles to flocculate the particles. After centrifugation (4300 rpm, 10 min) the sediments were smeared in 13-mm copper molds, dewatered with a paper tissue and immediately frozen in liquid nitrogen. The samples were kept frozen until analysis. To evaluate whether the reacted AgNP were efficiently flocculated

and incorporated into the pellets, the remaining Ag content in the supernatant after centrifugation was determined by ICP-MS (for further details see Appendix B).

XAS was performed at the Ag K-edge (25'514 eV) at the Dutch Belgian Beamline (DUBBLE, BM01B) at the European Synchrotron Radiation Facility (ESRF, Grenoble, France) and at the SuperXAS beamline (X10DA) at the Swiss Light Source (SLS, Villigen, Switzerland). A closed-cycle He-cryostat adjusted to 80 K (DUBBLE) or a CryoJet (Oxford Instruments, UK) with a N_2 gas stream adjusted to 100 K (SuperXAS) were used to cool the samples. The reference samples Ag^0 (metal foil), Ag_2S (acanthite) and Ag-CuS were measured in transmission mode. The reference Ag-CuS corresponds to Ag^+ reacted with CuS. It was prepared by adding 0.9 mmol HS^- to 200 mL of a 5 mM $CuNO_3$ solution to form colloidal CuS. The precipitated CuS (~0.9 mmol) was separated by centrifugation (5 min, 4300 rpm), re-dispersed in 100 mL 1 mM $AgNO_3$ solution, resulting in a total molar Ag/Cu ratio of ~0.11 and an (Ag+Cu)/S ratio of ~1.1. The dissolved Ag^+ was reacted with the colloidal CuS for 24 h at room temperature. The Ag-CuS solid was separated and prepared for XAS analysis as described for the sulfidized AgNP.

Data extraction and evaluation was performed using Athena (Ravel and Newville 2005) as described previously (Kaegi et al. 2013, Kaegi et al. 2011). Briefly, E_0 was set to 25'514 eV. A first-order polynomial was fit to the data from 25'414 to 25'484 eV and subtracted from the raw data. A second-order polynomial fit to the data from 25'554 to 25'714 eV was used to normalize the edge-jump at E_0 to unity and to flatten the spectrum. For linear combination fit (LCF) analysis of extended X-ray absorption fine structure (EXAFS) spectra from 2.5 to 8 $Å^{-1}$, individual fitted fractions were constrained to values between 0 and 1 and the sum of all fractions was constrained to unity. Details on the LCF analysis of the X-ray absorption near edge structure (XANES) spectra are given in Appendix B.

3.4 Results

Metal sulfide characterization

All metals sulfides were characterized by XRD. The average size of the metal sulfides was determined by DLS and zeta potentials were derived from electrophoretic mobilities (Table 3.1).

The zeta potentials were in agreement with values reported in the literature (Fullston et al. 1999, Ma et al. 2013b, Vergouw et al. 1998). The XRD patterns of the samples CuS_{cryst} and ZnS_{cryst} were in line with the patterns of covellite and sphal-

Table 3.1: Characteristics of AgNP and metal sulfides.

	Diameter DLS (PDI)[1] [nm]	Zeta potential [mV]	Diameter[2] [nm]	Surface plasmon resonance [nm]
10 nm AgNP	ND	ND	8.2(2.8), (n=224)	393
20 nm AgNP	ND	ND	21.4(3.5), (n=278)	403
40 nm AgNP	48.4 (0.190)[3]	-49.5	41.6(4.2), (n=218)	413
70 nm AgNP	69.0 (0.131)[3]	-55.1	65.3(4.9), (n=348)	440
100 nm AgNP	96.6 (0.089)[3]	-55.9	98.7(5.4), (n=286)	492
CuS_{ppt}	8161 (0.659)[4]	-20.4	2.8	NA
CuS_{cryst}	624 (0.503)[4]	-23.3	NA	NA
ZnS_{ppt}	1013 (0.571)[4]	7.72	18.5	NA
ZnS_{cryst}	973 (0.415)[4]	-13.0	NA	NA

[1]PDI = Polydispersity Index

[2]: AgNP: diameter of (primary) particles from TEM. Standard error (1σ) is given in brackets; CuS / ZnS: crystallite size (diameter) from XRD.

[3]: Aliquots of the stock suspensions (2 mg/l) were (1:5 diluted with buffer) sonicated for 10 minutes in a sonication bath and measured before the sulfidation experiments. The pH of the suspensions was 7.5. The data refer to number weighted particle size distributions using the cumulant method.

[4]: In 10 mL buffer (pH 7.5) 1 mg of the respective metal sulfide was dispersed and sonicated for 10 min. The data refer to number weighted particle size distributions using the cumulant method. The high PDI index indicate a very broad particle size distribution and make the size analysis from the DLS measurement very unreliable.

ND: not detectable (concentration too low); NA: not analyzed

erite, respectively, and confirmed their crystalline structure (Figure B.2). Corresponding SEM images are shown in Figure B.3. The XRD patterns of CuS_{ppt} and ZnS_{ppt} exhibited considerably broader peaks with maxima in line with the patterns of covellite and sphalerite, respectively. Crystallite sizes of ~3 nm for ZnS_{ppt} and 19 nm for CuS_{ppt} were estimated from the peak widths based on the Scherrer equation (for more details see Appendix B).

Oxidative dissolution of metal sulfides in absence of Ag

An increase of dissolved Cu^{2+} was observed for both types of CuS and indicated slower oxidative dissolution of CuS_{cryst} (Figure 3.1A) than CuS_{ppt} (Figure B.5). In contrast, the dispersion of both types of ZnS in buffer solution did not result in any detectable release of Zn^{2+} into solution, suggesting that the oxidation of zinc sulfide to sulfate was negligible (Figure B.5).

Reaction of metal sulfides with $Ag^{+}_{(aq)}$

To assess the availability of sulfide from the different metal sulfides for the reaction with Ag, we first investigated the reaction of metal sulfide with dissolved Ag^{+}. In the experiments with CuS_{cryst}, CuS_{ppt} or ZnS_{ppt}, dissolved Cu^{2+} and Zn^{2+} concentrations strongly increased over time and indicated significantly faster dissolution in the presence of Ag^{+} than under conditions of oxidative dissolution alone (Figure B.5), as exemplified for CuS_{cryst} in Figure 3.1A. Reaction of ZnS_{cryst} with dissolved Ag^{+} on the other hand did not result in a detectable Zn^{2+} release, indicating that the ZnS_{cryst} was rather inert in line with previous observations (Acero et al. 2007).

Reaction of metal sulfides with AgNP

To assess the reaction kinetics of metal sulfides with AgNP, we used CuS_{cryst} and ZnS_{ppt} because experiments with Ag^{+} showed that ZnS_{cryst} reacted too slowly and CuS_{ppt} oxidized too fast in the absence of Ag. During the reaction of the AgNP with CuS_{cryst} or ZnS_{ppt}, dissolved Cu^{2+} or Zn^{2+} increased monotonously as exemplarily shown for the reaction of 10-nm AgNP with CuS_{cryst} in Figure 3.1A. The decreasing metallic fraction of the AgNP was derived from the increasing M^{2+} concentration, taking the oxidative dissolution of the metal sulfide into account (Figure 3.1B and Figure B.5). XAS measurements confirmed that the release of metal cations (corrected for the oxidative dissolution) reflected the progress of the AgNP sulfidation (Table 3.2). Reacting AgNP of different sizes with different concentrations of CuS_{cryst} and ZnS_{ppt} resulted in a set of experiments that all followed a pseudo first-order rate law (Eq. 3.3):

$$[Ag]_t = [Ag]_0 * e^{-k*t} \qquad \text{Eq. 3.3}$$

$[Ag]_t$: metallic fraction at time t, $[Ag]_{0:}$ metalliuc fraction at the beginning of the experiment, k: rate constant (s^{-1}), t: time (s).

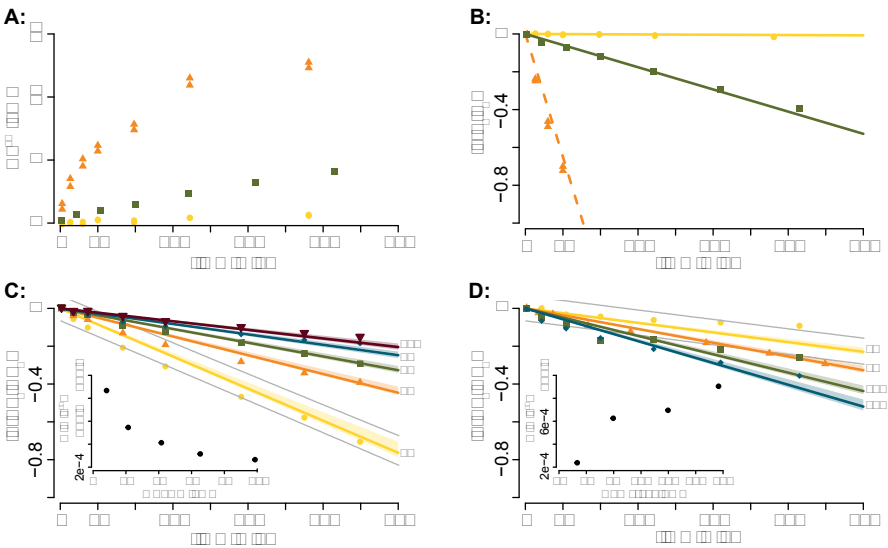

Figure 3.1: A: Increase of dissolved Cu^{2+} over time during *i)* oxidative dissolution of 40 µM CuS_{cryst} (yellow circles) *ii)* reaction of 40 µM CuS_{cryst} with Ag^{+} (18.6 µM) (orange upward triangles, two replicates are indicated) and iii) reaction of 40 µM CuS_{cryst} with 10-nm AgNP (18.6 µM) (green squares). **B:** Fraction of CuS during oxidative dissolution (40 µM CuS_{cryst}) derived from measurements of dissolved Cu^{2+} against time (yellow dots, the y-axis represents CuS_t / $CuS_{t=0}$). Fraction of metallic AgNP (18.6 µM, 10 nm, y axis representing Ag_t^0 / Ag_0^0) (green) and fraction of ionic Ag (18.6 µM $AgNO_3$,y axis representing Ag_t^+ / Ag_0^+) (orange) over time. Both types of Ag were reacted with 40 µM CuS_{cryst}. The Ag fractions (metallic or ionic) were calculated by subtracting the Cu^{2+} resulting from the oxidative dissolution from the spectrophotometrically measured Cu^{2+} concentrations The lines represent the calculated fractions using Eq. 3.4 in combination with the parameters given in Table 3.2. **C:** Fraction of metallic Ag against time displayed for different AgNP sizes reacted with of 40 µM CuS_{cryst}. The diameters of the AgNP in nm are given on the right side of each line. Inset: Reaction rate coefficients calculated for the 40 µM CuS_{cryst} experiments against the diameter of the AgNP. **D:** Fraction of metallic Ag against time displayed for 40-nm AgNP reacted with CuS_{cryst}. The CuS concentrations in µM are indicated on the right hand side. Inset: Reaction rate coefficients for the 40-nm AgNP experiments against CuS_{cryst} concentrations. C and D: The lines represent the calculated metallic Ag fractions using the Eq. 3.4 in combination with the parameters given in Table 3.2. Shaded areas in the panels exemplify the confidence interval and the grey lines (around yellow lines) indicate the predictive error of the model calculations.

The temporal decrease of the metallic fraction ($[Ag]_t$) of the AgNP for experiments performed with different AgNP sizes (10, 20, 40, 70, 100 nm) reacting with 80 µM CuS_{cryst} is given in Figure 3.1C. The reaction rate coefficient increases (slope becomes more negative) with decreasing AgNP size. Plotting the reaction rate coefficient against the AgNP size revealed an $1/d_{AgNP}$ dependence of the reaction rate coefficient on the size of the AgNP (Figure 3.1C, inset). Increasing reaction rate coefficients were observed with increasing CuS_{cryst} concentrations (40, 80, 130 and 200 µM) (Figure 3.1D). Comparable trends were also observed for all other AgNP sizes and metal sulfide concentrations as well as for ZnS_{ppt} (Figure B.6). Based on these findings, the rate constant k was described by the equation

$$k = k' * [MS]_{initial}^{\ a} * \left(\frac{1}{d_{Ag-NP}} \right)^{b} \qquad \text{Eq. 3.4}$$

where $[MS]_{initial}$ represents the initial concentration of metal sulfide in µM and d_{AgNP} the diameter of the AgNP in nm, derived from TEM analysis. k' as well as the exponents *a* and *b* were derived by fitting the entire datasets (all AgNP sizes and metal sulfide concentrations for a specific metal sulfide type) simultaneously by non-linear least squares regression. In Figure 3.1C and D, lines represent the model

Table 3.2: Kinetic parameters for the oxidative dissolution of metal sulfides (Eq. 3.2) and for the sulfidation of dissolved Ag^+ and AgNP (10, 20, 40, 70, 100 nm) by reaction with metal sulfides (Eq. 3.3 and Eq. 3.4).

		ZnS_{ppt}	CuS_{ppt}	CuS_{cryst}
oxidative dissolution of metal sulfides	k (min^{-1})	ND	$9.6(2) \times 10^{-5}$	$1.3(1) \times 10^{-5}$
Sulfidation of $AgNO_3$	k (min^{-1})	$2.7(7) \times 10^{-2}$	$1.4(2) \times 10^{-2}$	$1.08(6) \times 10^{-2}$
	k' ($nm^b\ \mu M^{-a}\ min^{-1}$)	$3.2(4) \times 10^{-4}$	NA	$4.7(8) \times 10^{-4}$
Sulfidation of AgNP	a	0.78(3)	NA	0.52(3)
	b	0.53(2)	NA	0.60(2)

Number in brackets refer to the last digit of the value and correspond to the standard error (1σ).

calculations based on the rate coefficients derived using Eq. 3.4 for the selected treatments. All experimental results and model fits (Figure B.6) and additional plots to assess the fit quality are provided in Appendix B.

Ag K-edge X-ray absorption spectroscopy

To obtain additional structural information about the solids and to confirm that the spectrophotometric analysis of the kinetic experiments reflected the sulfidation progress, we investigated partially and completely sulfidized AgNP using Ag K-edge XAS. The EXAFS spectra of the reacted AgNP and of reference materials are given in Figure 3.2. The speciation of Ag was assessed by a LCF analysis using the reference spectra of metallic Ag, Ag_2S and Ag-CuS as references (Table 3.2, Figure 3.2). The Ag-CuS reference accounted for a significant portion of the Ag-sulfide fraction. Based on its XANES and its Fourier-transformed EXAFS spectrum, this reference was considered to represent dominantly S-coordinated Ag (Figure B.11),

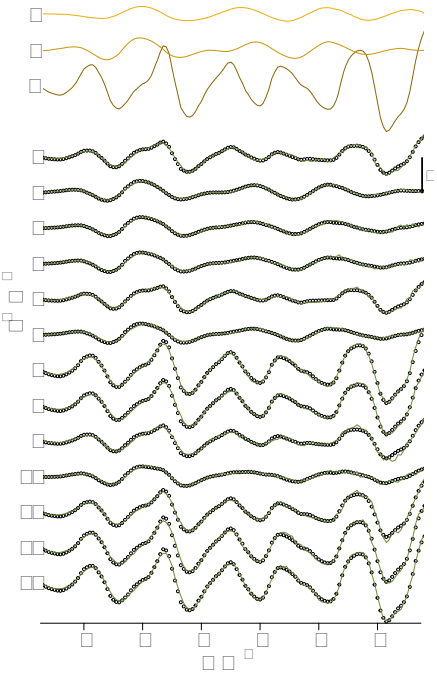

Figure 3.2: EXAFS spectra (lines) and LCF results (dots) using Ag-CuS (A), Ag_2S (B), and Ag-foil (C) as references. Numbers on the left correspond to the numbers given in Table 3.2. Spectra are plotted with an offset of 2 for clarity.

most probably adsorbed Ag^{+} or amorphous Ag-sulfide on CuS. . The fraction of metallic Ag derived from LCF analysis of either EXAFS or XANES (Figure B.9) spectra were very similar (Figure B.10). Furthermore, the fraction of metallic Ag derived from XAS analysis was in line with the metallic fraction of Ag calculated from the spectrophotometrically measured Cu^{2+} or Zn^{2+} release (Table 3.2).

Table 3.2: Metallic Ag fractions derived from UV-Vis measurements and from speciation analysis resulting from LCF of EXAFS spectra using Ag^0, Ag-CuS, and Ag_2S as reference spectra. MS refers to metal sulfides and size to the diameter of the AgNP.

No.	**MS**	**AgNP size**	**Reaction time**	**UV-Vis**	**EXAFS LCF**		
		(nm)	(h)	Ag^0	Ag^0	Ag-CuS	Ag_2S
1	CuS_{ppt}	10	6	45%	36%	27%	37%
2	CuS_{ppt}	10	72	0%	2%	18%	80%
3	CuS_{ppt}	100	22	15%	7%	19%	74%
4	CuS_{ppt}	100	72	10%	8%	13%	79%
5	ZnS_{ppt}	10	8	36%	30%	19%	51%
6	ZnS_{ppt}	10	72	0%	8%	13%	78%
7	ZnS_{ppt}	100	26	69%	72%	14%	14%
8	ZnS_{ppt}	100	72	48%	63%	32%	5%
9	CuS_{cryst}	10	9	50%	37%	29%	33%
10	CuS_{cryst}	10	72	7%	14%	18%	68%
11	CuS_{cryst}	100	72	61%	54%	19%	27%
12	ZnS_{cryst}	10	72	94%	75%	25%	0%
13	ZnS_{cryst}	100	72	94%	84%	16%	0%

Electron microscopy analysis

Additional insights into the mechanism of AgNP sulfidation were gained from TEM analysis of AgNP (100 nm) reacted with ZnS_{ppt} for 26 h, which resulted in the sulfidation of about 50 % of the total Ag. We found particles, which were comparable in size and shape to the starting materials (Figure 3.3).

High-resolution elemental distribution maps recorded on selected particles further indicated the development of complex sulfidation patterns. The distribution of the S, however, did not form a homogeneous and concentric shell around the metallic Ag core of the particles, but seemed to follow distinct migration patterns (Figure 3.4). In addition to Ag_2S closely associated with the reacted AgNP, smaller nanoparticles (<10 nm) were observed (Figure 3.3). Elemental analysis (EDX, inset Figure 3.3) and d-spacings (Figure B.13) calculated from diffraction patterns derived from high-resolution (HR)-TEM images (Figure B.12) confirmed that these nanoparticles were Ag_2S precipitates. Similar associations between larger and smaller particles were also reported resulting from sulfidation during sample

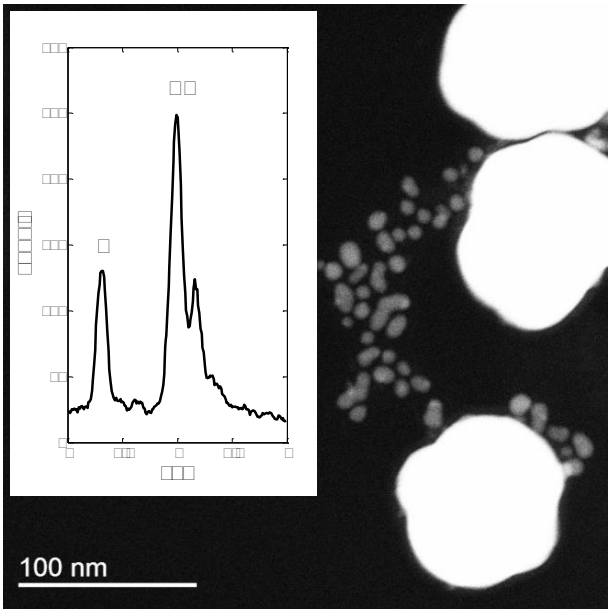

Figure 3.3: High-angle annular dark-field (HAADF) image of partially sulfidized 100-nm AgNP showing small (5-10 nm) Ag_2S particles next to partially sulfidized AgNP. Inset shows the EDX analysis of small Ag_2S particles.

storage under air (Glover et al. 2011). However, such an artifact seems unlikely in the present study, since the samples were stored in a dry (relative humidity <20%) N_2 atmosphere.

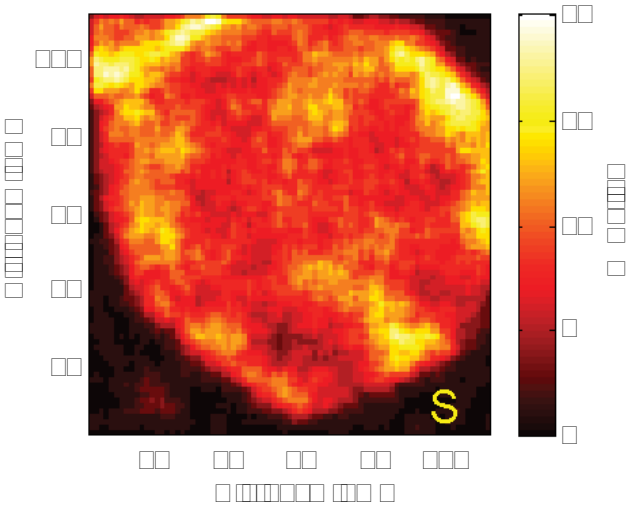

Figure 3.4: Sulfur distribution map derived from STEM–EDX measurements recorded on a partially sulfidized 100 nm AgNP. Inhomogeneous sulfidation patterns are clearly visible on the Sulfur distribution map. The color bar indicates the signal intensities.

3.5 Discussion

In aquatic environments, Ag(0) is oxidized under oxic conditions (Liu and Hurt 2010). The efficient scavenging of Ag^+ by the formation of poorly soluble Ag_2S (Haynes 2014) accelerates the Ag^0 oxidation in presence of sulfides (Liu et al. 2011). Sulfides preserved in the form of metal sulfides represent a large pool of sulfide which, depending on the metal type, can be more resistant towards oxidation by O_2 (Rozan et al. 1999) but can still be available for the sulfidation of Ag^0.

The sulfidation of AgNP in the presence of suspended metal sulfides followed pseudo- first-order kinetics. The pseudo-first-order reaction rate coefficients varied with the type and concentration of the metal sulfide and with the size of the AgNP. The initial concentration of the metal sulfide scaled exponentially with the parameter *a*, which equaled 0.52(3) for CuS_{cryst} and 0.78(3) for ZnS_{ppt} (numbers in parenthesis correspond to the last digit and represent 1σ). The larger value of the *a* parameter indicated a stronger dependence of the sulfidation rate on the concentration of ZnS_{ppt} than on the concentration of CuS_{cryst}. The exponent *a* likely represents a material property of the metal sulfide and, since the value of *a* was less than one, may also reflect the decreasing accessible surface area of the metal sulfide caused by particle aggregation at higher metal sulfide concentrations.

Furthermore, our results revealed a dependence of the rate coefficients on the AgNP size ($1/d_{AgNP}$, TEM size). This size-dependence scaled with the exponent *b* which was 0.53(2) for AgNP reacted with CuS_{cryst} and 0.60(2) for AgNP reacted with ZnS_{ppt}. The fact that the *b* parameters derived for experiments with CuS_{cryst} and ZnS_{ppt} are very similar suggests that this parameter is related to a property of the AgNP irrespective of the type of metal sulfide with which they react. The exponent *b* was smaller than one, indicating that larger particles sulfidize faster than expected from surface normalization compared to smaller particles, which can clearly be seen on Figure B.7. The surface areas of the different particle suspensions were calculated assuming equivalent masses, perfect spheres and TEM derived diameters of the AgNP.

Analytical electron microscopy revealed the formation of complex sulfidation patterns, which were different to core-shell structures reported from sulfidation of AgNP with hydrogen sulfides (Levard et al. 2011). High-resolution elemental distribution maps revealed a strongly heterogeneous distribution of S (Figure 3.4). This suggests that the sulfidation preferentially proceeds along subgrain boundaries that were observed on HR-TEM images of comparable AgNP as used in this study (Kaegi et al. 2013). This phenomenon has been described as intergranular corrosion (Wanhill 2011). The polycrystalline structure may thus lead to a larger available surface area of larger AgNP than expected from their external surface

area (Elechiguerra et al. 2005), in line with the parameter *b* smaller than one derived from the kinetic sulfidation experiments.

In addition to the direct heterogeneous sulfidation pathway at the AgNP surface (Liu et al. 2011) leading to complex sulfidation patterns, we observed freshly precipitated nanoscale Ag_2S particles indicating a dissolution-precipitation pathway.

LCF analyses of EXAFS spectra are in good agreement with results from the UV-Vis measurements. The LCF consistently revealed a small / moderate fraction of Ag-CuS that tended to decrease with increasing reaction time consistent with own previous findings from AgNP – wastewater batch experiments (Kaegi et al. 2013). This points towards an initial formation of less crystalline Ag-sulfide or adsorbed Ag species, which then transform into crystalline Ag_2S. The Ag-CuS fraction in ZnS_{cryst} experiments is likely due to Ag^+ adsorbed to the surface of ZnS, which did not yet result in the release of Zn^{2+} into the solution, and thus was not detected by the zincon method.

This study revealed that the sulfidation of AgNP in the presence of metal sulfides is possible under oxic conditions. The rate coefficients for the AgNP sulfidation reactions were dependent on AgNP size, metal sulfide concentration, type and structure. Furthermore, subgrain boundaries (inner surfaces) may explain the increased outer surface normalized reactivity of larger AgNP compared to smaller AgNP.

Environmental implications

The results from this study demonstrate that CuS and ZnS are sources of bisulfide for AgNP sulfidation. For total suspended solids (TSS) in municipal sewage sludge, contents of 120 - 4410 mg kg^{-1} Zn as ZnS and 135 to 2100 mg kg^{-1} Cu as CuS have been reported (Stover et al. 1976). The lowest of these reported amounts (120 mg kg^{-1} ZnS and 135 mg kg^{-1} CuS) are still sufficient for the complete sulfidation of 7.9 mmol Ag/kg TSS (850 mg Ag/kg TSS), which is about 1-2 orders of magnitudes above reported silver concentrations in sewage sludge (Shafer et al. 1998) and several orders of magnitudes higher than the modeled AgNP concentration in sewage sludge (17.4 µM (Gottschalk et al. 2010)).

Based on the AgNP sulfidation kinetics reported in this study, we can estimate the degree of AgNP sulfidation related to metal sulfides in urban wastewater systems. In a study on the transport and transformation of AgNP in a sewer channel (Kaegi et al. 2013), we did not observe any retardation, suggesting that AgNP transport can be approximated using a plug-flow reactor model. Based on the AgNP sulfidation kinetics observed for the reaction with ZnS_{ppt} in combination with the reported metal sulfide (CuS and ZnS) concentrations (19.5 - 500 µM in the sludge, derived from reported ZnS and CuS concentrations in sewage sludge on a dry mass basis and assuming 5 g_{TSS} L_{sludge}^{-1}) 10-nm AgNP are expected to almost completely sulfidize (70 - 100% Ag_2S) but 100-nm AgNP are predicted to remain partly metallic (26 – 98% Ag_2S) after a typical residence time of 24 h in wastewater systems

(sewers and wastewater treatment). Results from studies on pilot wastewater treatment plants spiked with AgNP indicated a near complete sulfidation of the AgNP (Kaegi et al. 2013, Kaegi et al. 2011, Lombi et al. 2013), which is in line with our predictions, considering the small particle sizes (mode 10 – 50 nm) used in these studies. In one of the studies (Kaegi et al. 2011) speciation analysis indicated a metallic fraction of up to 20% in the effluent of the wastewater treatment plant, which may be explained by the presence of larger aggregates / particles, causing reduced sulfidation rates. On the other side, considerable amounts of bisulfides (up to 30 µM) in the sewer systems (Nielsen et al. 2008) likely result in an accelerated sulfidation of the AgNP (Liu et al. 2011). The results from this study refer to citrate capped AgNP reacted with metal sulfides under oxygen saturated conditions at pH 7.5. A different surface coating, such as PVP, gum Arabic or PEG, may additionally influence the sulfidation rates. However, in batch experiments (although conducted under different experimental settings), where another type of AgNP (NM-300)(Klein et al. 2011) was reacted with activated sludge, near complete sulfidation was achieved after two hours indicating comparable sulfidation rate coefficients (Kaegi et al. 2011). Also different pH and O_2 levels may alter the sulfidation rates, but oxygen saturation and circumneutral pH values are typically observed in surface waters.

In oxic surface waters ZnS concentrations are reported from 1.5 nM in rural areas up to 127 nM close to WWTP effluents (Priadi et al. 2012). The ZnS_{ppt} and CuS_{cryst} used in this study exhibited half-life times longer than 35 days in oxygenated water in the absence of Ag and half-life times of ZnS and CuS in surface waters longer than 15 days have been observed (Rozan et al. 1999). Half-life times for the sulfidation of AgNP reported in this study ranged from 2 h to 2.4 days for the reaction with ZnS_{ppt} and from 5 h to 2.7 days for the reaction with CuS_{cryst}. From a mass flow analysis on the basis of current AgNP production volumes in Switzerland, AgNP concentrations in surface waters of ~7 pM have been predicted (Gottschalk et al. 2010). Since the concentrations of ZnS and CuS in oxic surface waters largely exceed this predicted AgNP concentration and since the half-life times for the AgNP sulfidation by reaction with ZnS or CuS are much shorter than the half-life times of the metal sulfides in the absence of Ag, complete sulfidation of AgNP in urban surface waters within hours to days can be expected even in the absence of free bisulfide.

The established sulfidation kinetics in combination with sulfide levels including metal sulfides and HS^- in wastewater and urban surface waters indicate that AgNP can completely be transformed into sulfides within a few hours to a few days.

Acknowledgements

We acknowledge the Electron Microscopy Centers at ETH Zurich (EMEZ, Zurich, Switzerland) and at Empa (Swiss Federal Institute for Materials Science and Technology, Duebendorf, Switzerland) for providing access to the microscopes. The Swiss Light Source (SLS, Villigen, Switzerland) and the Swiss Norwegian Beamline at the European Synchrotron Radiation Facility (SNBL, ESRF, Grenoble, France) are acknowledged for the allocation of beamtime. We thank Maarten Nachtegaal (SLS) for support at the SuperXAS beamline (SLS) and Sergey Nikitenko and Dipanjan Banerjee (both ESRF) for support at the Dutch Belgian Beamline (DUBBLE) at ESRF. This work is part of the project "Behavior of silver nanoparticles in a wastewater treatment plant" within the Swiss National Research Program NRP 64 "Opportunities and Risks of Nanomaterials". Additionally we would like to thank Andreas Scheidegger for support on statistical data analysis.

References

Acero, P., Cama, J. and Ayora, C. (2007) Sphalerite dissolution kinetics in acidic environment. Applied Geochemistry 22(9), 1872-1883.

Benn, T., Cavanagh, B., Hristovski, K., Posner, J.D. and Westerhoff, P. (2010) The Release of Nanosilver from Consumer Products Used in the Home Supplemental data file available online for this article. J. Environ. Qual. 39(6), 1875-1882.

Benn, T.M. and Westerhoff, P. (2008) Nanoparticle silver released into water from commercially available sock fabrics. Environ Sci Technol 42(11), 4133-4139.

Dobias, J. and Bernier-Latmani, R. (2013) Silver release from silver nanoparticles in natural waters. Environ Sci Technol 47(9), 4140-4146.

Doolette, C., McLaughlin, M., Kirby, J., Batstone, D., Harris, H., Ge, H. and Cornelis, G. (2013) Transformation of PVP coated silver nanoparticles in a simulated wastewater treatment process and the effect on microbial communities. Chemistry Central Journal 7(1), 1-18.

Elechiguerra, J.L., Larios-Lopez, L., Liu, C., Garcia-Gutierrez, D., Camacho-Bragado, A. and Yacaman, M.J. (2005) Corrosion at the Nanoscale: The Case of Silver Nanowires and Nanoparticles. Chemistry of Materials 17(24), 6042-6052.

Farkas, J., Peter, H., Christian, P., Gallego Urrea, J.A., Hassellov, M., Tuoriniemi, J., Gustafsson, S., Olsson, E., Hylland, K. and Thomas, K.V. (2011) Characterization of the effluent from a nanosilver producing washing machine. Environ Int 37(6), 1057-1062.

Fullston, D., Fornasiero, D. and Ralston, J. (1999) Zeta potential study of the oxidation of copper sulfide minerals. Colloids and Surfaces A: Physicochemical and Engineering Aspects 146(1–3), 113-121.

Geranio, L., Heuberger, M. and Nowack, B. (2009) The behavior of silver nanotextiles during washing. Environ Sci Technol 43(21), 8113-8118.

Glover, R.D., Miller, J.M. and Hutchison, J.E. (2011) Generation of Metal Nanoparticles from Silver and Copper Objects: Nanoparticle Dynamics on Surfaces and Potential Sources of Nanoparticles in the Environment. ACS Nano 5(11), 8950-8957.

Gorham, J., MacCuspie, R., Klein, K., Fairbrother, D.H. and Holbrook, R.D. (2012) UV-induced photochemical transformations of citrate-capped silver nanoparticle suspensions. Journal of Nanoparticle Research 14(10), 1-16.

Gottschalk, F., Sonderer, T., Scholz, R.W. and Nowack, B. (2009) Modeled environmental concentrations of engineered nanomaterials (TiO(2), ZnO, Ag, CNT, Fullerenes) for different regions. Environ Sci Technol 43(24), 9216-9222.

Gottschalk, F., Sonderer, T., Scholz, R.W. and Nowack, B. (2010) Possibilities and limitations of modeling environmental exposure to engineered nanomaterials by probabilistic material flow analysis. Env Tox and Chem 29(5), 1036-1048.

Haynes, W.M. (2014) CRC Handbook of Chemistry and Physics, CRC Press, Boca Raton, Fla.

Impellitteri, C.A., Harmon, S., Silva, R.G., Miller, B.W., Scheckel, K.G., Luxton, T.P., Schupp, D. and Panguluri, S. (2013) Transformation of silver nanoparticles in fresh, aged, and incinerated biosolids. Water Research 47(12), 3878-3886.

Kaegi, R., Voegelin, A., Ort, C., Sinnet, B., Thalmann, B., Krismer, J., Hagendorfer, H., Elumelu, M. and Mueller, E. (2013) Fate and transformation of silver nanoparticles in urban wastewater systems. Water Res 47(12), 3866-3877.

Kaegi, R., Voegelin, A., Sinnet, B., Zuleeg, S., Hagendorfer, H., Burkhardt, M. and Siegrist, H. (2011) Behavior of metallic silver nanoparticles in a pilot wastewater treatment plant. Environ Sci Technol 45(9), 3902-3908.

Kittler, S., Greulich, C., Diendorf, J., Koller, M. and Epple, M. (2010) Toxicity of Silver Nanoparticles Increases during Storage Because of Slow Dissolution under Release of Silver Ions. Chemistry of Materials 22(16), 4548-4554.

Klein, C.L., Comero, S., Locoro, G., Gawlik, B.M., Linsinger, T., Stahlmecke, B., Romazanov, J., Kuhlbusch, T.A.J., Van Doren, E., De Temmerman, P.J., Mast, J., Wick, P., Krug, H.F., Friedrichs, S., Maier, G., Werner, J., Hund-Rinke, K. and Kördel, W. (2011) NM-Series of representative manufactured nanomaterials: NM-300 silver characterisation, stability, homogeneity, p. 86 pp., European Union.

Levard, C., Mitra, S., Yang, T., Jew, A.D., Badireddy, A.R., Lowry, G.V. and Brown, G.E., Jr. (2013) Effect of chloride on the dissolution rate of silver nanoparticles and toxicity to E. coli. Environ Sci Technol 47(11), 5738-5745.

Levard, C., Reinsch, B.C., Michel, F.M., Oumahi, C., Lowry, G.V. and Brown, G.E. (2011) Sulfidation processes of PVP-coated silver nanoparticles in aqueous solution: impact on dissolution rate. Environ Sci Technol 45(12), 5260-5266.

Liu, J. and Hurt, R.H. (2010) Ion release kinetics and particle persistence in aqueous nano-silver colloids. Environ Sci Technol 44(6), 2169-2175.

Liu, J., Pennell, K.G. and Hurt, R.H. (2011) Kinetics and mechanisms of nanosilver oxysulfidation. Environ Sci Technol 45(17), 7345-7353.

Lombi, E., Donner, E., Taheri, S., Tavakkoli, E., Jämting, Å.K., McClure, S., Naidu, R., Miller, B.W., Scheckel, K.G. and Vasilev, K. (2013) Transformation of four silver/silver chloride nanoparticles during anaerobic treatment of wastewater and post-processing of sewage sludge. Environmental Pollution 176, 193-197.

Luther, G.W., 3rd, Findlay, A.J., Macdonald, D.J., Owings, S.M., Hanson, T.E., Beinart, R.A. and Girguis, P.R. (2011) Thermodynamics and kinetics of sulfide oxidation by oxygen: a look at inorganically controlled reactions and biologically mediated processes in the environment. Frontiers in Microbiology 2.

Ma, R., Levard, C., Judy, J.D., Unrine, J.M., Durenkamp, M., Martin, B., Jefferson, B. and Lowry, G.V. (2013a) Fate of zinc oxide and silver nanoparticles in a pilot waste water treatment plant and in processed biosolids. Environ Sci Technol.

Ma, R., Levard, C., Marinakos, S.M., Cheng, Y., Liu, J., Michel, F.M., Brown, G.E. and Lowry, G.V. (2012) Size-controlled dissolution of organic-coated silver nanoparticles. Environ Sci Technol 46(2), 752-759.

Ma, R., Levard, C., Michel, F.M., Brown, G.E. and Lowry, G.V. (2013b) Sulfidation Mechanism for Zinc Oxide Nanoparticles and the Effect of Sulfidation on Their Solubility. Environ Sci Technol 47(6), 2527-2534.

Nielsen, A.H., Vollertsen, J., Jensen, H.S., Madsen, H.I. and Hvitved-Jacobsen, T. (2008) Aerobic and anaerobic transformations of sulfide in a sewer system--field study and model simulations. Water Environ Res 80(1), 16-25.

Page, A.L. (1974) Fate and effects of trace elements in sewage when applied to agricultural lands: A literature review study., U.S. EPA.

Pomeroy, R. and Bowlus, F.D. (1946) Progress Report on Sulfide Control Research. Sewage Works Journal 18(4), 597-640.

Priadi, C., Le Pape, P., Morin, G., Ayrault, S., Maillot, F., Juillot, F., Hochreutener, R., Llorens, I., Testemale, D., Proux, O. and Brown, G.E. (2012) X-ray Absorption Fine Structure Evidence for Amorphous Zinc Sulfide as a Major Zinc Species in Suspended Matter from the Seine River Downstream of Paris, Ile-de-France, France. Environ Sci Technol 46(7), 3712-3720.

Ratte, H.T. (1999) Bioaccumulation and toxicity of silver compounds: A review. Environmental Toxicology and Chemistry 18(1), 89-108.

Ravel, B. and Newville, M. (2005) ATHENA , ARTEMIS , HEPHAESTUS : data analysis for X-ray absorption spectroscopy using IFEFFIT. Journal of Synchrotron Radiation 12(4), 537-541.

Reinsch, B.C., Levard, C., Li, Z., Ma, R., Wise, A., Gregory, K.B., Brown, G.E., Jr. and Lowry, G.V. (2012) Sulfidation of silver nanoparticles decreases Escherichia coli growth inhibition. Environ Sci Technol 46(13), 6992-7000.

Rozan, T.F., Benoit, G. and Luther, G.W. (1999) Measuring Metal Sulfide Complexes in Oxic River Waters with Square Wave Voltammetry. Environ Sci Technol 33(17), 3021-3026.

Russell, A.D. and Hugo, W.B. (1994) Antimicrobial activity and action of silver. Prog Med Chem 31, 351-370.

Säbel, C.E., Neureuther, J.M. and Siemann, S. (2010) A spectrophotometric method for the determination of zinc, copper, and cobalt ions in metalloproteins using Zincon. Analytical Biochemistry 397(2), 218-226.

Shafer, M.M., Overdier, J.T. and Armstong, D.E. (1998) Removal, partitioning, and fate of silver and other metals in wastewater treatment plants and effluent-receiving streams. Environmental Toxicology and Chemistry 17(4), 630-641.

Stover, R.C., Sommers, L.E. and Silviera, D.J. (1976) Evaluation of Metals in Wastewater-Sludge. Journal Water Pollution Control Federation 48(9), 2165-2175.

Sukola, K., Wang, F. and Tessier, A. (2005) Metal-sulfide species in oxic waters. Analytica Chimica Acta 528(2), 183-195.

Team, R.C. (2012) R: A Language and Environment for Statistical Computing, R Foundation for Statictical Computing.

Vergouw, J.M., Difeo, A., Xu, Z. and Finch, J.A. (1998) An agglomeration study of sulphide minerals using zeta potential and settling rate. Part II: sphalerite/pyrite and sphalerite/galena. Minerals Engineering 11(7), 605-614.

Wanhill, R.J.H. (2011) Case Histories of Ancient Silver Embrittlement. Journal of Failure Analysis and Prevention 11(3), 178-185.

Woodrow Wilson, I. (2015) Nanotechnology Consumer Products, Informa Healthcare.

Zhang, W., Yao, Y., Sullivan, N. and Chen, Y. (2011) Modeling the primary size effects of citrate-coated silver nanoparticles on their ion release kinetics. Environ Sci Technol 45(10), 4422-4428.

4. Effect of Ozone Treatment on Nano-Sized Silver Sulfide in Wastewater Effluent

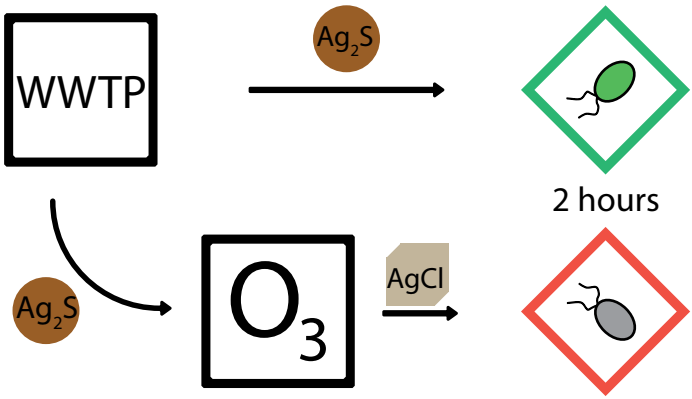

Published in Environmental Science & Technology, (DOI: 10.1021/acs.est.5b02194)
Basilius Thalmann[a, b, c, d], Andreas Voegelin[d], Urs von Gunten[a, d], Renata Behra[d], Eberhard Morgenroth[d] and Ralf Kaegi[a, b, c, d]

[a] Study concept and design; [b] Acquisition, analysis and interpretation of data; [c] Drafting of manuscript; [d] Critical revision

4.1 Abstract

Silver nanoparticles used in consumer products are likely to be released into municipal wastewater. Transformation reactions, most importantly sulfidation lead to the formation of nanoscale silver sulfide (nano-Ag_2S) particles. In wastewater treatment plants (WWTP), ozonation can enhance the effluent quality by eliminating organic micropollutants. The effect of ozonation on the fate of nano-Ag_2S, however, is currently unknown. In this study we investigate the interaction of ozone with nano-Ag_2S and evaluate the effect of ozonation on the short-term toxicity of WWTP effluent spiked with nano-Ag_2S.

The oxidation of nano-Ag_2S by ozone resulted in a stoichiometric factor (number of moles of ozone required to oxidize one mole of sulfide to sulfate) of 2.91, which is comparable to the results obtained for the reaction of bisulfide (HS^-) with ozone. The second order rate constant for the reaction of nano-Ag_2S with ozone ($k = 3.1\times10^4\ M^{-1}\ s^{-1}$) is comparable to the rate constant of other fast reacting micropollutants. Analysis of the ozonation products of nano-Ag_2S by transmission electron microscopy (TEM) and X-ray absorption spectroscopy (XAS) revealed that ozonation dominantly led to the formation of silver chloride in WWTP effluent. After ozonation of the Ag_2S-spiked effluent, the short-term toxicity for the green algae *Chlamydomonas reinhardtii* increased and reached EC_{50} values comparable to Ag^+. This study thus reveals that ozone treatment of WWTP effluent results in the oxidation of Ag_2S, and hence, an increase of the Ag toxicity in the effluent, which may become relevant at elevated Ag concentrations.

4.2 Introduction

Silver nanoparticles (Ag-NP) are incorporated into many consumer products (Woodrow Wilson 2015), such as textiles and cosmetics (Windler et al. 2013) because of their antimicrobial activity.(Ratte 1999, Russell and Hugo 1994) Several reports document that Ag-NP become detached from the bulk fabric during washing of the textiles and will thus be released to the sewer system (Benn et al. 2010, Benn and Westerhoff 2008, Geranio et al. 2009). Results from mass flow analyses indicate that the largest fraction of Ag-NP will reach a wastewater treatment plant (WWTP) (Sun et al. 2014). A high removal efficiency of ~95% has been observed for Ag-NP in WWTP. Consequently, ~5% of the Ag introduced as Ag-NP will reach the surface waters through the effluent of the WWTP (Gottschalk et al. 2009).

In sewer systems and in WWTP, Ag-NP (including both metallic Ag- and AgCl-NP) are mainly transformed by sulfidation, resulting in nano-sized silver sulfide particles (nano-Ag_2S). Only a minor fraction of the metallic Ag-NP, at least partially sulfidized, is expected to reach surface waters (Kaegi et al. 2013, Kaegi et al. 2011, Kaegi et al. , Lombi et al. 2013, Ma et al. 2013). Due to the ongoing reaction of Ag-NP with metal sulfides in urban surface waters, it is expected that the sulfidation of Ag-NP continues in oxygenated surface waters and will be completed within days to weeks (Thalmann et al. 2014). Ag_2S shows a substantially reduced toxic response towards aquatic and terrestrial organisms compared to metallic Ag-NP (Fabrega et al. 2011, Levard et al. 2013, Reinsch et al. 2012), due to its very low solubility in aquatic systems. Ag_2S is rather resistant towards oxidation and it remained stable for 30 days in oxic waters (Levard et al. 2011) and in sewage sludge during a composting period of 6 months (Lombi et al. 2013).

Considerable loads of organic micropollutants pass WWTPs and negative impacts on the aquatic fauna and flora in the receiving waters are expected on a long-term (Schwarzenbach et al. 2006). To mitigate the ecological impacts of micropollutants, an ozone treatment of the effluent water has been suggested to degrade the micropollutants (Joss et al. 2008, von Sonntag and von Gunten 2012). In Switzerland, about 100 WWTP will, therefore, be upgraded with an additional treatment (ozone and powdered activated carbon (PAC)) stage and similar measures are currently discussed in Germany and other countries.

In addition to the beneficial effect of degrading micropollutants, the treatment of effluent water with ozone may also affect the speciation of inorganic redox-sensitive compounds, including nano-Ag_2S. The oxidative dissolution of metallic Ag-NP with ozone has been investigated in aqueous solutions (Morozov et al. 2011, Yuan et al. 2013). The reaction of ozone with Ag_2S, the most relevant form of Ag in treated wastewater, however, has not been addressed to date.

The objectives of this study were, thus, to investigate the reaction of nano-Ag_2S particles with ozone and to evaluate the effect of the ozone treatment on the Ag induced short-term toxicity of the WWTP effluent. We determined the stoichiometry for the reaction of ozone with nano-Ag_2S and derived the second order rate constant for the reaction of nano-Ag_2S with ozone by competition kinetics. The size, morphology and chemical speciation of the reaction products in effluent water were determined using transmission electron spectroscopy (TEM) and X-ray absorption spectroscopy (XAS) at the Ag K-edge. Furthermore, we assessed the toxicity of effluent water spiked with nano-Ag_2S before and after ozonation by measuring the decrease of the photosynthetic yield of the freshwater algae *Chlamydomonas reinhardtii* exposed to the respective solutions.

4.3 Materials and Methods

Starting Materials

Nano-Ag_2S was synthesized by rapidly mixing 50 mL 3.7 mM silver nitrate solution ($AgNO_3$, Merck) with 50 mL of a 1.9 mM sodium hydrogen sulfide solution (NaSH, Alfa Aesar) (both solutions prepared in doubly deionized water (DDI; Millipore, 18.2 MΩ cm) and with 10^{-5} M NaOH). This resulted in the immediate precipitation of nanoscale Ag_2S. The suspension was sonicated for 20 min in a sonication bath (38 W L^{-1}, Bioblock Scientific) to disperse the particles. For the synthesis no stabilizing agents (organics) were used due to possible reactions of the organics with ozone. The nano-Ag_2S were collected for analysis by transmission electron microscopy (TEM), dynamic light scattering (DLS) and electrophoretic mobility measurements (zeta potential) as described in Thalmann, et al. (Table C.1) (Thalmann et al. 2014). The negative zeta potential (-39.8 mV) of the nano-Ag_2S particles prevented their agglomeration and the colloidal suspensions remained stable over several months.

Ozone stock solutions (1.3-1.5 mM O_3) were produced by bubbling ozone-containing O_2 gas (produced with an ozone generator CMG 3-3, Innovatec) through deionized water (for all experiments doubly deionized (DDI) water was used, Millipore, 18.2 MΩ cm), which was cooled in an ice bath. The ozone concentration of the stock solution was determined in a UV-Vis spectrometer (ε = 3200 L mol^{-1} cm^{-1} at 260 nm, Cary 100, Varian) (Lee et al. 2013).

Effluent water was obtained from a pilot WWTP (activated sludge process including primary clarification, nitrification, denitrification and secondary clarification) operated at Eawag (Kaegi et al. 2011). The WWTP effluent was characterized for dissolved organic carbon (DOC, Shimadzu TOC-L CSH), pH (SevenEasy, Mettler Toledo), chloride (Compact IC Flex 930, Metrosep A Supp 5 100/4.0, Metrohm), nitrate (Dr. Lange cuvettes LCK 339), ortho-phosphate (LCK 348) and chemical oxygen demand (COD, LCK 414). In addition, the concentration of copper (Cu) and zinc (Zn) in the effluent water was determined using inductively coupled plasma – optical emission spectroscopy (ICP-OES). Samples were filtered (GF/F filters, 0.7 µm, Whatman) before analysis, except for the pH measurements and for the elemental analysis.

Stoichiometry of the nano-Ag_2S-Ozone Reaction

The reaction of ozone with Ag_2S results in the oxidation of sulfide to sulfate (SO_4^{2-}), the production of O_2 and the release of two Ag^+ per SO_4^{2-} (Eq. 4.1, up to 7.8 g Ag_2SO_4 L^{-1} is soluble in water) (Haynes 2014).

$$Ag_2S + aO_3 \xrightarrow{k_{Ag2S}} 2Ag^+ + SO_4^{2-} + bO_2 \qquad \text{Eq. 4.1}$$

The stoichiometry of the reaction ($b=(a\times3-4)/2$) can thus be determined by reacting known amounts of ozone with Ag_2S and measuring the newly formed SO_4^{2-}. Selected doses of ozone ranging from 0 to 100 µM were mixed with 12.5 µM nano-Ag_2S. The pH of the solution was buffered with borate (pH 8.0, 10 mM). Tert-butanol (5 mM) was used as a radical scavenger to exclude unspecific side reactions through hydroxyl radicals (Lee et al. 2013). During the ozone addition, the solution was vigorously stirred. The amount of nano-Ag_2S reacting with ozone was derived from the total sulfate concentration measured by ionic chromatography after completion of the reaction (IC; ICS3000, AS9HC, Dionex, eluent: 9 mM Na_2CO_3 / 2 mM NaOH, QL = 5 µg L^{-1}). Samples for IC analysis were prepared by filtration through 10 kDa centrifugal membranes (Vivaspin 20, santorius stedim biotech, 10 min, 3100 g), followed by the removal of Ag^+ from the filtrates with OnGuard II H-cartridges (Dionex). Dissolved (<10 kDa) Ag in the filtrates was measured by inductively coupled plasma – mass spectroscopy (ICP-MS).

Rate Constant of the nano-Ag_2S-Ozone Reaction

The reaction of nano-Ag_2S with ozone was too fast to be monitored by online UV-Vis measurements and absorption spectra of ozone were affected by the presence of nano-Ag_2S. Therefore, the rate constant (k_{Ag2S}) of the rate-determining step of the reaction of nano-Ag_2S with ozone was determined with an approach based on competition kinetics described in detail by von Sonntag and von Gunten (2012). The method relies on accurate data of the rate constant of the competitor (buten-2-ol, $k_{Bu} = 7.9 * 10^4$ M^{-1} s^{-1}) and has successfully been applied to determine the rate constants for the reaction of ozone with micropollutants such as diclofenac (Sein et al. 2008). Competition experiments were conducted with buten-2-ol as a competitor to nano-Ag_2S (Munoz and von Sonntag 2000). The rate-determining step was assumed to be a second-order type reaction (Eq. 4.2).

$$r_{Ag_2S} = \frac{d[Ag_2S]}{dt} = k_{Ag_2S} \times [Ag_2S] \times [O_3] \qquad \text{Eq. 4.2}$$

At constant and relatively low ozone doses ($[O_3] < \Sigma$ ($[Ag_2S]$, [Buten-2-ol])) the rate constant for the reaction of ozone with Ag_2S can be derived from Eq. 4.3 (see Appendix C for a more detailed derivation).

$$\frac{[CH_2O]_0}{[CH_2O]} - 1 = \frac{k_{Ag_2S}}{k_{Bu}} \times \frac{[Ag_2S]}{[Buten-2-ol]} \qquad \text{Eq. 4.3}$$

$[CH_2O]_0$ and $[CH_2O]$ refer to the formaldehyde produced by the reaction of buten-2-ol with ozone in absence and presence of nano-Ag_2S, respectively. Nano-Ag_2S (16, 32, 48, 72 or 92 µM) and buten-2-ol (50, 80 or 100 µM) were spiked to 50 mL of 5 mM tert-butanol containing DDI water buffered to pH 8.0 (10 mM borate buffer), resulting in varying nano-Ag_2S to buten-2-ol ratios ($[Ag_2S]$ / [buten-2-ol]). A specific ozone dose (48 µM) was added to every vial. Formaldehyde (CH_2O) was determined according to the Hantzsch method (Nash 1953). One mL of solution was mixed with Nash's reagent (2 M ammonium acetate, 0.05 M acetic acid, 0.02 M acetylacetone) and reacted for 5 min in a water bath at 58°C. Before measuring the UV-Vis absorption at 412 nm, 2 mL of the reacted suspensions were centrifuged (1h, 27000 g) to remove the interfering nano-Ag_2S.

Ozone Treatment of Nano-Ag_2S Spiked Effluent Water

Hundred mL of WWTP effluent was collected in glass bottles (250 mL). Based on the measured DOC concentration, DDI water was added to adjust the DOC concentration in the effluent to 4 mg L^{-1}. Nano-Ag_2S (11.5 µM) was spiked to the samples which were then reacted with varying specific ozone doses defined as g O_3 per g DOC (g_{O3} / g_{DOC} = 0.25 – 1.5) in batch experiments. The ozone-treated solutions (0.5 mL) were filtered through centrifugal membranes (10 kDa, Vivaspin 500, santorius stedim biotech) to isolate dissolved Ag present as Ag^+ or bound to low molecular organic substances. This Ag fraction is referred to as Ag_{free} fraction. Additionally 0.5 mL of the ozone-treated solutions were mixed with 50 µL concentrated ammonia (25%, analysis, Merck) before centrifugal ultra-filtration. Ammonia forms a diammine-complex with Ag^+ (dissociation constant $K = [Ag^+]\times[NH_3]^2 = 6\times10^{-8}$ mol^2 L^{-2}) (Derr et al. 1941), leading to the dissolution of AgCl ($K_{sp} = 1.8\times10^{-10}$ mol^2 L^{-2}) and other silver salts at elevated NH_3 concentration but preserving Ag_2S ($K_{sp} = 6\times10^{-51}$ mol^3 L^{-3}).(2014) The fraction of Ag extracted with NH_3 is referred to as Ag_{NH3}.

The influence of chloride, phosphate and organics on the speciation and transformation during ozonation of nano-Ag_2S was assessed in separate experiments. Humic acid (Sigma Aldrich, 53680, technical grade) was used as a proxy for dissolved organic matter (DOM). Four mg L^{-1} humic acid with 5.6 µM nano-Ag_2S buffered to pH 8.0 (borate buffer, 10mM) were spiked with ozone (g_{O3} / g_{DOC} = 0.24

– 1.5) in absence and presence of typical effluent water concentrations of chloride (3.75 mM) and phosphate (0.1 mM).

Effect of Ozone Treatment on the Toxicity of nano-Ag_2S in WWTP Effluent

To assess the toxicity of the ozone treated and untreated effluent water spiked with Ag_2S, dose-response experiments with the single cell green algae *Chlamydomonas reinhardtii* were performed. *Chlamydomonas reinhardtii* (CC-125) obtained from the Chlamydomonas Genetics Center (Durham, USA) was cultured in the model fresh water growth medium Talaquil (pH 7.5) as described in Scheidegger et al. (2011). Cells were separated from the medium by centrifugation (10 min, 1500 g) during the exponential growth phase of the algal culture and the cell number was determined using a cell counter (Z2 Coulter Counter, Beckman Coulter). Algae were spiked to 15 mL of exposure medium to obtain a final concentration of 1.7 x 10^5 cells mL^{-1}.

As an exposure media either untreated or ozone treated WWTP effluent buffered to pH 7.5 using MOPS buffer (10 mM) was used. For experiments that included an ozone treatment, pristine and spiked (5 µM Ag_2S) WWTP effluents were treated with ozone. A typical specific ozone dose for the treatment of WWTP effluent is ~ 1 g_{O3} / g_{DOC} (Lee et al. 2013). To account for the ozone consumed by the sulfide oxidation the ozone doses were adjusted based on the stoichiometry of this reaction (for 5 µM Ag_2S additional 14.3 µM O_3 were added). Ozonated samples (pristine and spiked with Ag_2S) were stored in PE plastic bottles in the dark overnight. Exposure media of differing Ag concentrations (0 – 10 µM) were prepared by mixing the two ozonated solutions at the respective ratios. In addition, analogous experiments were conducted without ozone treatment (0 – 175 µM Ag as Ag_2S). Additional exposure media containing $AgNO_3$ in untreated effluent water were prepared in the same manner.

The toxicity was determined by measuring the algal photosynthetic yield of the photosystem II in light after 1 h and 2 h. The photosynthetic yield was measured by fluorometry using a PHYTO-PAM (Heinz Walz GmbH) equipped with an optical unit (ED-101US/MP). The yield was expressed as percentage of the respective control sample and plotted against the total Ag concentrations. A four-parameter logistic curve was fitted to the data using the statistic program R including the drc (analysis of dose-response curve data) package (Ritz and Streibig 2005, Team 2012). Experiments with nano-Ag_2S were performed in triplicates, $AgNO_3$ as singles.

Inductively Coupled Plasma - Mass Spectrometry (ICP-MS)

Total Ag concentrations from the toxicity tests and total Zn and Cu concentrations in the effluent water were determined by digesting 1 mL of sample with 1 mL HNO_3 (65%, ultrapure, Merck) and 200 µL H_2O_2 (35%, Merck) using a microwave assisted acid digestion system (UltraClave 3, MLS GmbH). For Ag analyses, acidified samples from centrifugal ultra-filtration (1% HNO_3) and samples from total

digestion were diluted to obtain Ag concentrations of ~1-10 µg L^{-1}. Measurements were performed against an external calibration using inductively coupled plasma mass spectrometry (ICP-MS, Agilent 7500cx, QL = 0.2 µg L^{-1}). Rhodium (m/z 103) was used as an internal standard to correct for non-spectral interferences. Zn and Cu were measured with a inductively coupled plasma optical emission spectrometer (ICP-OES, Cirus^{CCD}, SPECTRO Analytical Instruments GmbH, D).

Speciation of Ag

The speciation of Ag after ozone treatment of nano-Ag_2S spiked samples (11.5 µM Ag_2S) was determined by Ag K-edge X-ray absorption spectroscopy (XAS). The suspended particles were flocculated by adding $NaNO_3$ (analysis grade, Merck; to achieve a Na^+ concentration of 1 M) and 200 mg cellulose and separated by centrifugation (10 min, 3100 g). The sediments were pressed into a 13-mm diameter copper mold, dewatered with a paper tissue and immediately frozen in liquid nitrogen. The 13-mm pellets were kept frozen at -20°C until analysis.

XAS was performed at the Ag K-edge (25'414 eV) at the SuperXAS (X10DA) beamline at the Swiss Light Source (SLS, Villigen, Switzerland). During measurements the samples were cooled using a CryoJet (Oxford Instruments, UK) with a N_2 gas stream adjusted to 100 K. Reference samples of Ag_2S and AgCl (both from Alfa Aesar) were prepared as pellets and measured in transmission mode. XAS data extraction and evaluation was performed using Athena (Ravel and Newville 2005) as previously described (Kaegi et al. 2013, Kaegi et al. 2011, Thalmann et al. 2014).

Electron Microscopy

Particles from Ag_2S spiking experiments were characterized before and after O_3 treatment with a scanning transmission electron microscope (STEM, HD-2700-Cs, Hitachi, Japan). Samples for TEM analyses were prepared by either drop-on-grid deposition or direct on-grid centrifugation using carbon coated copper grids (PlanoEM or Quantifoil, DE) (Mavrocordatos et al. 1994, Mavrocordatos and Perret 1995). Images were recorded using either a bright field (BF) or a high-angular annular dark field (HAADF) detector. High resolution images were processed using Digital Micrograph (v1.85, Gatan). Elemental analysis of individual particles was performed using an energy dispersive X-ray detector (EDAX) and the spectra were recorded and processed using Digital Micrograph.

4.4 Results

Nano-Ag_2S and Effluent Water Characterization

Electrophoretic mobility and dynamic light scattering measurements of the fresh nano-Ag_2S indicated a zeta potential of -39.8 mV and a hydrodynamic diameter of ~60 nm (polydispersity index (PDI) = 0.41), respectively (90 µM Ag_2S measured in 10 mM borate buffer, pH 8.0). TEM images revealed rod-shaped Ag_2S particles (maximum particle diameter > 1.5 minimum particle diameter; ~60% of 105 analyzed particles) with dimensions of 57.5±15.2 × 19.3±3.9 nm and spherical Ag_2S nanoparticles with a diameter of 25.1±9.3 nm (Figure C.1). A more detailed summary of the particle characteristics is given in Table C.1. The characteristics of the effluent water are given in Table C.2.

Stoichiometry of the Reaction of Nano-Ag_2S with Ozone

To determine the stoichiometry of the reaction of Ag_2S with ozone, the sulfate concentrations resulting from the oxidation of the sulfide were plotted against the applied ozone dose (Figure 4.1A). The sulfate increased with increasing ozone dose and reached a plateau of ~12.5 µM sulfate at 35.6 µM ozone, corresponding to the maximum amount of sulfate that can be produced from 12.5 µM of Ag_2S. This indicates that at an ozone dose of 35.6 µM, all Ag_2S-sulfur has been oxidized to sulfate. Linear regression of the sulfate concentration against the ozone dose (excluding the last measurement point where ozone was present in excess), resulted in a straight line with a slope of 0.343(5) ($r^2 = 1.0$, standard error (1σ) in brackets). This slope corresponds to moles of SO_4^{2-} molecules produced by the reaction of Ag_2S with one mole ozone. Thus, 2.91 moles ozone were required to oxidize 1 mole S(-II) in Ag_2S to S(+VI) (Eq. 4.1, $a = 2.91$, $b = 2.37$).

Rate Constant for the Reaction of Nano-Ag_2S with Ozone

The rate constant of the reaction of nano-Ag_2S with ozone was determined from competition kinetics with buten-2-ol as competitor. Formaldehyde, the oxidation product of buten-2-ol, was measured. The rate constant of the reaction was derived according to Eq. 4.3 by linear regression (Figure 4.1B; for details see Appendix C). The slope of the regression line (0.40(1)) corresponding to the ratio of the second order rate constants k_{Bu}/k_{Ag2S} was used to calculate k_{Ag2S} ($3.1(1)\times10^4$ M^{-1} s^{-1}, Eq. 4.2).

Ozone Treatment of WWTP Effluent Spiked with Nano-Ag_2S

During the ozonation of effluent, DOM oxidation will be in competition to the oxidation of nano-Ag_2S. To study the influence of DOM on the extent of the oxidation of Ag_2S, experiments were conducted in a simplified system with DDI water spiked with 2.8 µM Ag_2S in the presence of humic acid as a proxy for DOM. Both the Ag_{free} fraction and the Ag_{NH3} fraction representing the sum of the "free" fraction and NH_3-soluble Ag species, reached the concentration expected for total oxi-

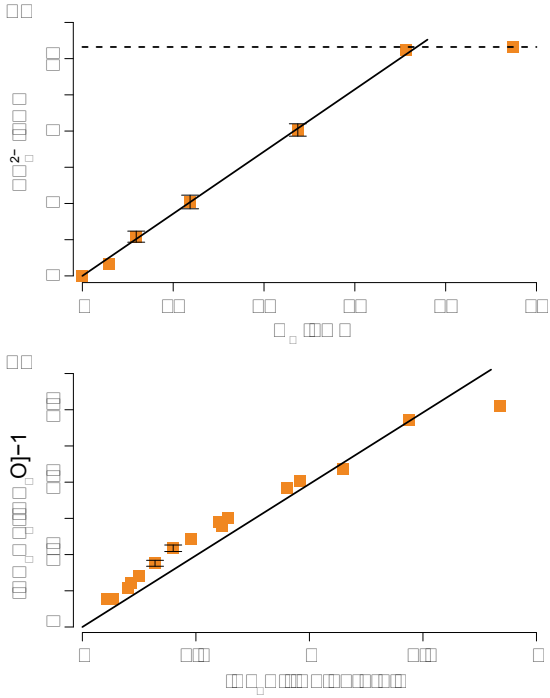

Figure 4.1: A: Ozone concentrations plotted against sulfate (SO_4^{2-}) concentrations (error bars = 1σ from triplicate experiments). Dashed line represents the sulfate concentration resulting from the complete oxidation of the spiked nano-Ag_2S (12.5 µM). The slope of the linear regression (line) to the first six sulfate measurements is equal to 0.343(5) with r^2 = 1.00. **B:** $[CH_2O]_0/[CH_2O]$-1, derived from measured formaldehyde concentrations, against $[Ag_2S]/[Buten\text{-}2\text{-}ol]$. The slope of the linear regression is 0.40(1) (r^2 = 0.95) which corresponds to k_{Bu}/k_{Ag2S}, resulting in a rate constant (k_{Ag2S}) of 3.1(1) ×10^4 M^{-1} s^{-1} (error bars = 1σ from experiments with the same $[Ag_2S]/[Buten\text{-}2\text{-}ol]$ ratio (0.x and 0.y), but different absolute concentrations ($[Ag_2S]/[Buten\text{-}2\text{-}ol]$ = 0.32: Ag_2S = 16 and 48 µM; $[Ag_2S]/[Buten\text{-}2\text{-}ol]$ = 0.40: $[Ag_2S]$ = 20 and 32 µM)

dation of the Ag_2S already at the lowest experimental ozone dose (0.24 g_{O3} / g_{DOC} corresponding to 20 µM O_3, Figure 4.2A).

To investigate the effects of anions (*e.g.* Cl^- and PO_4^{3-}) on the speciation of Ag after ozonation, experiments with humic acid, Cl^- and PO_4^{3-} were performed. The Ag_{NH3} fraction showed an almost identical trend as observed in the absence of these

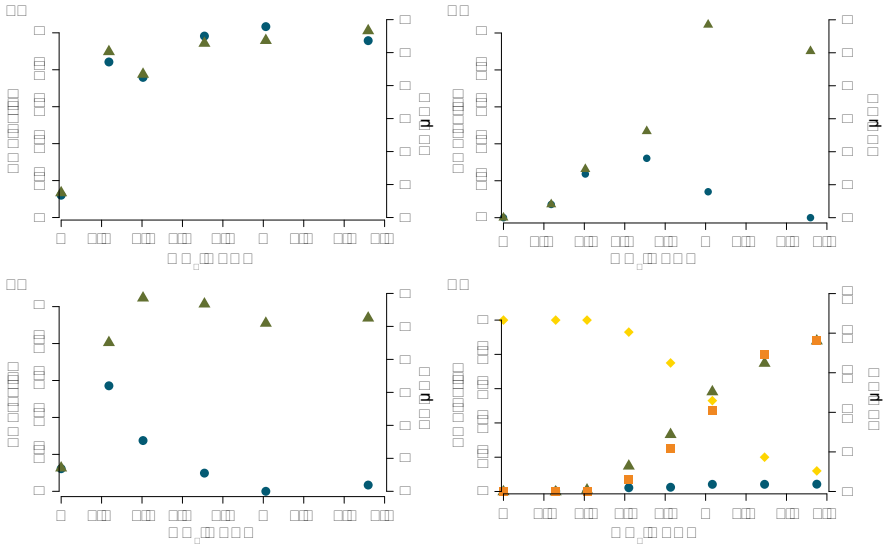

Figure 4.2: Dissolved Ag (Ag_{free}: blue circles), NH_3-soluble Ag (Ag_{NH3}: green triangles) and EXAFS LCF-derived Ag_2S (yellow diamonds) and AgCl (orange squares) fractions of the total Ag concentrations (**A, B & C:** 2.8 µM, **D:** 11.5 µM) versus specific ozone to DOC (4 mg L^{-1}) doses. Nano-Ag_2S was spiked to DDI water (buffered with 10 mM borate to pH 8.0) containing humic acid (4 mg L^{-1}, used as a proxy for DOM) in the absence (**A**) and presence (**B**) of chloride (3.75 mM) and phosphate (0.1 mM) and to WWTP effluent (**C & D**). The right axis refers to the Ag concentrations of the respective Ag fractions. The LCF fractions are scaled to the total Ag concentration spiked to the WWTP effluent.

anions (Figure 4.2B). However, the Ag_{free} fraction was only elevated at the lowest specific ozone dose and then gradually decreased to below the detection limit at a specific ozone dose of 1 g_{O3} / g_{DOC}.

To assess the impact of an ozone treatment on the fate of Ag_2S under WWTP-relevant conditions, nano-Ag_2S (2.8 µM and 11.5 µM) was spiked to WWTP effluent and the speciation of Ag was investigated as a function of the specific ozone dose (Figure 4.2C, D. At lower nano-Ag_2S concentrations, the Ag_{NH3} fraction increased steadily with specific ozone doses and reached the concentration corresponding to the total oxidation of Ag_2S at a specific ozone dose of 1 g_{O3} / g_{DOC}. The Ag_{free} fraction reached a maximum between 0.4 and 0.6 g_{O3} / g_{DOC} (Figure 4.2C). At higher nano-Ag_2S concentrations the Ag_{NH3} fraction only increased at O_3 doses > 0.4 g_{O3} / g_{DOC} and did not reach the expected Ag concentration based on a total oxidation of the

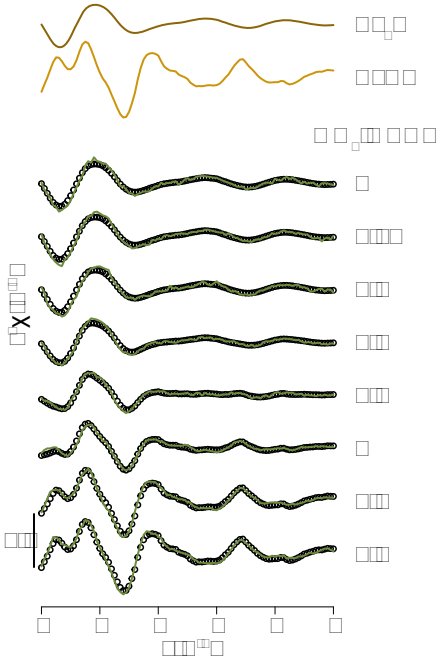

Figure 4.3: EXAFS spectra of reference and experimental samples from Figure 2D (lines) and reconstructed LCF spectra (open circles) using Ag_2S and AgCl as reference spectra. For clarity the spectra are plotted with an offset of 0.1. The LCF-derived fractions of Ag_2S and AgCl are given in Figure 4.2D.

spiked Ag_2S. The Ag_{free} fraction only slightly increased with specific ozone dose but always stayed below 1 µM (Figure 4.2D).

To determine the Ag speciation in the ozone treated WWTP effluent bulk suspension in more detail and to better characterize the Ag_{NH3} fraction, Ag K-edge XAS was performed. The EXAFS spectra of the ozone treated samples and of reference materials are given in Figure 4.3. Ag speciation was assessed by a LCF analysis using the spectra of Ag_2S and AgCl as references. The resulting fractions using the EXAFS spectra for the linear-combination fitting (LCF) analysis are given in Figure 4.2D and comparable results were also obtained with the XANES spectra (Figure C.2 and C.3). The increase of the AgCl fraction with increasing ozone dose closely matched the increase of the Ag_{NH3} fraction, supporting the assumption that NH_3 allowed to selectively probe dissolved Ag and AgCl but not Ag_2S (Figure 4.2D).

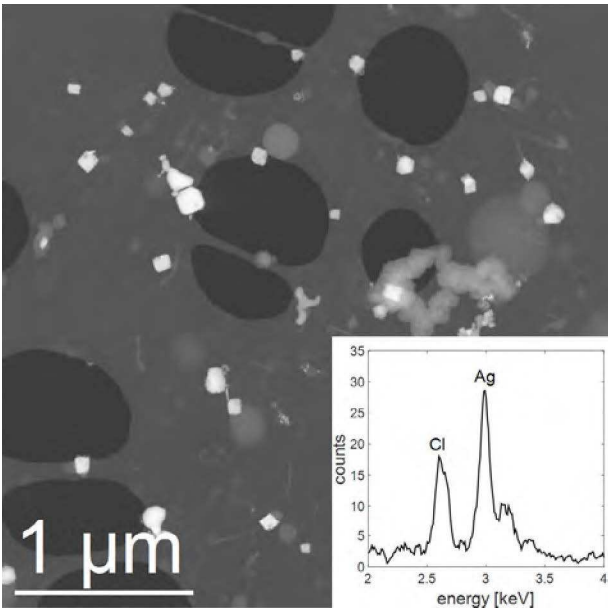

Figure 4.4: TEM (HAADF) image and EDX spectrum (inset) of particles collected from Ag_2S-spiked WWTP effluent after ozonation.

TEM analysis of samples collected from the effluent water after ozonation revealed the formation of cubic particles with an equivalent spherical diameter of 50 nm – 200 nm (Figure 4.4). EDX analysis of selected cubes clearly indicated Ag and Cl and no detectable S (Figure 4.4 inset) confirming that the cubes represented AgCl particles that most probably formed after the release of Ag+ by Ag2S oxidation.

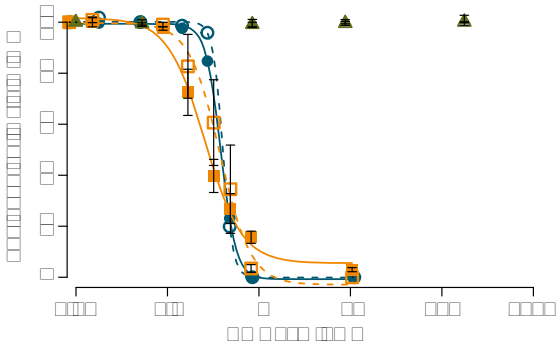

Figure 4.5: Dose-response curves of the photosynthetic yield of *Chlamydomonas reinhardtii* after 1 h (filled symbols and solid line) and 2 h (open symbols and dashed line) of exposure to nano-Ag_2S-spiked WWTP effluent after ozonation (orange squares) and to $AgNO_3$-spiked untreated effluent water (blue circles). The dose-response curve for nano-Ag_2S spiked to untreated WWTP effluent is displayed in green triangles. Nano-Ag_2S experiments and measurements were done in triplicates, $AgNO_3$ experiments were done as singles.

Table 4.1: Effect Concentration (EC) Values Derived from the Photosynthetic Yield of *Chlamydomonas reinhardtii* Determined with a Logistic Model[a] and Expressed as Total Ag Concentration.

Treatment	Time [h]	EC_{50} (Ag) [µM][b]	Number of experiments
Ag_2S and O_3	1	0.256(15)	3
	2	0.375(31)	3
$AgNO_3$ in untreated effluent water	1	0.383(4)	1
	2	0.403(6)	1

No short-term effect was found for Ag_2S (triplicates) spiked to untreated WWTP effluent water.

[a]Logistic model: %photosynthetic yield = min + ((max-min)/1+($[Ag]_{total}/EC_{50}$)^{Hillslope})

[b]Standard error (1σ) is given in brackets

Effect of the Ozonation on the Toxicity of Nano-Ag_2S Spiked WWTP Effluent

Increasing concentrations of nano-Ag_2S (up to 175 µM) spiked to WWTP effluent did not show any influence on the algal photosynthetic yield (n = 3). However, ozonation of effluent water spiked with increasing amounts of Ag_2S reduced the photosynthetic yield (Figure 4.5). The dose-response curve was described with a logistic model (Table 4.1). The EC_{50} value increased from 0.256(15) µM after 1 h exposure time to 0.375(31) µM after 2 h exposure time (n = 3, Table 4.1). EC_{50} values obtained for $AgNO_3$-spiked effluent water were comparable to the EC_{50} values obtained for nano-Ag_2S-spiked effluent after ozonation (Table 4.1, Figure 4.5).

4.5 Discussion

Oxidative Dissolution of Nano-Ag_2S by Ozonation

Ozone is a strong oxidant with a maximum of two accepted electrons for oxygen transfer reactions (von Sonntag and von Gunten 2012). Thus, for the oxidation of sulfide (-II) to sulfate (+VI), releasing eight electrons, four ozone molecules would be required. However, experimental observations of the oxidation of bisulfide (HS^-) with ozone suggest that only 2.4 ozone molecules are needed to oxidize one sulfide to sulfate. Density functional theory (DFT) investigations of the reaction of sulfide with ozone identified two major reaction pathways. One pathway needs the postulated four ozone molecules, but the other requires only two ozone molecules as sulfinic peracid ($HS(O)OO^-$) is formed as an intermediate and, therefore, more than two electrons can be transferred to one ozone molecule (Mark et al. 2011). We found that 2.91 mole of ozone are required to fully oxidize the sulfide from one mole of nano-Ag_2S. Hence, slightly more ozone is needed to oxidize the Ag-bound sulfide compared to the HS^-, but still significantly less than predicted based on the assumption of a two electron transfer per ozone molecule.

Increasing ozone doses also resulted in increasing Ag^+ concentration but only at ozone doses > ~15 µM (Figure C.2). Furthermore, Ag^+ concentration did not exceed 20 µM (25 µM would have been expected for complete Ag_2S oxidation) which most probably reflected losses of Ag^+ to the walls of the reaction tubes.

The oxidation of bisulfide with ozone (k = ~10^9 M^{-1} s^{-1}; $t_{1/2}$ = 3.5×10^{-5} s, assuming pseudo-first-order kinetics with [O_3] = 20 µM) (Hoigné et al. 1985) is much faster than the oxidation of nano-Ag_2S (k = 3.1×10^4 M^{-1} s^{-1}, $t_{1/2}$ = 1.1 s). The slight deviation of the measurements from linearity (Figure 4.1B) may be taken as an indication that the reaction rate was limited by mass transfer (diffusion). We conducted our experiments with nano-Ag_2S that included individual particles close to 100 nm. If the reaction is mass-transfer limited, then smaller nano-Ag_2S will be oxidized even faster during the ozone treatment of the wastewater effluent. For the oxidation of nano-Ag_2S in effluent water the rate constant was comparable to bisphenol A (1.7×10^4 M^{-1} s^{-1}, $t_{1/2}$ = 2.0 s, pH = 7), an endocrine disruptor found in wastewater (Deborde et al. 2005). Even a 2.91 times smaller rate constant for the oxidation of Ag_2S (1.1×10^4 M^{-1} s^{-1}) as obtained when assuming complete oxidation of S(-II) to S(+VI) in the competitive reaction kinetics experiment (see Appendix C) would still be in the same range as the second order rate constant of other micropollutants. Furthermore, the Ag_2S particles used in this study were synthesized in the absence of organics. Ag_2S nanoparticles formed in the presence of organic compounds may be less crystalline than the particles studied here and may exhibit a higher sulfide oxidation rate. Based on these considerations, it is therefore reasonable to assume

that Ag_2S nanoparticles in WWTP effluent will be completely dissolved if the effluent is treated with ozone to remove micropollutants such as bisphenol A.

Ozone Treatment of WWTP Effluent Spiked with Nano-Ag_2S

In the experiments in which nano-Ag_2S spiked to WWTP effluent was treated with ozone, Ag_2S was oxidized and Ag was found in the Ag_{NH3} fraction. However, at higher nano-Ag_2S concentration (11.5 μM) the Ag_{NH3} fraction increased slowly and did not reach the expected concentration based on complete oxidation of the spiked Ag_2S (Figure 4.2D). Competition of DOM with Ag_2S for the reaction with ozone may explain the delayed and slow increase of Ag_{NH3} in the effluent water. As ozone was additionally consumed by DOM, there was not enough ozone available to oxidize all nano-Ag_2S even at higher specific ozone doses. In the experiments with less Ag_2S (2.8 μM), nano-Ag_2S was completely oxidized during treatment with a specific ozone dose of 1 g_{O3} / g_{DOC} (Figure 4.2C). The experiments conducted in the presence of humic acid and absence of other organics showed that the complete oxidation of the spiked nano-Ag_2S (2.8 μM) is immediate with a specific ozone dose of 0.24 g_{O3} /g_{DOC}, suggesting that humic acid only marginally interfered with the oxidation of Ag_2S (Figure 4.2A, B).

Based on thermodynamic calculations silver sulfate (Ag_2SO_4) is predicted to completely dissolve at the applied Ag concentrations but AgCl will precipitate (Figure C.5) (Puigdomenech 2013). LCF analysis of XAS spectra indicated that Ag was dominantly present in the form of Ag_2S and AgCl and at high ozone dosages, mainly AgCl was observed suggesting that the ozone treatment resulted in the oxidation of Ag_2S followed by precipitation of AgCl particles. The addition of NH_3 to the experimental suspensions containing AgCl resulted in the dissolution of AgCl due to the formation of a soluble complex $[Ag(NH_3)_2]^+$. The Ag fractions derived from the NH_3 extractions were in good agreement with the fraction of Ag assigned to AgCl resulting from LCF analysis of XAS spectra, supporting the hypothesis that the NH_3 extractions represent AgCl.

The Ag_{free} fraction found in experiments conducted at lower ozone doses most likely represented Ag complexed with DOM moieties, since equilibrium calculations including Ag-chloride complexes indicated an about eight times lower total dissolved Ag concentration (Figure 4.2C). These moieties may have become oxidized at higher specific ozone doses, and, therefore, this fraction decreased with increasing ozone dose. In the presence of humic acid, Cl^- and PO_4^{3-}, a similar pattern was observed for the Ag_{free} fraction, suggesting that the humic acid was to some extent able to complex the Ag at low ozone doses (Figure 4.2B).

The differences in shape (rod-like vs. cube-like) and size between the Ag_2S particles spiked to WWTP effluent and the AgCl particles formed after ozonation revealed by TEM analysis indicated that the transformation from Ag_2S to AgCl proceeded via an oxidative dissolution - reprecipitation pathway.

Effect of the Ozonation on the Toxicitity of Nano-Ag_2S Spiked to WWTP Effluent

Pristine nano-Ag_2S added to ozone treated effluent water showed no toxicity upon short-term exposure towards *Chlamydomonas reinhardtii*. Ag_2S is about four orders of magnitudes less toxic than Ag^+ (Leblanc et al. 1984, Ratte 1999), due to its very limited solubility and inertness under oxic conditions (Levard et al. 2011). These results indicate that nano-Ag_2S does not increase the toxicity towards *Chlamydomonas reinhardtii* compared to bulk-Ag_2S.

During ozone treatment nano-Ag_2S was oxidized, Ag cations were released into the experimental media and in the presence of Cl^- precipitated as AgCl. The EC_{50} values from respective experiments were only slightly higher than the reported EC_{50} values for $AgNO_3$ in MOPS buffer (Navarro et al. 2008). Thermodynamic calculations for a simplified system (Figure C.5) revealed that about 200 nM Ag are present as dissolved species (mainly $AgCl_2^-$ and Ag^+) under these experimental conditions. Thus, the observed toxicity may be explained by the dissolved Ag fraction in equilibrium with AgCl.

Chlamydomonas reinhardtii exposed to $AgNO_3$ spiked to (untreated) WWTP effluent resulted in EC_{50} values that were *i)* twice as high as EC_{50} values reported for Ag^+ (Navarro et al. 2008) and *ii)* substantially higher than EC_{50} values derived from exposure experiments conducted with nano-Ag_2S spiked effluent water after ozonation. The reduced toxicity of Ag^+ observed in this study compared to literature data can be explained by the formation of AgCl precipitates and the presence of organics in the effluent water which may complex or bind Ag cations strongly enough to further limit their bioavailability and therefore reduce the toxicity of Ag. Furthermore, we did not observe any significant differences for short-term toxicological effects towards *Chlamydomonas reinhardtii* between ozone treated and untreated effluent water.

Environmental Implications

The sulfidation of Ag-NP is known to strongly decrease the short and long term toxicity of Ag (Levard et al. 2013). Results from this study demonstrate that during an ozone treatment of WWTP effluent at specific ozone doses comparable to recommended values in full-scale WWTPs, nano-Ag_2S will be oxidized along with other micropollutants. Therefore, depending on the composition of the wastewater (concentration of Cl^- and other Ag ligands), the short-term toxicity of the effluent water may increase, due to the oxidation of Ag_2S and the concomitant release of Ag cations. In a recent study we reported Ag concentrations of a few tens of ng L^{-1} in the effluent of a full-scale WWTP (Kaegi et al.). Under such conditions, short term toxicological effects as observed in the current study are unlikely, which is in agreement with a recent study reporting a consistent decrease of the algal toxicity after ozonation of different wastewater effluents (Schindler Wildhaber et al. 2015).

However, considerably higher Ag concentrations in wastewater effluent (several µg L^{-1}) (Holler et al. 2007) and in sludge (800 mg kg^{-1}) (Kim et al. 2010) have been reported and ecotoxicological effects caused by the ozonation of such Ag-rich effluents cannot be completely ruled out.

Acknowledgements

We acknowledge the Electron Microscopy Centers at ETH Zurich (EMEZ, Zurich, Switzerland) and at Empa (Swiss Federal Institute for Materials Science and Technology, Duebendorf, Switzerland) for providing access to the microscopes. The Swiss Light Source (SLS, Villigen, Switzerland) is acknowledged for the allocation of beamtime. We thank Maarten Nachtegaal and Grigory Smolentsev (SLS) for support at the SuperXAS beamline (SLS). This work is part of the project "Behavior of silver nanoparticles in a wastewater treatment plant" within the Swiss National Research Program NRP 64 "Opportunities and Risks of Nanomaterials". Additionally we would like to thank Brian Sinnet, Bettina Wagner and Elisabeth Sahli for the support in the laboratories at Eawag.

References

Benn, T., Cavanagh, B., Hristovski, K., Posner, J.D. and Westerhoff, P. (2010) The Release of Nanosilver from Consumer Products Used in the Home Supplemental data file available online for this article. J. Environ. Qual. 39(6), 1875-1882.

Benn, T.M. and Westerhoff, P. (2008) Nanoparticle silver released into water from commercially available sock fabrics. Environ Sci Technol 42(11), 4133-4139.

Deborde, M., Rabouan, S., Duguet, J.-P. and Legube, B. (2005) Kinetics of Aqueous Ozone-Induced Oxidation of Some Endocrine Disruptors. Environ Sci Technol 39(16), 6086-6092.

Derr, P.F., Stockdale, R.M. and Vosburgh, W.C. (1941) Complex Ions. II. The Stability and Activity Coefficients of the Silver-Ammonia Ion1. J Am Chem Soc 63(10), 2670-2674.

Fabrega, J., Luoma, S.N., Tyler, C.R., Galloway, T.S. and Lead, J.R. (2011) Silver nanoparticles: behaviour and effects in the aquatic environment. Environ Int 37(2), 517-531.

Geranio, L., Heuberger, M. and Nowack, B. (2009) The behavior of silver nanotextiles during washing. Environ Sci Technol 43(21), 8113-8118.

Gottschalk, F., Sonderer, T., Scholz, R.W. and Nowack, B. (2009) Modeled environmental concentrations of engineered nanomaterials (TiO(2), ZnO, Ag, CNT, Fullerenes) for different regions. Environ Sci Technol 43(24), 9216-9222.

Haynes, W.M. (2014) CRC Handbook of Chemistry and Physics, CRC Press, Boca Raton, Fla.

Hoigné, J., Bader, H., Haag, W.R. and Staehelin, J. (1985) Rate constants of reactions of ozone with organic and inorganic compounds in water—III. Inorganic compounds and radicals. Water Research 19(8), 993-1004.

Holler, J.S., Nordberg, G.F. and Fowler, B.A. (2007) Handbook on the Toxicology of Metals (Third Edition). Nordberg, G.F., Fowler, B.A., Nordberg, M. and Friberg, L.T. (eds), pp. 809-814, Academic Press, Burlington.

Joss, A., Siegrist, H. and Ternes, T.A. (2008) Are we about to upgrade wastewater treatment for removing organic micropollutants? Water Science & Technology 57(2), 251-255.

Kaegi, R., Voegelin, A., Ort, C., Sinnet, B., Thalmann, B., Krismer, J., Hagendorfer, H., Elumelu, M. and Mueller, E. (2013) Fate and transformation of silver nanoparticles in urban wastewater systems. Water Res 47(12), 3866-3877.

Kaegi, R., Voegelin, A., Sinnet, B., Zuleeg, S., Hagendorfer, H., Burkhardt, M. and Siegrist, H. (2011) Behavior of metallic silver nanoparticles in a pilot wastewater treatment plant. Environ Sci Technol 45(9), 3902-3908.

Kaegi, R., Voegelin, A., Sinnet, B., Zuleeg, S., Siegrist, H. and Burkhardt, M. (2015) Transformation of AgCl nanoparticles in a sewer system - A field study. Sci Total Environ (0).

Kim, B., Park, C.-S., Murayama, M. and Hochella, M.F. (2010) Discovery and Characterization of Silver Sulfide Nanoparticles in Final Sewage Sludge Products. Environ Sci Technol 44(19), 7509-7514.

Leblanc, G.A., Mastone, J.D., Paradice, A.P., Wilson, B.F., Jr, H.B.L. and Robillard, K.A. (1984) The influence of speciation on the toxicity of silver to fathead minnow (Pimephales promelas). Environmental Toxicology and Chemistry 3(1), 37-46.

Lee, Y., Gerrity, D., Lee, M., Bogeat, A.E., Salhi, E., Gamage, S., Trenholm, R.A., Wert, E.C., Snyder, S.A. and von Gunten, U. (2013) Prediction of Micropollutant Elimination during Ozonation of Municipal Wastewater Effluents: Use of Kinetic and Water Specific Information. Environ Sci Technol 47(11), 5872-5881.

Levard, C., Hotze, E.M., Colman, B.P., Dale, A.L., Truong, L., Yang, X.Y., Bone, A.J., Brown, G.E., Jr., Tanguay, R.L., Di Giulio, R.T., Bernhardt, E.S., Meyer, J.N., Wiesner, M.R. and Lowry, G.V. (2013) Sulfidation of silver nanoparticles: natural antidote to their toxicity. Environ Sci Technol 47(23), 13440-13448.

Levard, C., Reinsch, B.C., Michel, F.M., Oumahi, C., Lowry, G.V. and Brown, G.E. (2011) Sulfidation processes of PVP-coated silver nanoparticles in aqueous solution: impact on dissolution rate. Environ Sci Technol 45(12), 5260-5266.

Lombi, E., Donner, E., Taheri, S., Tavakkoli, E., Jämting, Å.K., McClure, S., Naidu, R., Miller, B.W., Scheckel, K.G. and Vasilev, K. (2013) Transformation of four silver/silver chloride nanoparticles during anaerobic treatment of wastewater and post-processing of sewage sludge. Environmental Pollution 176, 193-197.

Ma, R., Levard, C., Judy, J.D., Unrine, J.M., Durenkamp, M., Martin, B., Jefferson, B. and Lowry, G.V. (2013) Fate of zinc oxide and silver nanoparticles in a pilot waste water treatment plant and in processed biosolids. Environ Sci Technol.

Mark, G., Naumov, S. and von Sonntag, C. (2011) The Reaction of Ozone with Bisulfide (HS−) in Aqueous Solution – Mechanistic Aspects. Ozone: Science & Engineering 33(1), 37-41.

Mavrocordatos, D., Lienemann, C.-P. and Perret, D. (1994) Energy filtered transmission electron microscopy for the physico-chemical characterization of aquatic submicron colloids. Microchimica Acta 117(1-2), 39-47.

Mavrocordatos, D. and Perret, D. (1995) Non-artifacted specimen preparation for transmission electron microscopy of submicron soil particles. Communications in Soil Science & Plant Analysis 26(15-16), 2593-2602.

Morozov, P.A., Abkhalimov, E.V., Chalykh, A.E., Pisarev, S.A. and Ershov, B.G. (2011) Interaction of silver nanoparticles with ozone in aqueous solution. Colloid Journal 73(2), 248-252.

Munoz, F. and von Sonntag, C. (2000) Determination of fast ozone reactions in aqueous solution by competition kinetics. Journal of the Chemical Society, Perkin Transactions 2 (4), 661-664.

Nash, T. (1953) The colorimetric estimation of formaldehyde by means of the Hantzsch reaction. Biochem. J. 55(3), 416-410.

Navarro, E., Piccapietra, F., Wagner, B., Marconi, F., Kaegi, R., Odzak, N., Sigg, L. and Behra, R. (2008) Toxicity of Silver Nanoparticles to Chlamydomonas reinhardtii. Environ Sci Technol 42(23), 8959-8964.

Puigdomenech, I. (2013) MEDUSA (Making Equilibrium Diagrams/Using Sophisticated Algorithms), Royal Institute of Technology: Stockholm.

Ratte, H.T. (1999) Bioaccumulation and toxicity of silver compounds: A review. Environmental Toxicology and Chemistry 18(1), 89-108.

Ravel, B. and Newville, M. (2005) ATHENA , ARTEMIS , HEPHAESTUS : data analysis for X-ray absorption spectroscopy using IFEFFIT. Journal of Synchrotron Radiation 12(4), 537-541.

Reinsch, B.C., Levard, C., Li, Z., Ma, R., Wise, A., Gregory, K.B., Brown, G.E., Jr. and Lowry, G.V. (2012) Sulfidation of silver nanoparticles decreases Escherichia coli growth inhibition. Environ Sci Technol 46(13), 6992-7000.

Ritz, C. and Streibig, J. (2005) Bioassay Analysis using R. Journal of Statistical Software 12(5).

Russell, A.D. and Hugo, W.B. (1994) Antimicrobial activity and action of silver. Prog Med Chem 31, 351-370.

Scheidegger, C., Behra, R. and Sigg, L. (2011) Phytochelatin formation kinetics and toxic effects in the freshwater alga Chlamydomonas reinhardtii upon short- and long-term exposure to lead(II). Aquatic Toxicology 101(2), 423-429.

Schindler Wildhaber, Y., Mestankova, H., Schärer, M., Schirmer, K., Salhi, E. and von Gunten, U. (2015) Novel test procedure to evaluate the treatability of wastewater with ozone. Water Research 75(0), 324-335.

Schwarzenbach, R.P., Escher, B.I., Fenner, K., Hofstetter, T.B., Johnson, C.A., von Gunten, U. and Wehrli, B. (2006) The Challenge of Micropollutants in Aquatic Systems. Science 313(5790), 1072-1077.

Sein, M.M., Zedda, M., Tuerk, J., Schmidt, T.C., Golloch, A. and Sonntag, C.v. (2008) Oxidation of Diclofenac with Ozone in Aqueous Solution. Environ Sci Technol 42(17), 6656-6662.

Sun, T.Y., Gottschalk, F., Hungerbühler, K. and Nowack, B. (2014) Comprehensive probabilistic modelling of environmental emissions of engineered nanomaterials. Environmental Pollution 185(0), 69-76.

Team, R.C. (2012) R: A Language and Environment for Statistical Computing, R Foundation for Statictical Computing.

Thalmann, B., Voegelin, A., Sinnet, B., Morgenroth, E. and Kaegi, R. (2014) Sulfidation kinetics of silver nanoparticles reacted with metal sulfides. Environ Sci Technol 48(9), 4885-4892.

von Sonntag, C. and von Gunten, U. (2012) Chemistry of Ozone in Water and Wastewater Treatment, IWA Publishing.

Windler, L., Height, M. and Nowack, B. (2013) Comparative evaluation of antimicrobials for textile applications. Environment International 53(0), 62-73.

Woodrow Wilson, I. (2015) Nanotechnology Consumer Products, Informa Healthcare.

Yuan, Z., Chen, Y., Li, T. and Yu, C.-P. (2013) Reaction of silver nanoparticles in the disinfection process. Chemosphere 93(4), 619-625.

5. Conclusions and Research Outlook

Metallic AgNP were shown to have toxic effects on the aquatic environment. Most of them are caused either by a direct interaction with the AgNP or through the release of Ag^+ due to their slow oxidative dissolution (Fabrega et al. 2009, Navarro et al. 2008). Knowledge about transformations of AgNP is crucial to understand the fate and behavior of AgNP in the environment and to reliably asses the potential risks associated with the increased use of AgNP. Sulfidation of AgNP reduces the toxicity by several orders of magnitude, resulting in great research interest (Peijnenburg et al. 2015, Reinsch et al. 2012). The sulfidation of AgNP has been reported to take place in sewers (Brunetti et al. 2015, Kaegi et al. 2013) and WWTP (Doolette et al. 2013, Kaegi et al. 2011, Kent et al. 2014), but also in freshwater wetlands (Lowry et al. 2012).

However, before this thesis was initiated the knowledge about the reaction rates and mechanisms of AgNP sulfidation was very limited. Environmental predictions of AgNP were either omitting the sulfidation reaction (Mueller and Nowack 2008) or including it based on very limited experimental data (Barton et al. 2015), which may result in the under- or overestimation of the potential environmental risk of AgNP. Therefore, this thesis investigated the transformations of AgNP in the urban wastewater and water system. The following chapter is divided in a summary of the results, their environmental implications, and a research outlook identifying knowledge gaps and further research needs.

5.1 Results Summary

The first aim of this thesis was to provide more detailed insights into the mechanistic and kinetic aspects of the sulfidation reaction of AgNP with two different sulfide sources: *i)* HS^- and *ii)* metal sulfides. The sulfidation of AgNP with *i)* HS^- had half-life times between 1 and 12 min, with decreasing half-life times for decreasing particle diameters and increasing HA concentrations (Chapter 2). The kinetics were best described by the parabolic rate law, a solid state kinetic model based on the limited diffusion of Ag through the reacted part of the particle. TEM analysis revealed that in the absence of HA the particles were more likely to only get sulfidized from one side of the particle, while at increased HA concentrations the sulfidation proceeded through a concentrically core-shell type structure. Furthermore, the sulfidized AgNP showed typical patterns of Kirkendall voids in their center, most likely originating from the faster diffusion of Ag than that of S through the Ag_2S layer resulting in an inward diffusion of voids.

The sulfidation of AgNP with *ii)* metal sulfides as sulfide source, proceeded with both CuS and ZnS under oxic conditions (Chapter 3). However, the half-life times

ranged from 2 to 65 h which is considerably longer than for HS^-. The reaction rate was increasing with decreasing AgNP size and increasing metal sulfide concentration and was further dependent on the metal sulfide type and crystallinity. The kinetics were best described by a pseudo-first-order kinetic model which was empirically expanded to include the rate dependency on the particle size and metal sulfide concentration. TEM analysis indicated that the metal sulfides were mostly adjacent to the AgNP, where also the sulfidation started to advance. Additional high resolution elemental distribution maps revealed complex sulfidation patterns.

The second aim of this thesis was to investigate the transformation of sulfidized AgNP in the effluent during ozone treatment (Chapter 4). Nano-Ag_2S was oxidized to Ag_2SO_4 by the consumption of 2.91 ozone per sulfide molecule and the rate constant was 3.1×10^4 M^{-1} s^{-1} which is comparable to fast reacting organic micropollutants. XAS and TEM confirmed that in effluent water the Ag_2S was oxidatively dissolved and AgCl crystals precipitated due to the lower solubility product of AgCl. Furthermore, the short-term toxicity of ozone treated and untreated nano-Ag_2S in WWTP effluent was assessed with the green algae *Chlamydomonas reinhardtii*. The 1 h toxicity of Ag in WWTP effluent increased from no detectable effect at 175 μM_{Ag} L^{-1} for untreated nano-Ag_2S to an EC_{50} of 0.256 μM_{Ag} L^{-1} for ozonized nano-Ag_2S, which was in a similar range as Ag^+.

5.2 Environmental Implications

The experimental results from the first part of this thesis revealed that the sulfidation of AgNP in the environment is possible with *i)* HS^- and *ii)* metal sulfides. Furthermore, sulfidation is faster than the oxidative-dissolution of AgNP under environmental conditions, such as waste and surface water, allowing the sulfidation of AgNP to occur in urban wastewater and water systems (Ma et al. 2012). Hence, the environmental risk of AgNP is expected to be mitigated as already partially sulfidized AgNP significantly reduce the toxicity of AgNP (Reinsch et al. 2012).

The sulfidation with *i)* HS^- is accelerated by environmentally ubiquitous HA and based on the parabolic model the rate is neither dependent on the HS^- nor on the Ag concentration. The sulfidation with HS^- is more likely to occur in the urban wastewater systems due to higher HS^- concentrations than in oxic surface waters. Hence, with hydraulic residence times of a few hours, it is expected that AgNP released to the sewers will already be completely or close to completely sulfidized when they reach the WWTP. Similar results were obtained in a lab scale sewer spiked with AgNP (Brunetti et al. 2015). Thus, negative impacts on the WWTP performance and the effluent quality due to toxic interactions of Ag with bacteria are not expected and have not yet been observed (Yang et al. 2012).

Based on these estimations and mass flow analysis most of the AgNP should be fully sulfidized when they leave the urban wastewater system due to their hydraulic residence time. However, some metallic AgNP might reach the surface waters through other pathways, *e.g.* rain overflow of sewers or direct washout from products to the surface waters. Current predictions for AgNP in the surface waters are in the range of a few picomolar (Gottschalk et al. 2009). Besides the oxidative-dissolution and the interaction with ligands such as chloride and NOM, also sulfidation of AgNP is likely to occur in urban waters due to the presence of metal sulfides. The sulfidation of AgNP in surface waters was estimated to be complete within days.

Experimental results from the second part of this thesis revealed that ozone oxidizes Ag_2S. Furthermore, the oxidation rate is comparable to other micropollutants, leading to an oxidative dissolution of the sulfidized AgNP. Therefore, nano-Ag_2S in the effluent of WWTP treated with ozone is likely to be oxidized. Depending on the concentrations of other ligands such as chloride and NOM, the dissolved Ag precipitates as AgCl or forms complexes with Cl^- (*e.g.* $AgCl_2^-$, $AgCl_3^{2-}$) and other complexes with organic molecules. The change in speciation of Ag led to an increased short-term toxicity toward algae with EC_{50} values close to ionic Ag^+ in WWTP effluent. Thus, besides the environmentally positive effect of ozonation of WWTP effluent due to the degradation of organic micropollutants, the additional treatment can lead to an increased toxicity of Ag. This could be of importance when choosing the best suited WWTP upgrade to remove micropollutants. However, it should be noted that current Ag concentrations in WWTP effluents are relatively low and it is not yet known if long-term effects due to increased Ag concentrations are likely to occur. Furthermore, it is possible that in the surface waters the Ag could again become sulfidized with metal sulfides.

This PhD thesis was conducted in the broader context of the national research program (NRP 64) about "Opportunities and Risks of Nanomaterials". This thesis, in combination with results from other researchers about mass flow modeling and environmental toxicity of AgNP, was able to show that the environmental exposure of hazardous Ag species at toxic doses is currently not of major concern, but under exceptional circumstances (*e.g.* direct spill of AgNP into the surface waters) adverse effects cannot be excluded (Levard et al. 2013, Reinsch et al. 2012, Sun et al. 2014). This new knowledge about sulfidation of AgNP should be considered for further governmental regulations.

Besides the possible risks for humans and the environment, AgNP may provide an opportunity to further replace more persistent antimicrobial agents of higher environmental concern. For example triclosan is an organic antimicrobial widely applied to consumer and medical products with an annual production volume of approximately 350 t. The application of AgNP could possibly substitute or comple-

ment triclosan in some products. Especially for medical applications this could be of great interest, as triclosan resistant bacteria have already been detected (Singer et al. 2002). The use of AgNP in medical devices is under development and some products are already on the market (Rai et al. 2009). Triclosan is reported in a wide concentration range in the environment, with up to 14 mg L^{-1} in wastewater. With predicted no effect concentrations (PNEC) of 50 ng L^{-1} it is highly toxic (Singer et al. 2002). The partial replacement of triclosan with AgNP could reduce the overall environmental risk, due to the efficient detoxification of AgNP through their sulfidation in the wastewater.

5.3 Research Outlook

In this study the sulfidation of AgNP with *i)* HS^- and *ii)* metal sulfides was found to be dependent on the AgNP size. Furthermore, the kinetics were dependent for *i)* HS^- on the concentration of HA and for *ii)* metal sulfides on the concentration and type of metal sulfides. However, in urban wastewater and water systems other environmental parameters may influence or govern the sulfidation kinetics. In a first part, further environmental factors worth investigating, such as AgNP surfactant, pH, ionic strength, HA and Ag-binding ligands like Cl^- or cysteine and proteins, are reviewed and discussed. Second, nitrate as an oxidant and polysulfides as sulfide source are proposed. In a third part, the oxidation of other metal sulfides in WWTP effluent with ozone is elaborated.

What is the influence of the AgNP surfactant on the sulfidation kinetics?

Individual surfactants (*e.g.* PEG or BPEI) are likely to more efficiently shield the AgNP surface from corrosive substances. Thus, the particles would be more persistent toward oxidation and sulfidation.

How does the pH influence the sulfidation rate?

Although mostly circumneutral, the pH in the environment can vary significantly from rather alkaline wastewaters to more acidic waters or other aquifers. The oxidative-dissolution rate of AgNP increases at lower pH due to the higher availability of protons necessary for the oxidation (Table 1.1) (Peretyazhko et al. 2014). For the sulfidation with *i)* HS^- a lower pH would lead to the formation of H_2S which easily degasses from the water and, hence, a low pH would likely inhibit the reaction. For the reaction with *ii)* metal sulfides the effect of the pH is unclear. At low pH ZnS for example dissolves, but CuS is persistent, hence, the influence of the metal sulfide type on the sulfidation rate is likely to be stronger.

What is the influence of the ionic strength and HA on the sulfidation kinetics?

Increasing ionic strength, especially increasing divalent cations, can destabilize AgNP suspensions leading to an increased hetero- and homo-agglomeration of the particles. HA, however, could stabilize the AgNP (Yin et al. 2015). Hence, for the sulfidation with *i)* HS^-, the rate is likely to be more strongly dependent on the presence of HA. On the other hand, for *ii)* metal sulfides TEM analysis suggested some kind of a solid-solid type reaction of AgNP with metal sulfides. Thus, increasing ionic strength could lead to hetero-agglomeration of AgNP with metal sulfide particles, which would increase the sulfidation rate due to higher local sulfide concentrations. The effect of HA has only been investigated for the sulfidation with *i)* HS^-. For *ii)* metal sulfides, the presence of HA could stabilize both particles and separate them, which most likely would result in a decrease in the sulfidation rate.

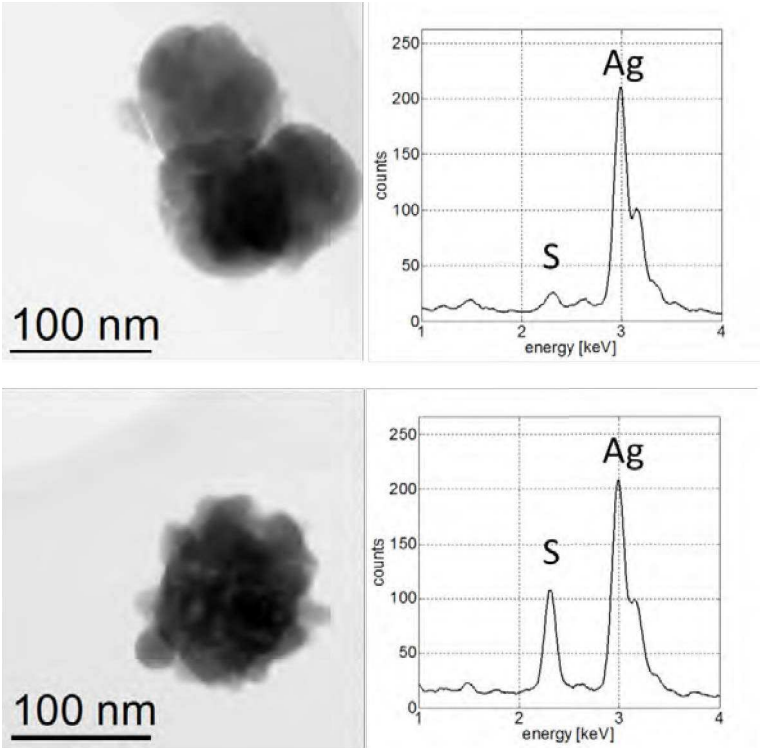

Figure 5.1: TEM (bright field) images of AgNP (100 nm) reacted for 2 h with either HS^- (top) or with polysulfides (bottom). Energy dispersive X-ray spectra of the respective particles are given on the right hand side.

What is the effect of other Ag-binding ligands on the sulfidation?

Other Ag ligands or chelating agents in water such as Cl^-, cysteine or proteins could lead to the formation of a passivation layer or shielding around the AgNP and substantially decrease the reaction rate for both sulfide sources. Furthermore, the reaction mechanisms could change from the observed parabolic and pseudo-first order kinetics to a reaction where first Ag is oxidized, dissolved and later precipitates as Ag_2S.

Is the sulfidation of AgNP also possible with another oxidant?

Apart from environmental conditions that are affecting the sulfidation reaction and its rate, the sulfidation might also proceed with other oxidants or sulfide sources. So far, dissolved molecular O_2 has been used for the oxidation of metallic Ag during the sulfidation of AgNP. The potential of other oxidants for the sulfi-

dation process has not yet been studied. Nitrate (NO_3^-) has a standard electrode potential which is, depending on the final product (NO_2 or NO), just above the potential of bulk Ag (Haynes 2014). Although the electrode potential of NO_3^- is strongly dependent on the pH, thermodynamic calculations suggest that due to the low solubility of Ag_2S NO_3^- could serve as an oxidant to oxidize Ag even at pH 7.5. Thus, the sulfidation of AgNP in anoxic waters could be dependent on NO^{3-} concentrations. Furthermore, HS^- is more persistent in the presence of NO_3^- than O_2, as the abiotic oxidation of HS^- with NO_3^- is unlikely to occur due to the thermodynamically unfavored one electron transfer reaction (Luther et al. 2011).

How does the sulfidation of AgNP proceed with polysulfides?

The two sulfide sources that were investigated in this work depend on an additional oxidant such as oxygen for the sulfidation of AgNP, hence, the transformation of AgNP is only possible in oxic waters. Polysulfides (S_n^{2-}) are another environmental sulfide source expected to be present in anoxic (waste-) waters. They are an intermediate species between HS^- and elemental sulfur with an overall oxidative state and charge of -2 and a typical chain length (n) of sulfur atoms between 2 and 8. Polysulfides can both act as sulfide source and as oxidant to oxidize AgNP in the same molecule which gives them great potential to sulfidize AgNP under anoxic conditions found in large parts of the urban wastewater system (Eq. 5.1).

$$2Ag + S_n^{2-} \rightarrow Ag_2S + S_{n-1}^{2-} \qquad \text{Eq. 5.1}$$

Zeng et al. (2011) have used the sulfidation of AgNP with polysulfides under anoxic conditions during the synthesis of selectively sulfidized Ag nanocrystals. Polysulfides could be the active sulfide specie for the sulfidation of AgNP under anoxic environmental conditions, as the sulfidation is known to also take place in anoxic wastewaters (Kaegi et al. 2013).

First proof-of-principle experiments were conducted within this work by reacting polysulfides or HS^- with 100-nm AgNP under anoxic conditions. After 2 h of reaction time, samples were collected and prepared for analytical TEM analysis. Results from the TEM analysis revealed that the AgNP reacted with polysulfides to a substantial degree under anoxic conditions, while with HS^- they remained almost completely metallic (Figure 5.1).

However, the rate of the sulfidation and the presence of polysulfides in wastewater is still unknown. The detection of polysulfides in environmental samples is rather difficult due to poor detection limits and their instability under oxic conditions, however, they have been found in sulfur rich water wells and pipes (Kamyshny et al. 2008, Kristiana et al. 2010).

How does ozone interact with other metal sulfides?

The reaction of ozone with particulate matter in WWTP effluent has been studied for the first time in this thesis. Nano-Ag_2S in WWTP effluent was found to become readily oxidized by ozone, which may lead to an increased toxicity of the Ag species. Ag is currently only found in minor concentrations (up to several µg L^{-1}) and, hence, is not of utter ecotoxicological concern. However, ozone may also react with other particulate metal sulfides or redox sensitive metals present in the WWTP effluent. For metal sulfides the highest concentrations in the effluent are expected for zinc and copper sulfide (ZnS and CuS) (Stover et al. 1976) and it is very likely that ozone oxidizes the sulfide to sulfate. Both of these metals are known to be of ecotoxicological concern, depending on their speciation. Hence, their reactin rates with ozone and metal speciation after ozonation is of high relevance for the environment.

Furthermore, the ozonation of other higher toxic but in wastewater less concentrated chalcophile metals such as cadmium and mercury could also affect the environment. The ozone consumption and oxidation rate of other metal sulfides with ozone is unknown, but likely to be in the range of the nano-Ag_2S oxidation. The metal speciation after ozonation is still unknown and very difficult to predict due to the harsh oxidative conditions during ozonation and the complexity of WWTP effluent.

References

Barton, L.E., Auffan, M., Durenkamp, M., McGrath, S., Bottero, J.-Y. and Wiesner, M.R. (2015) Monte Carlo simulations of the transformation and removal of Ag, TiO2, and ZnO nanoparticles in wastewater treatment and land application of biosolids. Science of The Total Environment 511, 535-543.

Brunetti, G., Donner, E., Laera, G., Sekine, R., Scheckel, K.G., Khaksar, M., Vasilev, K., De Mastro, G. and Lombi, E. (2015) Fate of zinc and silver engineered nanoparticles in sewerage networks. Water Research 77(0), 72-84.

Doolette, C., McLaughlin, M., Kirby, J., Batstone, D., Harris, H., Ge, H. and Cornelis, G. (2013) Transformation of PVP coated silver nanoparticles in a simulated wastewater treatment process and the effect on microbial communities. Chemistry Central Journal 7(1), 1-18.

Fabrega, J., Fawcett, S.R., Renshaw, J.C. and Lead, J.R. (2009) Silver nanoparticle impact on bacterial growth: effect of pH, concentration, and organic matter. Environ Sci Technol 43(19), 7285-7290.

Gottschalk, F., Sonderer, T., Scholz, R.W. and Nowack, B. (2009) Modeled environmental concentrations of engineered nanomaterials (TiO(2), ZnO, Ag, CNT, Fullerenes) for different regions. Environ Sci Technol 43(24), 9216-9222.

Haynes, W.M. (2014) CRC Handbook of Chemistry and Physics, CRC Press, Boca Raton.

Kaegi, R., Voegelin, A., Ort, C., Sinnet, B., Thalmann, B., Krismer, J., Hagendorfer, H., Elumelu, M. and Mueller, E. (2013) Fate and transformation of silver nanoparticles in urban wastewater systems. Water Res 47(12), 3866-3877.

Kaegi, R., Voegelin, A., Sinnet, B., Zuleeg, S., Hagendorfer, H., Burkhardt, M. and Siegrist, H. (2011) Behavior of metallic silver nanoparticles in a pilot wastewater treatment plant. Environ Sci Technol 45(9), 3902-3908.

Kamyshny, A., Jr., Zilberbrand, M., Ekeltchik, I., Voitsekovski, T., Gun, J. and Lev, O. (2008) Speciation of Polysulfides and Zerovalent Sulfur in Sulfide-rich Water Wells in Southern and Central Israel. Aquatic Geochemistry 14(2), 171-192.

Kent, R., Oser, J. and Vikesland, P.J. (2014) Controlled Evaluation of Silver Nanoparticle Sulfidation in a Full-Scale Wastewater Treatment Plant. Environ Sci Technol.

Kristiana, I., Heitz, A., Joll, C. and Sathasivan, A. (2010) Analysis of polysulfides in drinking water distribution systems using headspace solid-phase microextraction and gas chromatography–mass spectrometry. Journal of Chromatography A 1217(38), 5995-6001.

Levard, C., Hotze, E.M., Colman, B.P., Dale, A.L., Truong, L., Yang, X.Y., Bone, A.J., Brown, G.E., Jr., Tanguay, R.L., Di Giulio, R.T., Bernhardt, E.S., Meyer, J.N., Wiesner, M.R. and Lowry, G.V. (2013) Sulfidation of silver nanoparticles: natural antidote to their toxicity. Environ Sci Technol 47(23), 13440-13448.

Levard, C., Hotze, E.M., Lowry, G.V. and Brown, G.E., Jr. (2012) Environmental transformations of silver nanoparticles: impact on stability and toxicity. Environ Sci Technol 46(13), 6900-6914.

Levard, C., Reinsch, B.C., Michel, F.M., Oumahi, C., Lowry, G.V. and Brown, G.E. (2011) Sulfidation processes of PVP-coated silver nanoparticles in aqueous solution: impact on dissolution rate. Environ Sci Technol 45(12), 5260-5266.

Lowry, G.V., Espinasse, B.P., Badireddy, A.R., Richardson, C.J., Reinsch, B.C., Bryant, L.D., Bone, A.J., Deonarine, A., Chae, S., Therezien, M., Colman, B.P., Hsu-Kim, H., Bernhardt, E.S., Matson, C.W. and Wiesner, M.R. (2012) Long-term transformation and fate of manufactured ag nanoparticles in a simulated large scale freshwater emergent wetland. Environ Sci Technol 46(13), 7027-7036.

Luther, G.W., 3rd, Findlay, A.J., Macdonald, D.J., Owings, S.M., Hanson, T.E., Beinart, R.A. and Girguis, P.R. (2011) Thermodynamics and kinetics of sulfide oxidation by oxygen: a look at inorganically controlled reactions and biologically mediated processes in the environment. Frontiers in Microbiology 2.

Ma, R., Levard, C., Marinakos, S.M., Cheng, Y., Liu, J., Michel, F.M., Brown, G.E. and Lowry, G.V. (2012) Size-controlled dissolution of organic-coated silver nanoparticles. Environ Sci Technol 46(2), 752-759.

Mueller, N.C. and Nowack, B. (2008) Exposure modeling of engineered nanoparticles in the environment. Environ Sci Technol 42(12), 4447-4453.

Navarro, E., Piccapietra, F., Wagner, B., Marconi, F., Kaegi, R., Odzak, N., Sigg, L. and Behra, R. (2008) Toxicity of Silver Nanoparticles to Chlamydomonas reinhardtii. Environ Sci Technol 42(23), 8959-8964.

Peijnenburg, W.J.G.M., Baalousha, M., Chen, J., Chaudry, Q., Von Der Kammer, F., Kuhlbusch, T.A.J., Lead, J., Nickel, C., Quik, J.T.K., Renker, M., Wang, Z. and Koelmans, A.A. (2015) A review of the properties and processes determining the fate of engineered nanomaterials in the aquatic environment. Critical Reviews in Environmental Science and Technology, 00-00.

Peretyazhko, T., Zhang, Q. and Colvin, V.L. (2014) Size-Controlled Dissolution of Silver Nanoparticles at Neutral and Acidic pH Conditions: Kinetics and Size Changes. Environ Sci Technol.

Rai, M., Yadav, A. and Gade, A. (2009) Silver nanoparticles as a new generation of antimicrobials. Biotechnology Advances 27(1), 76-83.

Reinsch, B.C., Levard, C., Li, Z., Ma, R., Wise, A., Gregory, K.B., Brown, G.E., Jr. and Lowry, G.V. (2012) Sulfidation of silver nanoparticles decreases Escherichia coli growth inhibition. Environ Sci Technol 46(13), 6992-7000.

Singer, H., Müller, S., Tixier, C. and Pillonel, L. (2002) Triclosan: Occurrence and Fate of a Widely Used Biocide in the Aquatic Environment: Field Measurements in Wastewater Treatment Plants, Surface Waters, and Lake Sediments. Environ Sci Technol 36(23), 4998-5004.

Stover, R.C., Sommers, L.E. and Silviera, D.J. (1976) Evaluation of Metals in Wastewater-Sludge. Journal Water Pollution Control Federation 48(9), 2165-2175.

Sun, T.Y., Gottschalk, F., Hungerbühler, K. and Nowack, B. (2014) Comprehensive probabilistic modelling of environmental emissions of engineered nanomaterials. Environmental Pollution 185(0), 69-76.

Yang, Y., Chen, Q., Wall, J.D. and Hu, Z. (2012) Potential nanosilver impact on anaerobic digestion at moderate silver concentrations. Water Research 46(4), 1176-1184.

Yin, Y., Shen, M., Tan, Z., Yu, S., Liu, J.-f. and Jiang, G. (2015) Particle Coating-dependent Interaction of Molecular Weight Fractionated Natural Organic Matter: Impacts on the Aggregation of Silver Nanoparticles. Environ Sci Technol.

Zeng, J., Tao, J., Su, D., Zhu, Y., Qin, D. and Xia, Y. (2011) Selective Sulfuration at the Corner Sites of a Silver Nanocrystal and Its Use in Stabilization of the Shape. Nano Letters 11(7), 3010-3015.

A. Appendix of Chapter 2

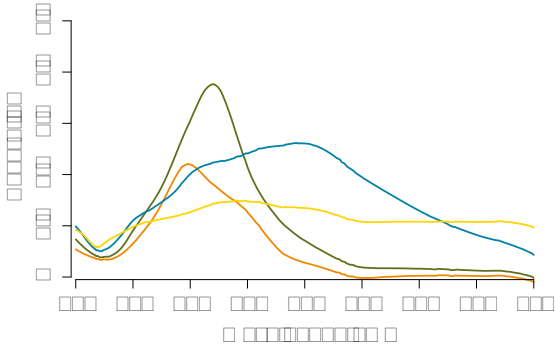

Figure A.1: Plasmon resonance of 20-nm (orange), 40-nm (green), 100-nm (blue) and 200-nm (yellow) AgNP.

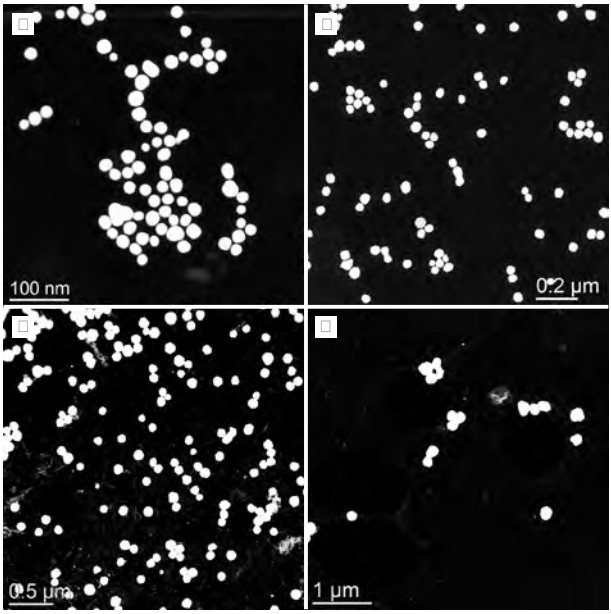

Figure A.2: TEM images of pristine AgNP with diameters of 20 (A), 40 (B), 100 (C) and 200 nm (D).

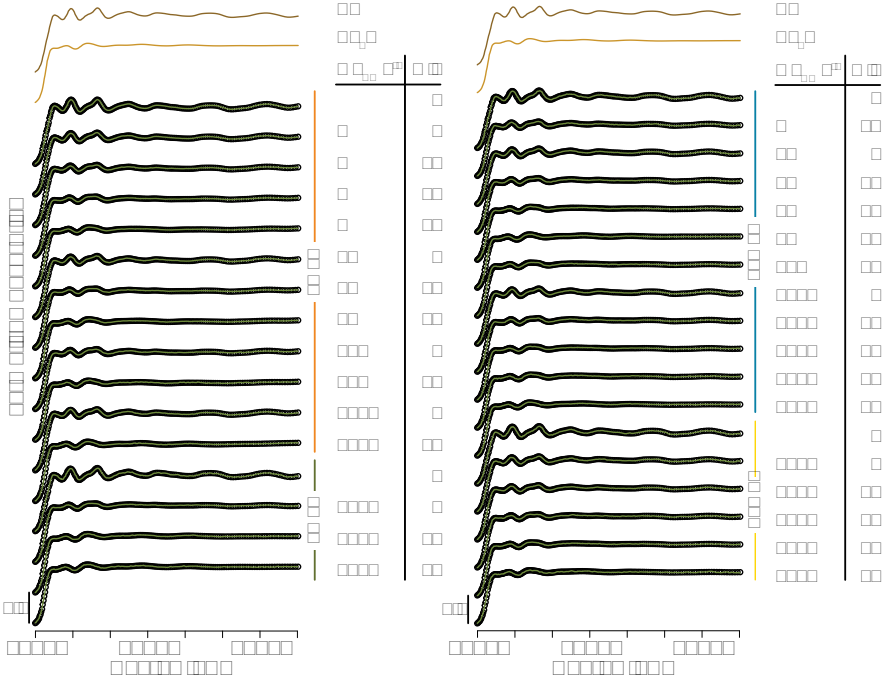

Figure A.3: XANES spectra of reference and experimental samples and reconstructed LCF spectra (open circles) using Ag and Ag_2S as reference spectra. For clarity the spectra are plotted with an offset of 0.5. The sum of all fractions was unconstrained for LCF analysis. A comparison of the LCF-derived Ag fraction from XANES and EXAFS is given in Figure A.5.

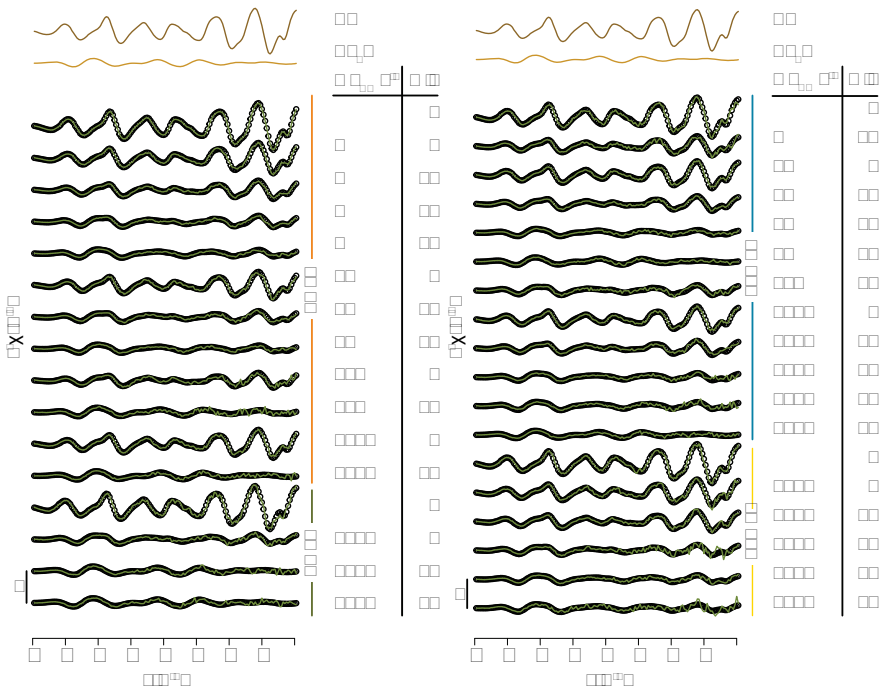

Figure A.4: EXAFS spectra of reference and experimental samples and reconstructed LCF spectra (open circles) using Ag and Ag_2S as reference spectra. For clarity the spectra are plotted with an offset of 2. The sum of all fractions was unconstrained for LCF analysis. A comparison of the LCF-derived Ag fraction from XANES and EXAFS is given in Figure A.5.

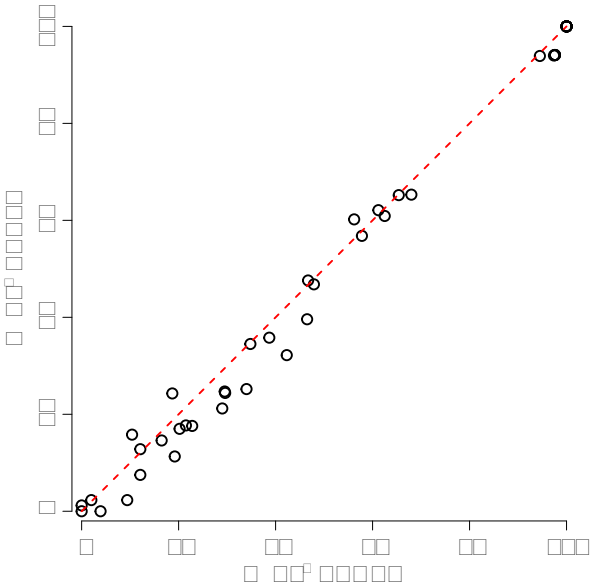

Figure A.5: Comparison of the metallic Ag fractions derived from LCF analysis of XANES and EXAFS spectra.

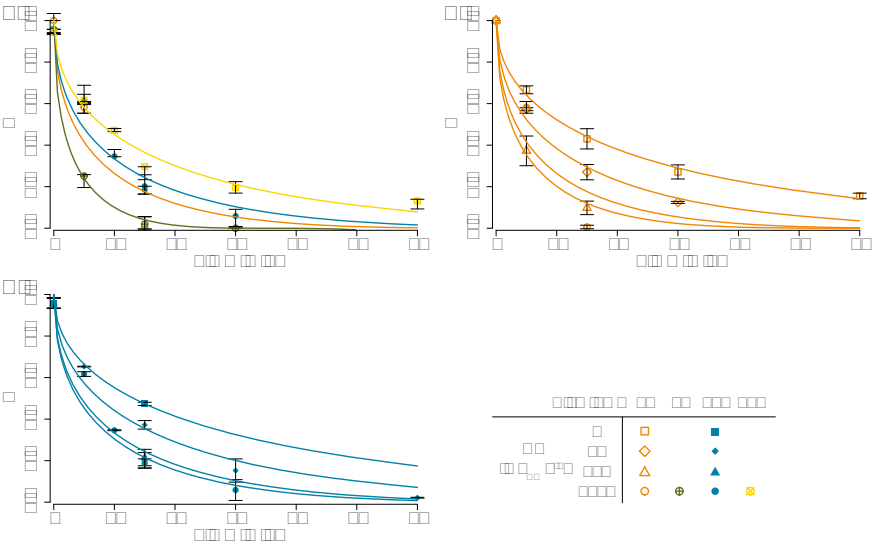

Figure A.6: Results of the parabolic rate model fit (lines) to the experimental data (**A:** AgNP sizes at constant HA concentration, **B:** 20-nm AgNP at differing HA concentrations, **C:** 100-nm AgNP at differing HA concentrations).

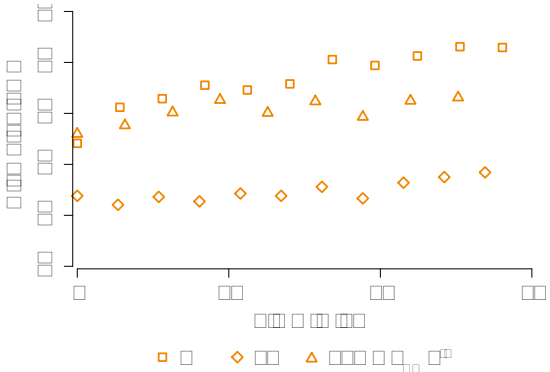

Figure A.7: Hydrodynamic diameter measured by DLS over time for 20-nm AgNP in the presence of HA (0, 50 and 250 mg_{HA} L^{-1}, squares, diamonds and triangles respectively) and HS^- (2.5 mM).

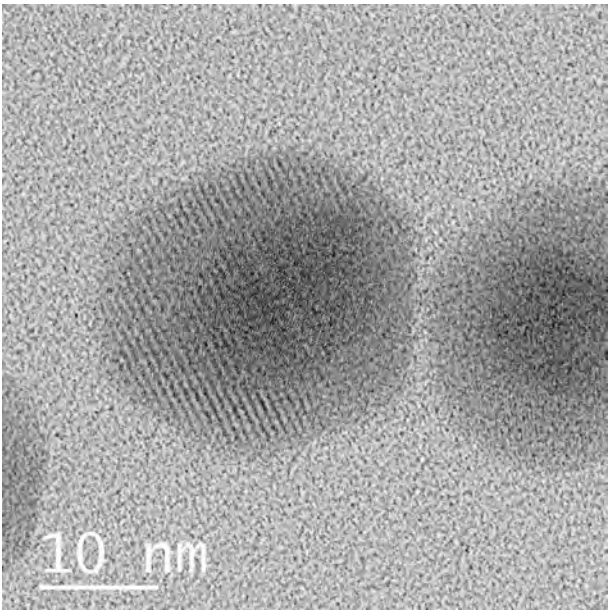

Figure A.8: High resolution TEM image of two 20-nm AgNP sulfidized for 5 min in the presence of 250 mg_{HA} L^{-1}. A core-shell type structure is visible.

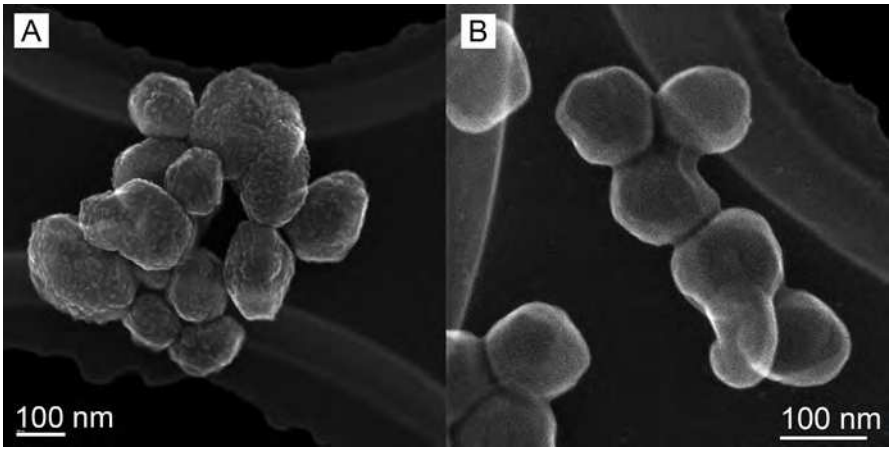

Figure A.9: Secondary electron (SE) image of 100-nm AgNP after **A:** 5 min sulfidation in presence of 1000 mg_{HA} L^{-1} and **B:** after 4 h sulfidation without HA.

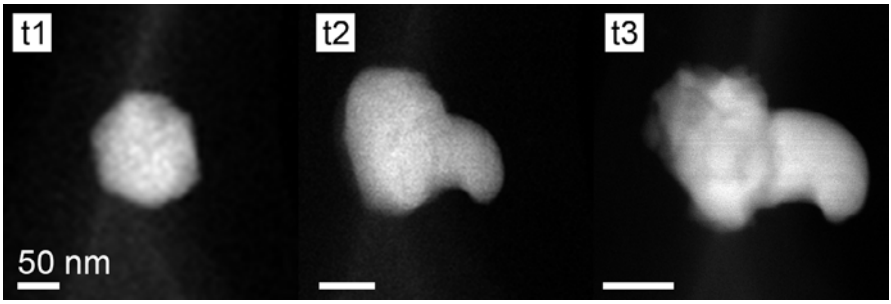

Figure A.10: Time sequence of partially sulfidized 100-nm AgNP (15 min with 1000 mg_{HA} L^{-1}) over one minute under the electron beam.

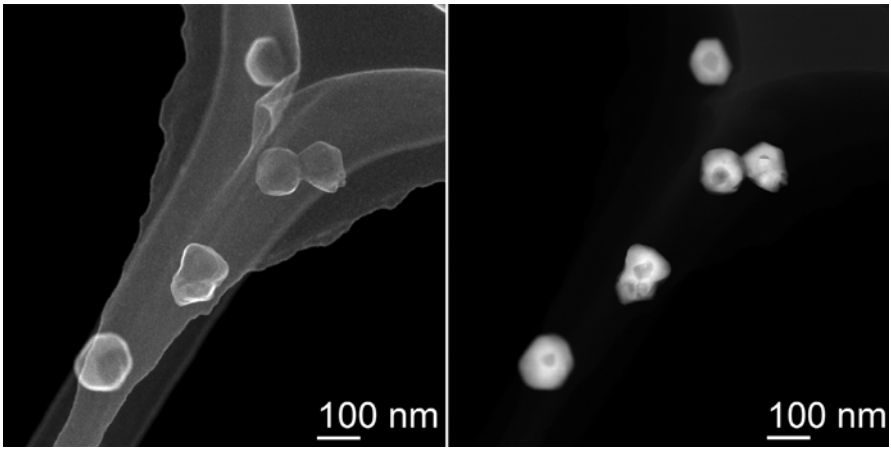

Figure A.11: TEM secondary-electron (SE) image of 100-nm AgNP after 15 min reaction with HS^- in the presence of 1000 mg_{HA} L^{-1} (left). Corresponding TEM image of the same particles recorded with HAADF detector (right).

Table A.1: AgNP characteristics

	DLS Size [nm] (PDI)[a,b]	zeta potential [mV][c]	TEM Size [nm] (particles sized)
20-nm AgNP	29.33 (0.285)	-40.43	19.0±3.7 (465)
40-nm AgNP	39.44 (0.189)	-42.47	38.2±5.0 (446)
100-nm AgNP	103.7 (0.22)	-48.7	92±14 (153)
200-nm AgNP	228.8 (0.234)	-52.47	207±34 (68)

[a]: PDI = Polydispersity Index

[b]: 100 ppm AgNP measured in 10 mM HEPES buffer at pH 7.5

[c]: 10 ppm AgNP measured in 10 mM HEPES buffer and 2 mM citrate at pH 7.5

Table A.2: Summary of Sulfidation Experiments Conducted and Investigated with XAS (X) and TEM (T)

Time	[mg_{HA} L^{-1}]	20 nm	40 nm	100 nm	200 nm
0 min	0	XT	T	XT	T
	50	X		X	
	250	X		X	
	1000	X	X	X	X
5 min	0	XT		T	
	50	X		X	
	250	XT			
	1000	X	X	XT	X
10 min	1000			X	X
15 min	0	X		X	
	50	X		X	
	250	X		X	
	1000	X	X	XT	X
30 min	0	X			
	50	X		X	
	1000		X	X	X
45 min	0	T			
	250	T			
60 min	0	X			
	50			X	
	1000				X
4 h	0			T	

Table A.3: Average of the LCF Derived Ag Fraction from XANES and EXAFS for Each Measured Sample with Standard Error (σ).

AgNP Size [nm]	HA [mg_{HA} L^{-1}]	Time [min]	F_{Ag}	σ	AgNP Size [nm]	HA [mg_{HA} L^{-1}]	Time [min]	F_{Ag}	σ
20	0	0	1.000	0.000	100	0	0	0.959	0.025
20	0	5	0.667	0.019	100	50	0	0.959	0.025
20	0	15	0.431	0.049	100	250	0	0.959	0.025
20	0	30	0.271	0.034	100	1000	0	0.959	0.025
20	0	60	0.156	0.013	100	250	15	0.215	0.040
20	50	0	1.000	0.000	100	0	15	0.474	0.008
20	50	5	0.573	0.007	100	1000	5	0.617	0.011
20	50	15	0.270	0.037	100	1000	10	0.347	0.002
20	50	30	0.125	0.005	100	1000	15	0.202	0.037
20	250	0	1.000	0.000	100	1000	15	0.186	0.023
20	250	5	0.373	0.071	100	1000	30	0.059	0.050
20	250	15	0.098	0.033	100	50	5	0.653	0.001
20	1000	0	1.000	0.000	100	50	15	0.373	0.021
20	1000	5	0.582	0.028	100	50	30	0.153	0.056
20	1000	15	0.006	0.008	100	50	60	0.022	0.002
40	1000	0	0.957	0.024	200	1000	0	0.942	0.004
40	1000	5	0.251	0.055	200	1000	5	0.617	0.006
40	1000	15	0.020	0.028	200	1000	10	0.472	0.006
40	1000	30	0.000	0.000	200	1000	15	0.296	0.062
					200	1000	30	0.196	0.027
					200	1000	60	0.131	0.038

Table A.4: Rate coefficients of the Parabolic Rate Model with Confidence Intervals of 1σ.

AgNP Size [nm]	20				40	100				200
HA [mg_{HA} L^{-1}]	0	50	250	1000	1000	0	50	250	1000	1000
k [nm^2 s^{-1}]	0.34	0.68	1.55	1.16	10.47	6.86	12.08	22.68	19.84	58.27
Standard error (1σ)	0.02	0.05	0.15	0.42	1.08	0.89	1.30	3.22	2.24	5.04

B. Appendix of Chapter 3

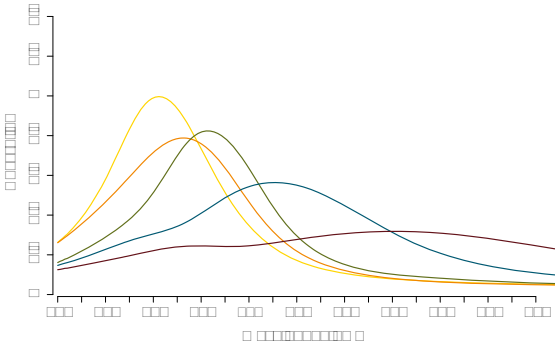

Figure B.1: Surface plasmon resonance of 10 (yellow), 20 (orange), 40 (green), 70 (blue) and 100 nm (brown) AgNP (concentration: 20 mg/L).

Pellets for X-ray absorption (XAS) measurements

To assess the efficiency of the separation of partially sulfidized AgNP from the reaction suspensions for analysis by XAS, the residual Ag in the supernatant after flocculation and centrifugation of the suspensions was quantified. The very high Na^+ in combination with the very low Ag concentration did not allow for a direct analysis by ICP-MS. Therefore, the residual Ag was precipitated as or transformed to Ag_2S by adding an excess of Na_2S (2 mg, 0.026mmol) to 10 mL supernatant, which would have allowed to transform 5.5 mg (0.051 mmol) of Ag to Ag_2S (the Ag concentration in the starting suspension was 0.02 mg/10 mL). After 2 days the precipitated Ag_2S was separated from the liquid by centrifugation (4300 rpm, 60 min) and the solids were dissolved overnight in 1 mL HNO_3 and 0.1 mL H_2O_2. The results suggested that about 70% of the Ag was collected in the pellets for XAS analysis. Nonetheless, the good correlation between unreacted AgNP fractions derived by spectrophotometric analysis and XAS (Table 3.2) suggested that the method for particulate Ag separation for XAS allowed to collect representative samples.

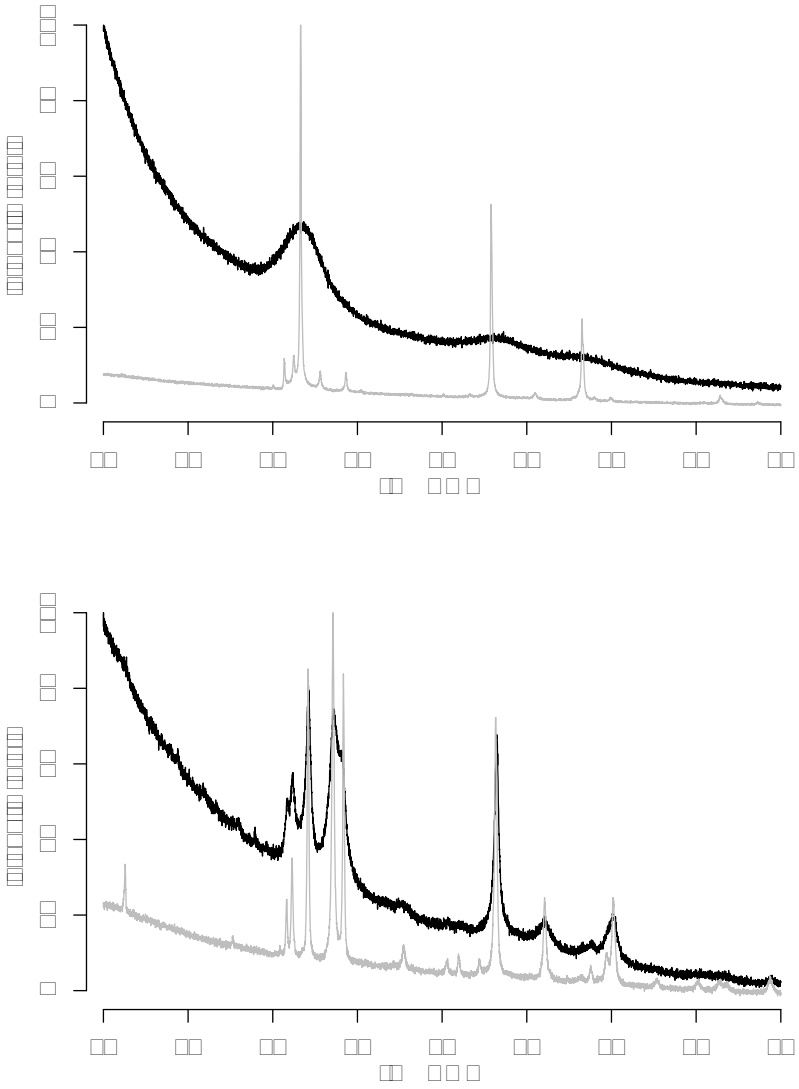

Figure B.2: XRD patterns of ZnS_{cryst}(upper, grey), ZnS_{ppt} (upper, black), CuS_{cryst} (lower, grey) and CuS_{ppt} (lower, black). The Scherrer equation to calculate the crystallite size was applied to the peaks at 33.2° for ZnS_{ppt} (sphalerite 111) and 34.2° for CuS_{ppt} (covellite 012).

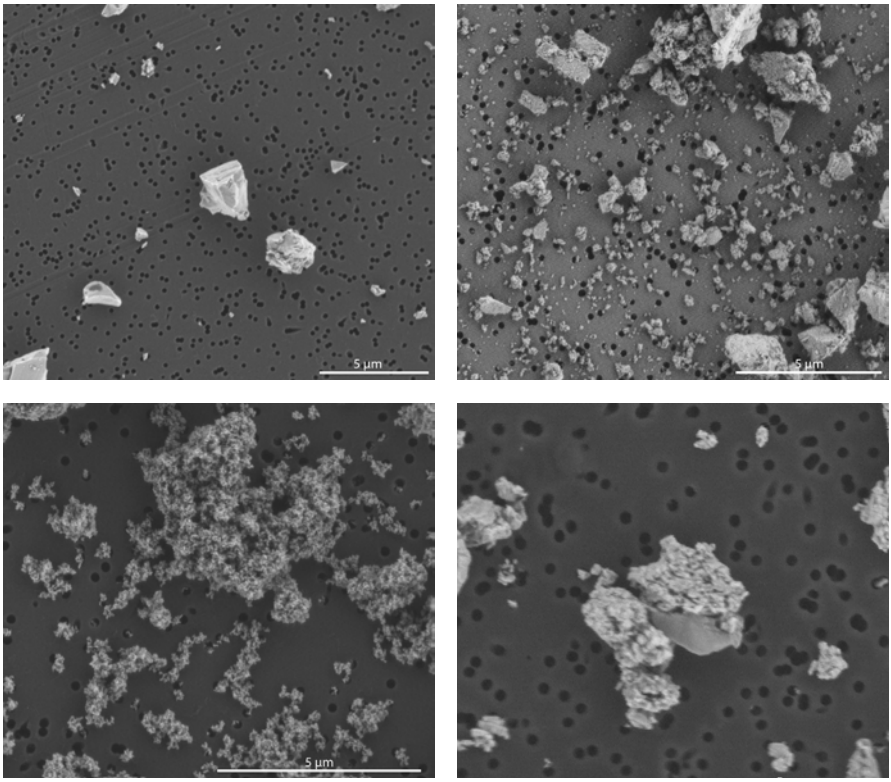

Figure B.3: Backscattered electron (BSE) images of: ZnS_{ppt} (upper, left), ZnS_{cryst} (upper, right), CuS_{ppt} (lower, left) and CuS_{cryst} (lower, right).

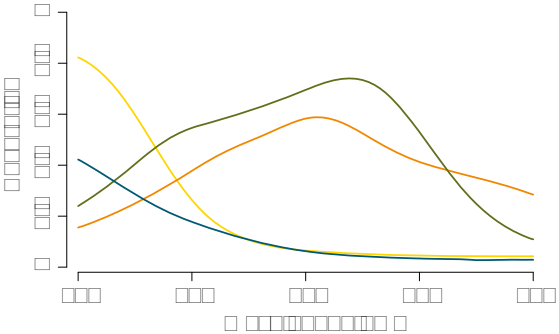

Figure B.4: UV-Vis spectra of zincon in the presence of Zn^{2+} (green), Cu^{2+} (orange), Ag^{+} (yellow) and blank (blue).

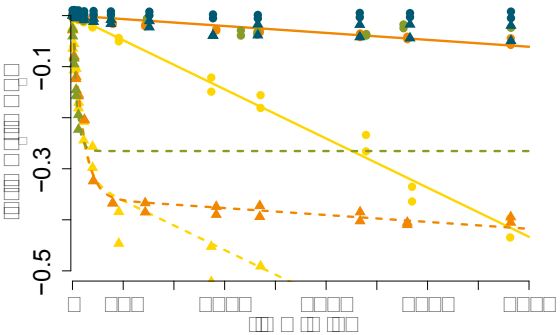

Figure B.5: Fraction of residual metal sulfide derived from UV-Vis measurements versus reaction time. Oxidative dissolution of CuS_{ppt} (yellow dots) and CuS_{cryst} (orange dots) measured in the absence of Ag: Solid lines indicate the fitted oxidative-dissolution kinetics. The oxidative dissolution for ZnS_{ppt} (green dots) and ZnS_{cryst} (blue dots) was at the limit of detection and thus fitting the data to a rate law is inadequate. Oxidative dissolution of CuS_{ppt} (yellow triangles), CuS_{cryst} (orange triangles) and ZnS_{ppt} (green triangles) measured in the presence of Ag^{+}: Dashed lines indicate the fitted CuS and ZnS fractions. No dissolution was detected when ZnS_{cryst} reacted with Ag^{+} (blue triangles). The sharp bend in the curves marks the exhaustion of the Ag.

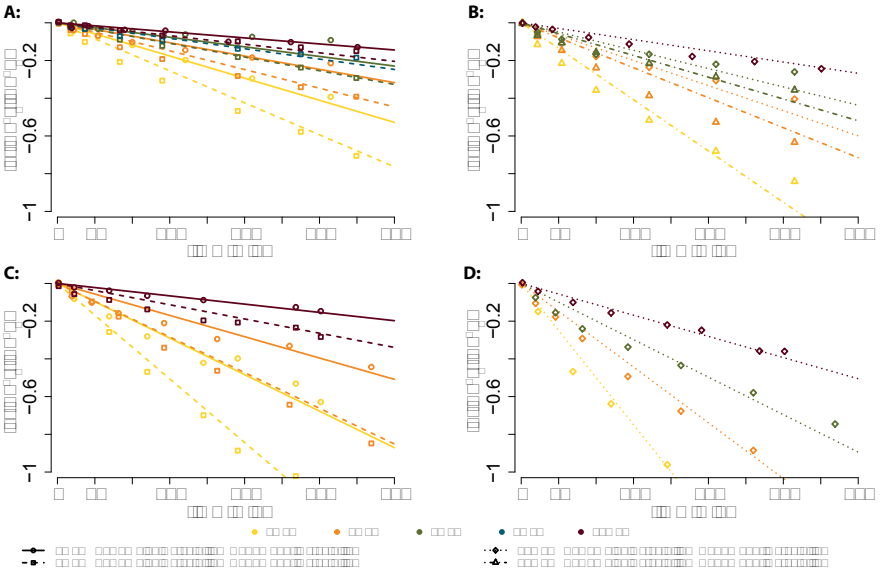

Figure B.6: Open symbols represent fractions of metallic Ag calculated from UV-Vis measurements of either Cu^{2+} or Zn^{2+}. The lines represent the calculated metallic Ag fractions using the Eq. 3.4 in combination with the parameters given in Table 3.2.

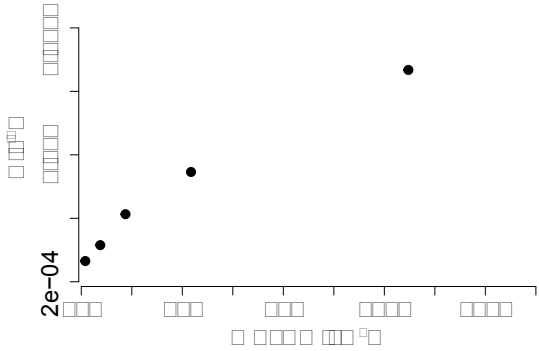

Figure B.7: Reaction rate coefficients calculated for 40 µM CuS_{cryst} experiments against the calculated total AgNP surface area.

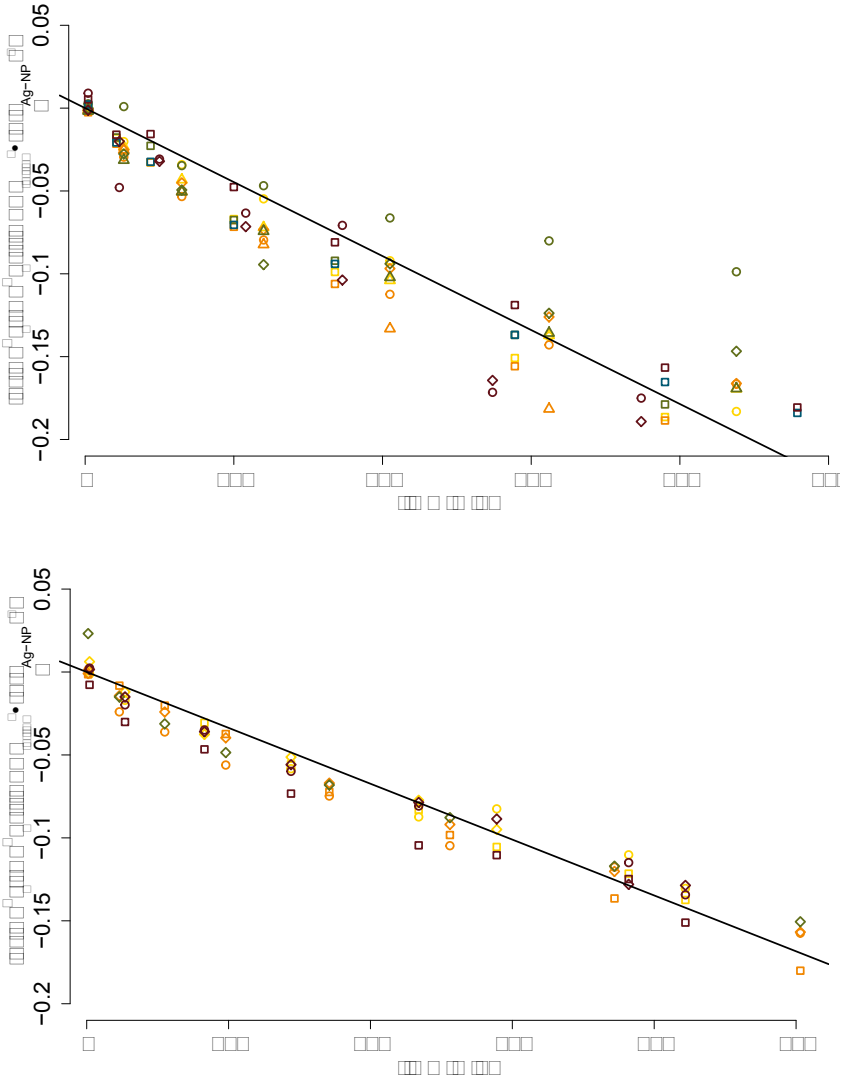

Figure B.8: All measurements for CuS (top) and ZnS (bottom) reacted with AgNP transformed according to $ln\left([Ag]_0 / [Ag]_t\right) \div [MS]^a_{initial} \times \left(1 / d_{Ag-NP}\right)^b = -k' \times t$. The slope of the regression line represents -k' (Eq. 3.4).

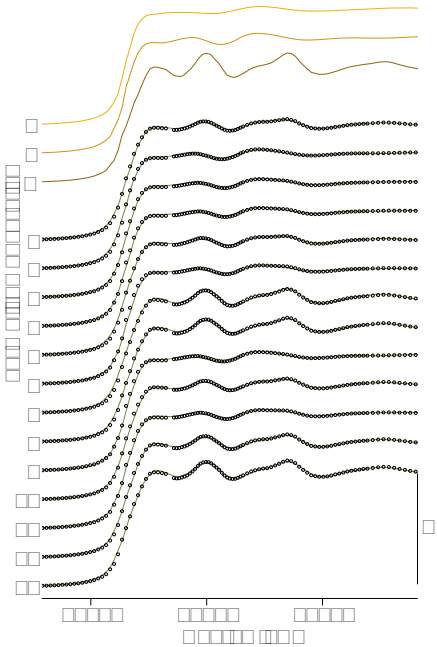

Figure B.9: X-ray absorption near edge structure (XANES) of samples (solid lines) and LCF results (open dots) using three standards (A: Ag-foil, B: Ag_2S, C: Ag-CuS). Numbers correspond to the sample names in Table 3.2. For clarity, the spectra are plotted with an offset of 0.25. For LCF the individual fractions were constrained to lie between 0 and 1 and the sum of all fractions was unconstrained.

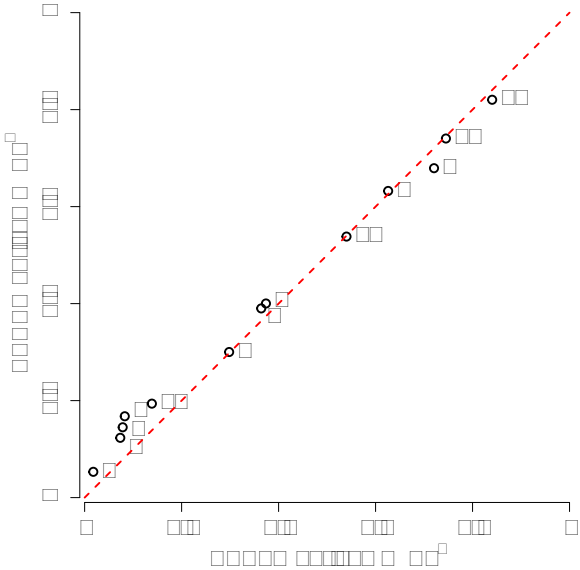

Figure B.10: Comparison of the metallic Ag fractions derived from LCF analysis of EXAFS and XANES spectra. The sum of all fractions was constrained to 1 for EXAFS and unconstrained for XANES LCF analysis.

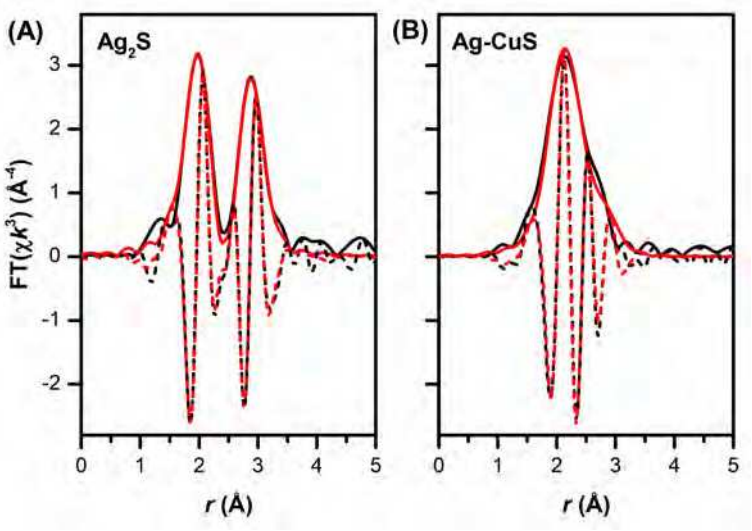

Figure B.11: Magnitude (solid black lines) and imaginary part (dashed black lines) of the Fourier-transformed reference spectra of Ag_2S (**A**) and Ag-CuS (**B**) and comparison with shell-fits (magnitude: red solid lines; imaginary part: red dashed lines). Details on the shell-fits and shell-fit parameters are given in Table B.2. For the Ag-CuS reference, the results suggest that Ag uptake was due to complexation on the surface of CuS and/or the formation of amorphous Ag-sulfide or mixed Ag-Cu-sulfide.

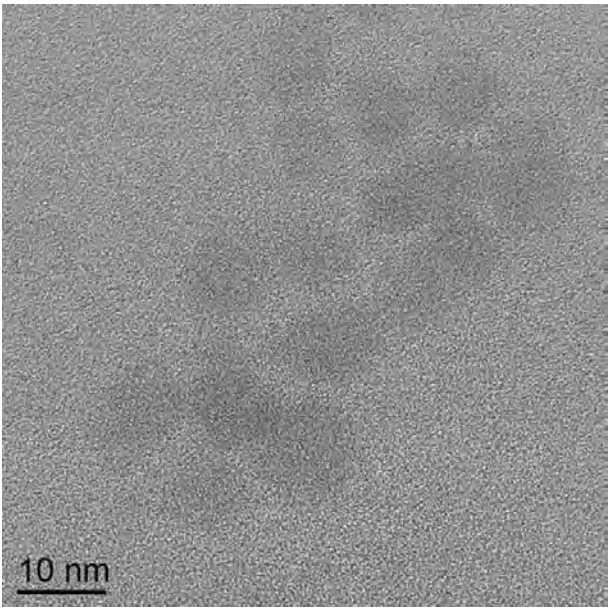

Figure B.12: High-resolution (HR)-TEM image (phase contrast) of ~ 5- 10 nm Ag_2S particles.

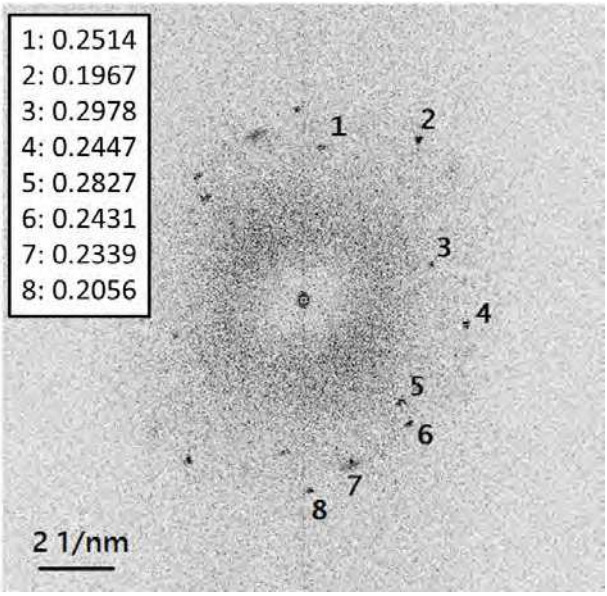

Figure B.13: Diffraction pattern calculated from the HR-TEM image by applying Fast Fourier Transform (FFT) analysis. D-spacings of individual reflections (1-8) are given in nm. The d-spacings match to the crystal structure of Ag_2S (Acanthite).

Table B.1: Summary of conducted experiments. Ag concentrations are measured with ICP-MS and metal sulfide concentrations are based on weighted amounts.

AgNP size [nm]	**Ag [mg L^{-1}]**	**Cus_{cryst} [µM]**	**Ag [mg L^{-1}]**	**ZnS_{ppt} [µM]**
	2.48	38.6	2.65	38.1
	2.8	78.8	2.59	77.7
10			2.57	128.4
	2.82	196.5		
	2.23	40.7	2.05	39.9
	2.16	78.7	2.15	77.2
20	2.72	139.5	2.13	136.8
	2.07	196.5		
	1.97	40		
	2	79.5		
40	2.44	139.6	2.03	137
	2.26	195.1		
70	2.29	79.6	1.78	78.1
	1.96	39.5	2.55	38.5
100	1.94	77.8	2.08	76.9
	1.99	130.9	2.31	128.2

Table B.2: Results from shell-fit analysis of the Ag K-edge EXAFS spectra of Ag_2S and Ag-CuS.[a]

	path	$CN \times S_0^2$	DW ($Å^2$)	r (Å)	r-factor (×1000)
Ag_2S [b]	Ag-S	2.0 (±0.3)	0.007 (±0.001)	2.50 (±0.01)	1.1
	Ag-Ag	5.5 (±1.0)	0.014 (±0.002)	3.06 (±0.01)	
Ag-CuS [c]	Ag-S	1.6 (±0.2)	0.007	2.55 (±0.01)	1.8
	Ag-Cu	2.2 (±0.6)	0.014	2.84 (±0.02)	
	Ag-Ag	1.5 (±0.5)	0.014	2.96 (±0.03)	

[a] The k^3-weighted EXAFS spectra were Fourier-transformed over the k-range 3-11 $Å^{-1}$ using a Kaiser-Bessel apodization window with a sill width of 2 $Å^{-1}$. Shell-fits were performed in r-space over the r-range 1.1 to 3.6 Å using the software code Artemis (Ravel and Newville 2005). Theoretical scattering paths were obtained using FEFF 8.2 (Ankudinov et al. 2003) based on the structure of acanthite (Ag_2S), replacing one second-shell Ag atom by Cu to generate the Ag-Cu path. From the fit of the Ag_2S spectrum, an energy shift of -0.7 (±1.0) eV was obtained which was kept constant in the fit of the Ag-CuS spectrum. Values reported include the product of coordination number and amplitude reduction factor ($CN \times S_0^2$), the Debye Waller parameter (DW), interatomic distance (r) and r-factor. Values in parentheses correspond to the statistical fit uncertainties.

[b] Fit parameters obtained from the analysis of the Ag_2S reference spectrum are in relatively good agreement with reported structural parameters.

[c] For the fit of the spectrum of Ag-CuS, the Debye Waller factors were fixed to the values obtained for Ag_2S and the value of the Ag-Cu path was set equal to the value of the Ag-Ag path. Addition of the both the Ag-Ag and the Ag-Cu path significantly improved the quality of the fit (reduction of reduced chi-square by more than factor 2). Fit results suggest that Ag uptake was dominantly due to complexation on the surface of CuS and/or formation of amorphous Ag-sulfide or mixed Ag-Cu-sulfide.

References

Ankudinov, A.L., Nesvizhskii, A.I. and Rehr, J.J. (2003) Dynamic screening effects in x-ray absorption spectra. Physical Review B 67(11), 115120.

Ravel, B. and Newville, M. (2005) ATHENA , ARTEMIS , HEPHAESTUS : data analysis for X-ray absorption spectroscopy using IFEFFIT. Journal of Synchrotron Radiation 12(4), 537-541.

C. Appendix of Chapter 4

Competition Kinetics

Ag_2S oxidation reaction:

$$Ag_2S + nO_3 \xrightarrow{k_{Ag_2S}} S^* + 2Ag^+ \qquad \text{Eq. C.1}$$

Competing reaction:

$$[Bu] + [O_3] \xrightarrow{k_{Bu}} [CH_2O] \qquad \text{Eq. C.2}$$

Mass balance for ozone:

$$n \times [S^*] = [CH_2O]_0 - [CH_2O] \qquad \text{Eq. C.3}$$

Rate of competition reaction:

$$r_{Bu} = k_{Bu} \times [Bu] \times [O_3] \qquad \text{Eq. C.4}$$

Combine Eq. 4.2 and Eq. C.4:

$$\frac{r_{Ag_2S}}{r_{Bu}} = \frac{k_{Ag_2S} \times [Ag_2S] \times [O_3]}{k_{Bu} \times [Bu] \times [O_3]} = \frac{[S^*]}{[CH_2O]} \qquad \text{Eq. C.5}$$

Eq. C.3 in Eq. C.5:

$$\frac{k_{Ag_2S} \times [Ag_2S]}{k_{Bu} \times [Bu]} = \frac{[CH_2O]_0 - [CH_2O]}{n \times [CH_2O]} \qquad \text{Eq. C.6}$$

Solve (y = m*x):

$$\frac{[CH_2O]_0}{[CH_2O]} - 1 = \frac{n \times k_{Ag_2S}}{k_{Bu}} \times \frac{[Ag_2S]}{[Bu]} \qquad \text{Eq. C.7}$$

The product of the rate-determining step of the reaction of Ag_2S with ozone remains silent as there are fast side reactions (Eq. C.1) and the rate coefficient of the reaction has to be determined with competition kinetics (Eq. C.2) (von Sonntag and von Gunten 2012). We assumed that *i)* the product (S^*) of the rate-determining step is formed by the reaction of one ozone with one Ag_2S (n = 1) and *ii)* the reaction can be described with a second order type rate law.

$[CH_2O]_0$ is the concentration of formaldehyde formed in absence of Ag_2S and corresponds to the ozone dose. $[CH_2O]$ is the measured formaldehyde in presence of Ag_2S. $[Ag_2S]$ and [Bu] are the initial concentrations of Ag_2S and Buten-2-ol. k_{Bu} is the second order rate constant for the Buten-2-ol-ozone reaction (Eq. C.4). Regressing $([CH_2O]_0/[CH_2O]\text{-}1)$ vs. $[Ag_2S]/[Bu]$ (Eq. C.7) results in a straight line with the slope corresponding to k_{Ag2S}/k_{Bu}.

If n is not equal to 1, meaning that n moles ozone are consumed by the formation of one mole of S^*, k_{Ag2S} will be reduced by the factor n.

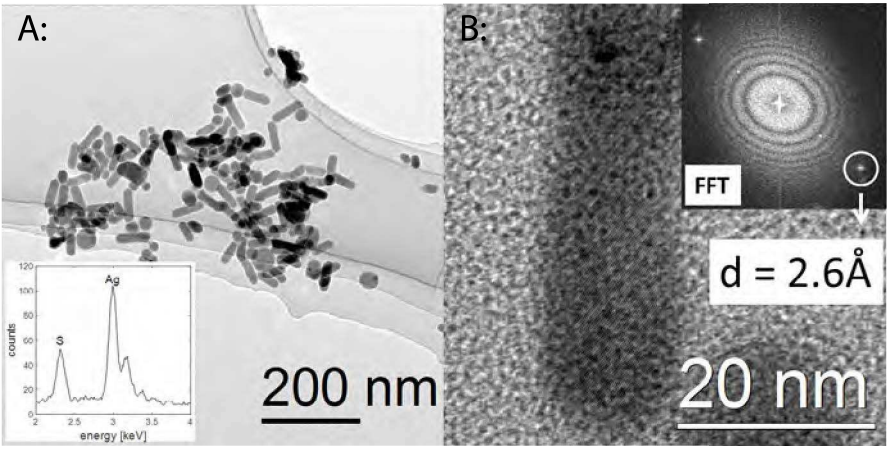

Figure C.1: Bright-field TEM images of Ag_2S particles used for the spiking experiments (A). EDX – spectrum of an Ag_2S particle revealing Ag and S signal intensities at ratio of roughly 2:1 (inset A). High resolution TEM image of an Ag_2S particle, the inset shows the forward Fourier transformation (FFT) of the high resolution image (B). Lattice spacing of 2.6 Å extracted from the FFT image are consistent with the structure of Ag_2S (Acanathite).

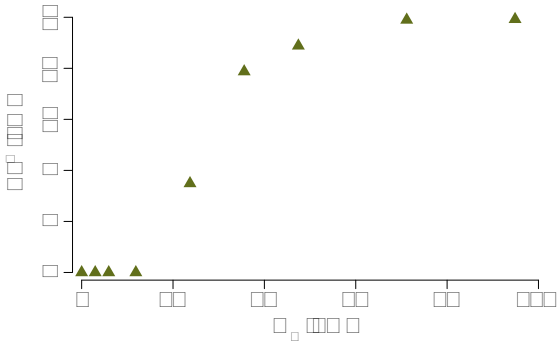

Figure C.2: Ag concentration in DDI water (buffered with 10 mM borate to pH 8.0) spiked with Ag_2S (11.5 µM) after ozonation versus the applied ozone dose.

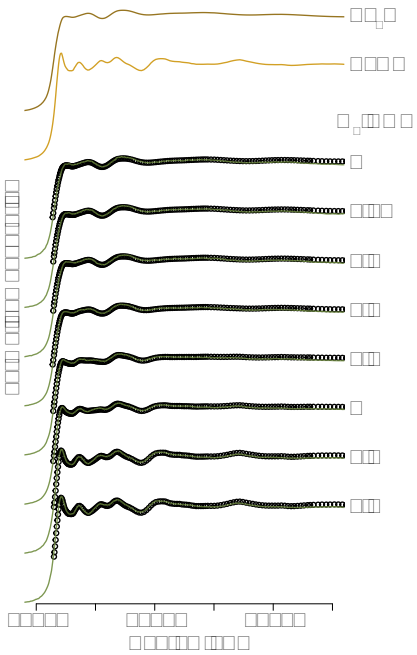

Figure C.3: X-ray absorption near edge structure (XANES) of samples (solid lines) and LCF results (open circles) using two references (Ag_2S and AgCl). For clarity, the spectra are plotted with an offset of 0.5. For LCF the individual fractions were constrained to lie between 0 and 1 and the sum of all fractions was unconstrained.

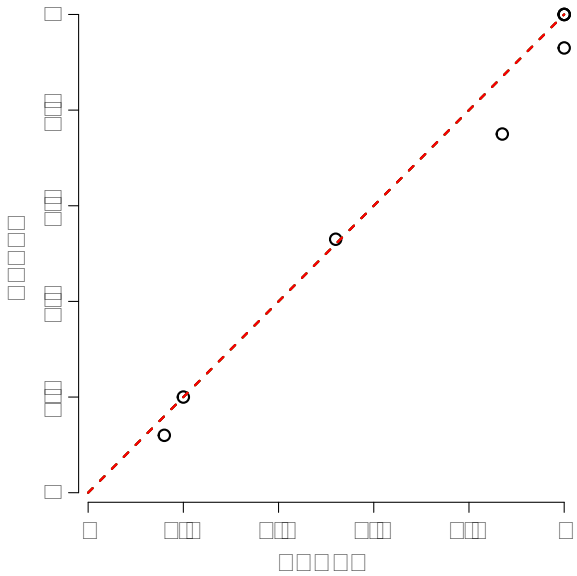

Figure C.4: Comparison of the Ag_2S fractions derived from LCF analysis of EXAFS and XANES spectra. The sum of all fractions was constrained to 1 for EXAFS (unconstrained sums of fractions are given in Table C.4) and unconstrained for XANES LCF analysis.

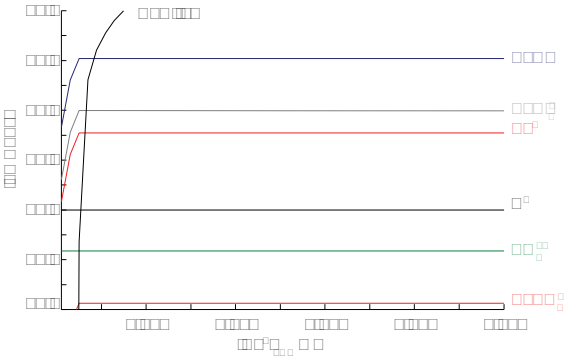

Figure C.5: Chemical equilibrium concentration plot for Ag in the presence of Cl^- (3 mM), PO_4^{3-} (0.1 mM) and SO_4^{2-} (1 mM) at pH 8.0. AgCl(c) is the dominating phase at Ag concentrations > ~ 1 µM, but also AgCl(aq), $AgCl_2^-$ and Ag^+ are predicted at (eco)toxicologically relevant concentrations. The calculations were conducted with Medusa-Hydra chemical equilibrium software (Puigdomenech 2013).

Table C.1: Properties of the Synthesized Ag_2S Particles used for the Spiking Experiments

	Diameter DLS (PDI)[a]	Zeta potential[b]	Size and shape[c]
	[nm]	[mV]	[nm]
nano-Ag_2S	59.0 (0.41)	-39.8	rod-shaped particles (61 %):[d] 57.5±15.2 × 19.3±3.9 nm spherical particles: 25.1±9.3 nm

[a]: z-average Zetasizer (NanoZS, Malvern Instruments, UK), PDI = Polydispersity Index

[b]: 90 µM Ag_2S measured in 10 mM borate buffer at pH 8.0

[c]: 105 particles measured by TEM

[d]: rod-shaped particles are defined as $d(Feret_{max}) > 1.5 * d(Feret_{min})$.

Table C.2: Effluent Water Characteristics and Concentrations of Cu and Zn

Parameter	Value
DOC	4.2 – 4.8 mg_{DOC} L^{-1}
COD	13.6 mg_{O2} L^{-1}
pH	8.0
Chloride	3 mM
Nitrate	0.3 mM
Phosphate	0.07 mM

Element	µmol L^{-1}
Copper	0.38
Zinc	0.80

Table C.3: Experiments Conducted and Methods Applied

	Nano-Ag_2S	$AgNO_3$
Stoichiometry & Kinetics (DDI water)	IC[a], ICP-MS, competition kinetics with UV-Vis measurements	NA
Ozonation of effluent water	11.5 µM Ag_2S: ICP-MS, XAS 2.8 µM Ag_2S: ICP-MS, TEM	NA
Toxicology in effluent water: untreated	ICP-MS, Phytopam[b]	ICP-MS, Phytopam
Ozone treated	ICP-MS, Phytopam[b]	NA

[a]: IC = Ion Chromatograph

[b]: Fluorometer to measure the algal photosynthetic yield of the photosystem II.

Table C.4: EXAFS Sum of Fractions for Unconstrained LCF

Sample: g_{O3} / g_{DOC}	unconstrained sum of fractions
0	1.00
0.25	1.00
0.4	1.00
0.6	1.09
0.8	1.10
1	0.96
1.3	0.95
1.5	1.00

References

Puigdomenech, I. (2013) MEDUSA (Making Equilibrium Diagrams/Using Sophisticated Algorithms), Royal Institute of Technology: Stockholm.

von Sonntag, C. and von Gunten, U. (2012) Chemistry of Ozone in Water and Wastewater Treatment, IWA Publishing.

Acknowledgment

This PhD thesis would not have been possible without the support of many people. I am most grateful to Ralf Kägi for all his hard work, support, encouragement and for being a great mentor. I highly enjoyed the intense discussions and our teamwork at the beamline. My sincere gratitude goes to Andreas Voegelin and Eberhard Morgenroth for many scientific discussions, arguments, inestimable critical feedback and all the support. I am very thankful to Prof. Greg Lowry for accepting to co-examine this thesis.

A special thanks goes to Brian Sinnet who always supported me with lab work and was there when I had a problem to solve. Furthermore, I thank Renata Behra and Urs von Gunten for the great collaboration work and support. Many thanks go to Alma Mašić, Ann-Kathrin McCall and Michele Laureni for being great colleagues and friends who always cheered me up with amazing office dinners and fun breaks. Thanks to Constanze Haupt, Dominic Looser, Jamile Wagner, Peter Desmond, Susanne Scheidegger and Theresa Rossboth for contributing to a great office atmosphere.

Thanks to my other PhD fellows (Alexandra Fumasoli, Andrea Portmann, Anna Chomiak, Christian Thürlimann, Christoph Egger, Dario del Giudice, Dorothee Spuhler, Hanspeter Zöllig, Jonathan Habermacher, Lena Mutzner, Mariane Schneider, Omar Wani, Pascal Wunderlin and Sven Eggimann) for their critical and helpful feedback during PhD seminars and for the good times at the PhD activities. I would like to thank the members of the staff representation at Eawag (Alois Zwyssig, Isabelle von Niederhäusern, Jacqueline Traber and Tom Gonser), it was a great experience being able to contribute and being part of this group.

My gratitude goes to all the people from the process engineering and urban water management group at Eawag for creating such a stimulating and friendly environment. I am thankful to the Swiss National Science Foundation for the financial support, and for creating an amazing network of researchers working in different fields of nanotechnology through the National Research Program 64 "Opportunities and Risks of Nanomaterials".

Thanks to all my friends that supported me during my PhD. I am very happy to have my good childhood friends Francesco Albizzati, Gopal Joshi and Simon Trüb, I always enjoy your company. Thanks to my wonderful Gourmet Friends: Loran Lampart, Manuela Bieri, Sandro Imhasly and Stefanie Peter; for the uplifting evenings with excellent food and intense discussions. Thanks to my band mates: Emanuel Albizzati and Timo Hegnauer; for the good times, you rock! Furthermore, I thank the "Super G Gang": Christian Wullschleger, Christoph Zuber, Jennifer Meyer, Jérôme Beeler, Jens Bergermann, Julia Brändli, Michael Mettler, Nora Rusterholz and Wolfgang Pallmann; for all the fun and spontaneous events and trips.

Einen speziellen Herzlichen Dank für die grosse Unterstützung in all den vielen Jahren geht an meine Eltern Bänz Zulliger und Marlise Thalmann und meine Grossmutter Claire Thalmann. I am also thankful to the family of Kylie for all their support: Calvin Graf, Nicole Russnaik, Oliver Graf and Soledad Graf.

Last but not least, I thank you, Kylie Russnaik, for the encouragement, for always being there for me and for making me smile. You are my biggest support.

Dankä

Basil, September 2015